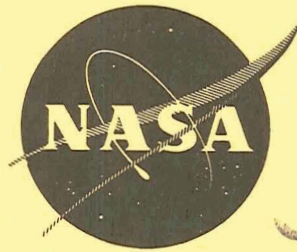


N71-35580

NASA CR-72901



CASE FILE COPY

DEVELOPMENT OF A CHROMIUM-THORIA ALLOY

by

N. D. Veigel, B. A. Wilcox, J. M. Blocher, Jr.,
A. H. Clauer, D. A. Seifert, K. E. Meiners,
M. F. Browning, and W. H. Pfeifer

BATTELLE
Columbus Laboratories

prepared for

NATIONAL AERONAUTICS AND SPACE ADMINISTRATION

NASA Lewis Research Center
Contract NAS 3-12435
T. P. Herbell and J. P. Merutka,
Project Managers
Materials and Structures Division



NOTICE

This report was prepared as an account of Government-sponsored work. Neither the United States, nor the National Aeronautics and Space Administration (NASA), nor any person acting on behalf of NASA:

- (A) Makes any warranty or representation, expressed or implied, with respect to the accuracy, completeness, or usefulness of the information contained in this report, or that the use of any information, apparatus, method, or process disclosed in this report may not infringe privately owned rights; or
- (B) Assumes any liabilities with respect to the use of, or for damages resulting from the use of, any information, apparatus, method or process disclosed in this report.

As used above, "person acting on behalf of NASA" includes any employee or contractor of NASA, or employee of such contractor, to the extent that such employee or contractor of NASA or employee of such contractor prepares, disseminates, or provides access to any information pursuant to his employment or contract with NASA, or his employment with such contractor.

Requests for copies of this report should be referred to

National Aeronautics and Space Administration
Scientific and Technical Information Facility
P. O. Box 33
College Park, Maryland 20740

1. Report No. NASA-CR-72901	2. Government Accession No.	3. Recipient's Catalog No.	
4. Title and Subtitle DEVELOPMENT OF A CHROMIUM-THORIA ALLOY		5. Report Date March 10, 1971	6. Performing Organization Code
		8. Performing Organization Report No.	
7. Author(s) N. D. Veigel, B. A. Wilcox, J. M. Blocher, Jr., A. H. Clauer, D. A. Seifert, K. E. Meiners, M. F. Browning, and W. H. Pfeifer		10. Work Unit No.	
9. Performing Organization Name and Address Battelle Columbus Laboratories 505 King Avenue Columbus, Ohio 43201		11. Contract or Grant No. NAS3-12435	
		13. Type of Report and Period Covered Contractor Report	
12. Sponsoring Agency Name and Address National Aeronautics and Space Administration Washington, D. C. 20546		14. Sponsoring Agency Code	
		15. Supplementary Notes	
16. Abstract A vapor-deposition apparatus was designed, constructed, and used to prepare chromium and chromium-3 w/o ThO ₂ powders in one-quarter to one-half pound (114-227 g) lots. The powders were consolidated by hot isostatic pressing, rolled to sheet, and evaluated in sheet form. The addition of thoria lowered the ductile-to-brittle transition temperature both in the as-rolled and annealed (1 hr, 1200 C) conditions. After high temperature annealing (up to 1427 C), the Cr-ThO ₂ alloys recrystallized with elongated grains. Although such a structure should have good high temperature strength, no improvement was observed, probably because the microstructure was less than optimum.			
17. Key Words (Suggested by Author(s)) Cr-ThO ₂ powder Cr-ThO ₂ alloys Cr-ThO ₂ properties		18. Distribution Statement Unclassified - unlimited	
19. Security Classif. (of this report) Unclassified	20. Security Classif. (of this page) Unclassified	21. No. of Pages 101	22. Price* \$3.00

* For sale by the National Technical Information Service, Springfield, Virginia 22151

FINAL REPORT

on

DEVELOPMENT OF A CHROMIUM-THORIA ALLOY

by

N. D. Veigel, B. A. Wilcox, J. M. Blocher, Jr.,
A. H. Clauer, D. A. Seifert, K. E. Meiners,
M. F. Browning, and W. H. Pfeifer

ABSTRACT

A vapor-deposition apparatus was designed, constructed, and used to prepare chromium and chromium-3 w/o ThO₂ powders in one-quarter to one-half pound (114-227 g) lots. The powders were consolidated by hot isostatic pressing, rolled to sheet, and evaluated in sheet form.

The addition of thoria lowered the ductile-to-brittle transition temperature both in the as-rolled and annealed (1 hr, 1200°C) conditions. After high temperature annealing (up to 1427°C), the Cr-ThO₂ alloys recrystallized with elongated grains. Although such a structure should have good high temperature strength, no improvement was observed, probably because the microstructure was less than optimum.

SUMMARY

The purpose of this investigation was to evaluate the low temperature ductility and high temperature strength of chromium and chromium-thoria prepared from powders produced by chemical vapor deposition. The initial objective was to scale-up a vapor-deposition process patterned after a smaller unit of the first phase of work used in a previous program (NASA-10492)⁽¹⁾ to produce one pound (454 g) lots of chromium/thoria powder in a one-day process run. This objective was partially achieved in that 0.30 to 0.55 pound (133-250 g) lots of powder product were collected in preparations of 8 to 11 hours duration. Development progressed to the extent that the preparation of one-pound (454 g) lots in about 20 hours of continuous operation appear to be attainable. The major problem encountered with the powder preparation unit, was the formation of a chromium plug on a nozzle that injected a helium-CrI₂ mixture into a hydrogen filled chamber, thereby causing early termination of powder preparation runs. An effective nozzle design was identified and used to prepare chromium and chromium/thoria powder.

The powders prepared for evaluation included a 250-g lot of pure chromium powder, and three other lots (133 to 232 g) of Cr-ThO₂ powder containing about 3 w/o ThO₂ (2.2 v/o).

Powder products were cold pressed at 50,000 psi (345 MN/m²) and densified by hot isostatic pressing (HIP) at 10,000 psi (69 MN/m²) and 1100°C for two hours. The consolidation was successful in that densification was achieved and no detectable leakage occurred during HIP. However, most of the consolidated billets were found to be cracked after decladding and surface grinding. Consequently, sectioning was required to obtain crack-free material for rolling. Successful hot rolling of the billets to sheets of 0.026 to 0.033 inch (0.066 to 0.084 cm) thickness was achieved. The billets were sheathed in a mild steel container and initially rolled at 1100°C. As rolling progressed the temperature was gradually lowered, and the final rolling temperature was 700°C.

Tension tests at a strain rate of $1.7 \times 10^{-4} \text{ sec}^{-1}$ showed that the ThO_2 particles lowered the ductile-to-brittle transition temperature (DBTT) compared with pure chromium. This ductilizing was evident both in the as-rolled condition, and after the materials had been annealed for one hour at 1200°C . The DBTT values were:

<u>Material</u>	<u>As-Rolled</u>	<u>Annealed</u>
Pure chromium	140°C	140°C
Cr- ThO_2 alloys	15°C	50°C

This ductilizing was interpreted as the result of three possible mechanisms:

(1) ThO_2 particles dispersing slip, such that critical stress concentrations for crack initiation were more difficult to achieve, (2) particles acting as dislocation sources providing mobile dislocations, and (3) particles in grain boundaries helping transmit slip across the boundaries.

Over the temperature range $150\text{-}200^\circ\text{C}$ the yield and ultimate strengths of Cr- ThO_2 alloys were about 10,000 psi (69 MN/m^2) higher than corresponding values for pure chromium. However, at 1093°C the strength of Cr- ThO_2 alloys was essentially the same as pure chromium. The relative lack of dispersion strengthening is attributed to a less than optimum dispersion of ThO_2 particles. In order to achieve better low and high temperature strengthening, the ThO_2 dispersion must be made more uniform, or another strengthening method such as solid solution alloying, e.g., with tantalum or niobium, must be used in conjunction with the dispersion.

INTRODUCTION

Dispersion-strengthened chromium is of interest for use in turbines which require materials having better high-temperature strength and oxidation resistance than present superalloys. To be effective in strengthening at elevated temperatures, the dispersoid must be stable in contact with the matrix and impurities associated with the matrix. Another requirement for turbine use is that the material must have sufficient ductility at low temperatures to withstand shock associated with turbine

"start-up". The limited ductility of chromium is well known and is recognized to be a severe design limitation. Consequently, the objective of the present research program was to develop and characterize a dispersion-strengthened chromium system that not only has improved strength and microstructural stability at elevated temperatures, but also has improved ductility at low temperatures.

The present research program is a continuation of work, concluded under a previous contract (NASA-10492)⁽¹⁾, which demonstrated that consolidation of small lots (5-16 g) of vapor-formed chromium/thoria powder yields a dispersion that is thermally stable during high temperature annealing, e.g., 1427°C for 100 hours. An expected result of this dispersion of thoria in chromium is an increase in the room temperature and high-temperature strength. Although mechanical-property data were not obtained for the chromium/thoria alloy prepared during the previous program, the strengthening effect of dispersed particles in other alloy systems is well known.

Another anticipated effect that may be obtained with particles dispersed in "brittle" metals is to lower the ductile-to-brittle transition temperature (DBTT). Although the possibility has not been demonstrated in the chromium/thoria system, it has been postulated by Hahn and Rosenfield⁽²⁾, and demonstrated in the Fe-ThO₂ system⁽³⁾. The basic premise is that particles would limit the free-slip distance, thus reducing the dislocation pile-up length, which in turn would raise the cleavage stress. If this occurs, there is a good possibility that yielding will occur before cleavage, and the ductile-to-brittle transition temperature will be shifted to lower temperatures.

The immediate and long range objectives of the present program were to:

(1) scale-up the vapor-deposition process to produce about one pound (454 g) of chromium or chromium-thoria powder in a one day process run, (2) to consolidate the powder and roll to sheet, and (3) to prepare specimens for evaluation of the ductilizing concept and to examine high temperature strength and thermal stability.

PROCESS DEVELOPMENT

Process Description

The feasibility of preparing small lots of chromium/thoria powder by deposition was demonstrated in the previous development program⁽¹⁾. On consolidation of the powder product, a thermally stable dispersion was obtained having an interparticle spacing of 3 to 5 μ m. In view of the promising results, scale-up of the process and further evaluation of the product were pursued.

The process involves the feeding of a CrI_2 -helium gas mixture into a hydrogen-filled chamber to cause the formation of chromium powder by hydrogen reduction of the CrI_2 . Simultaneously, thoria particles entrained in hydrogen are injected into the reaction zone. Thus, chromium powder is formed in the presence of the thoria particles. It has not been established that the thoria particles are coated in this process. However, the thoria and chromium are sufficiently blended so that on consolidation of the powder a promising material is obtained. The size of the as-prepared chromium powder is in the range of 0.02 to 0.4 μ m.

Design of the Powder-Preparation Unit

A schematic drawing of the apparatus is given in Figure 1, and photographs of the assembled unit are shown in Figures 2, 3, 4, and 5. Operation of the unit is described in the following discussion.

Iodine is vaporized and carried with helium from a three-liter flask housed in the heating jacket labeled A in Figure 2. The iodine-evaporation assembly is mounted on a platform balance in order to monitor the iodine feed rate. The helium/iodine gas mixture is fed to a 7 cm diameter x 38.1 cm long Vycor tube (labeled B in Figure 2) containing solid CrI_2 powder heated to about 700°C.

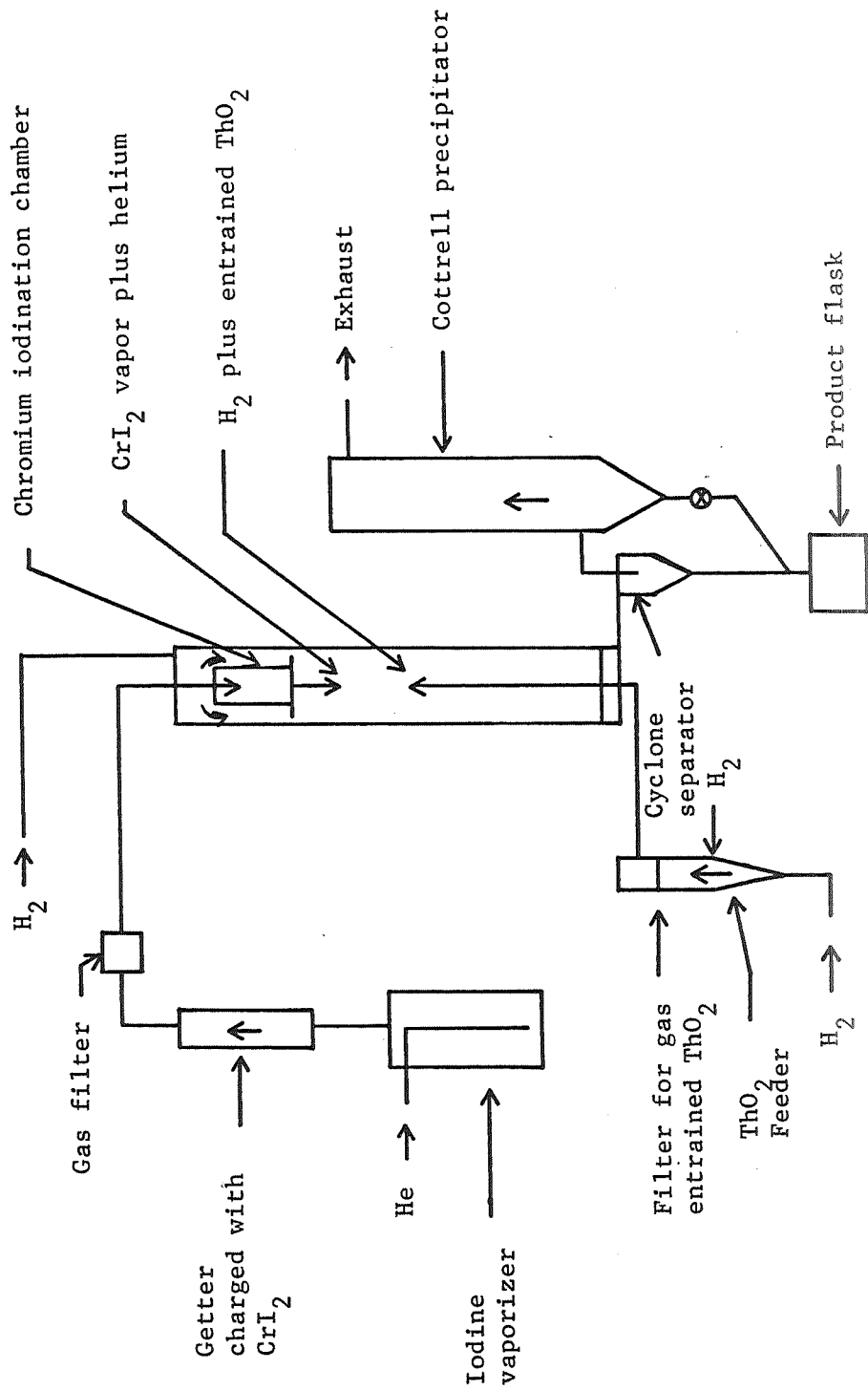
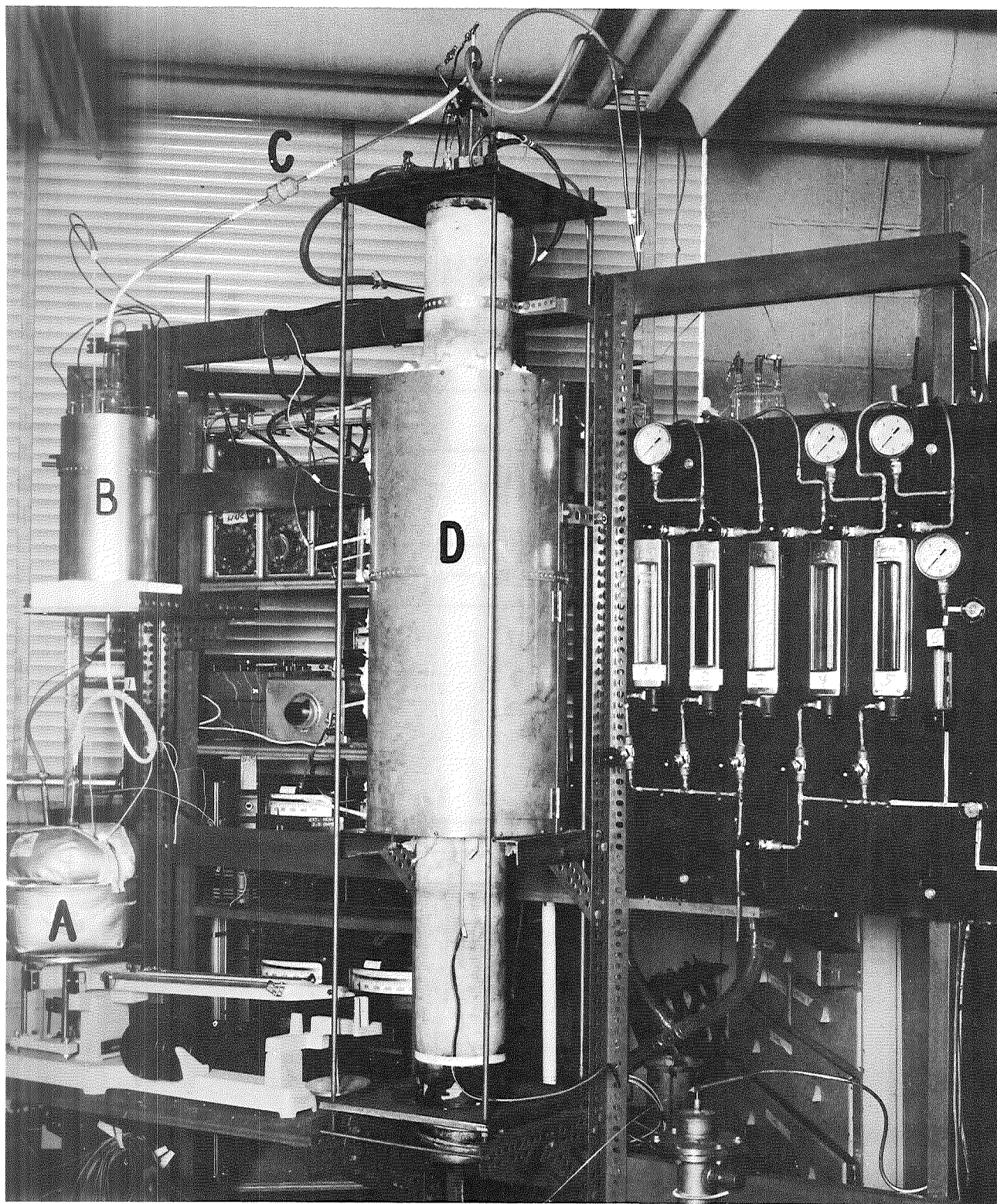
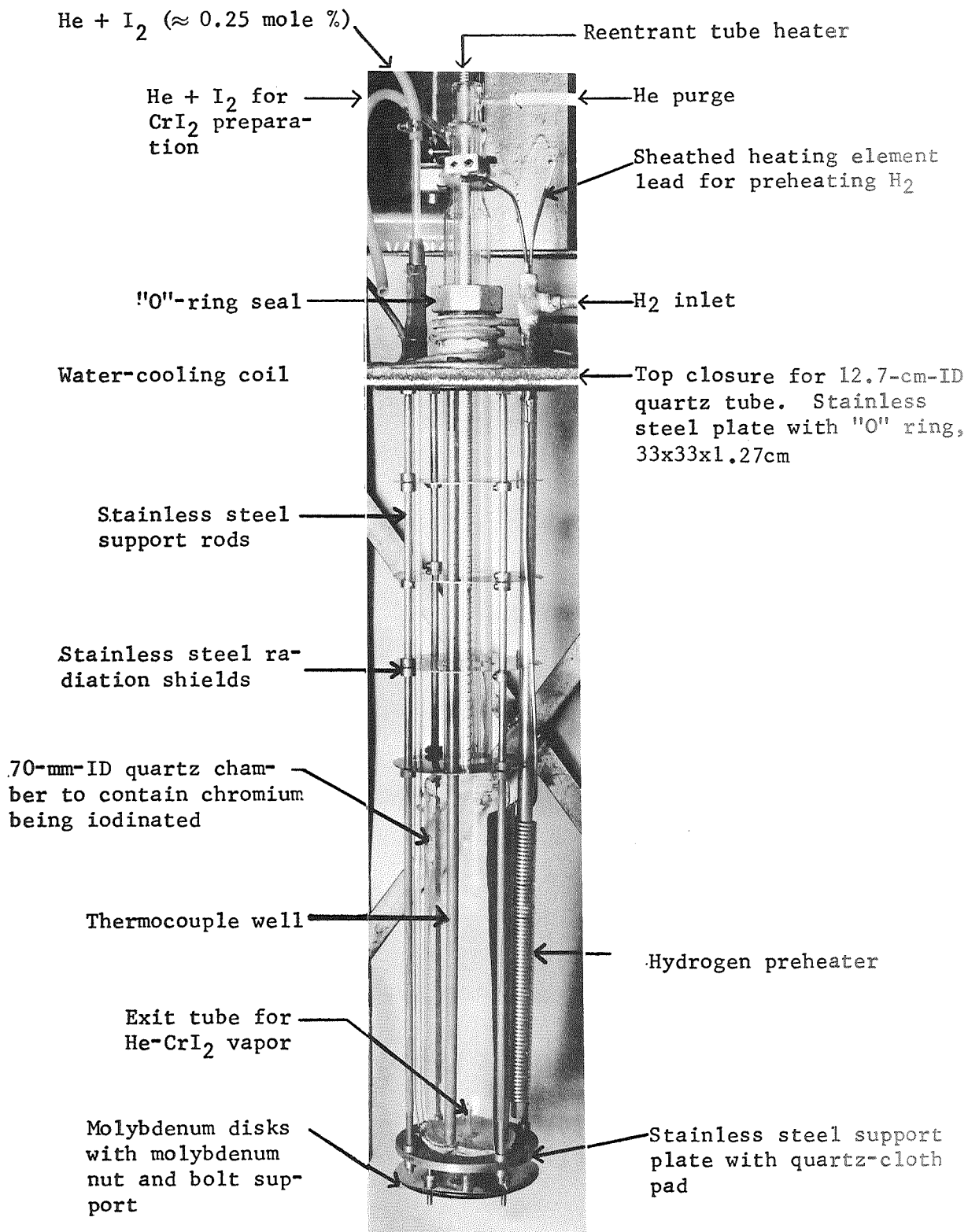


FIGURE 1. APPARATUS FOR THE PREPARATION OF CHROMIUM/ThO₂ POWDER



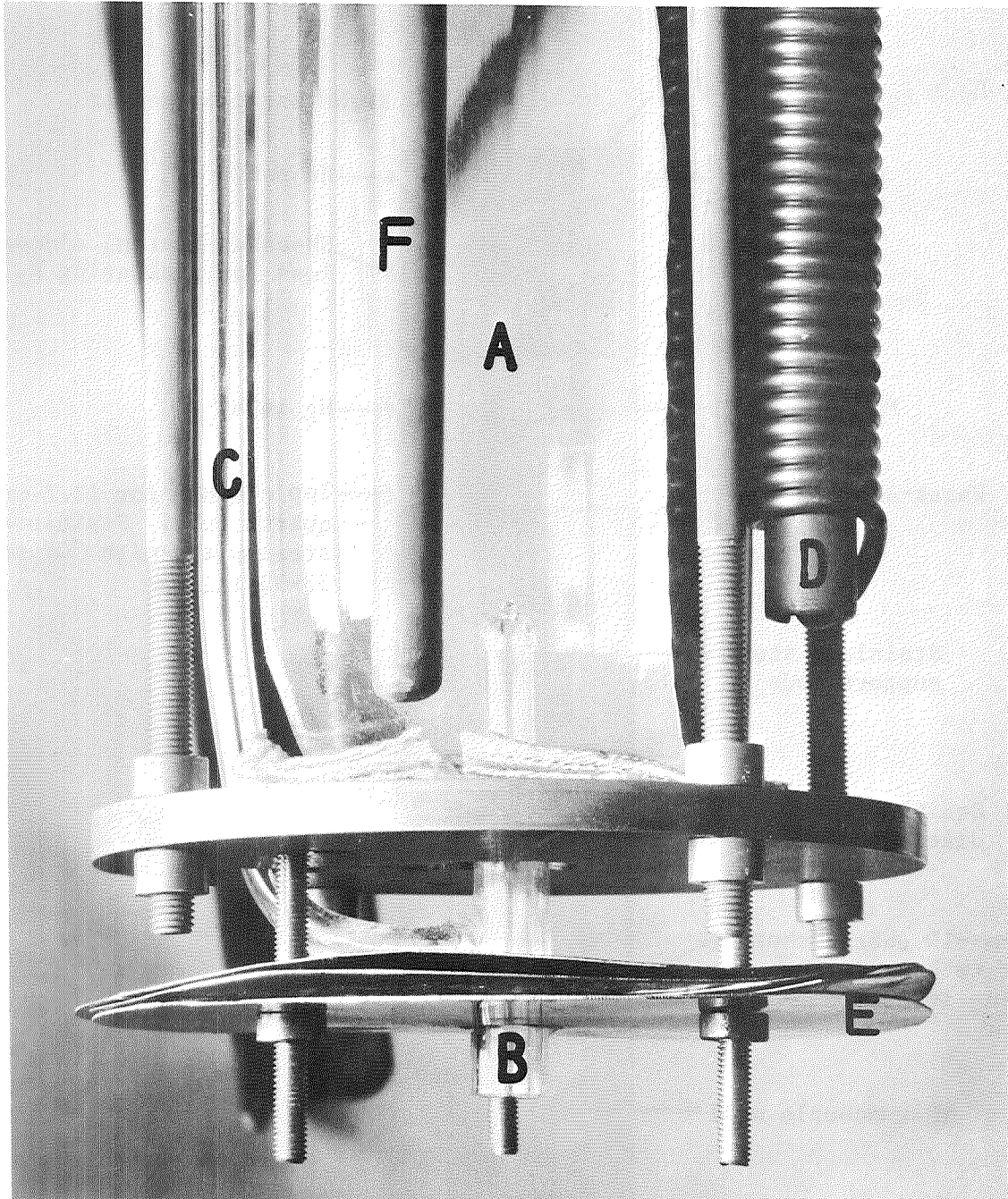
46923

FIGURE 2. VIEW OF ASSEMBLED CHROMIUM/THORIA POWDER-PREPARATION UNIT



46922

FIGURE 3. ASSEMBLY FOR IODINATION OF CHROMIUM AND PREHEATING HYDROGEN



46921

FIGURE 4. VIEW OF THE He-CrI₂-FEED NOZZLE

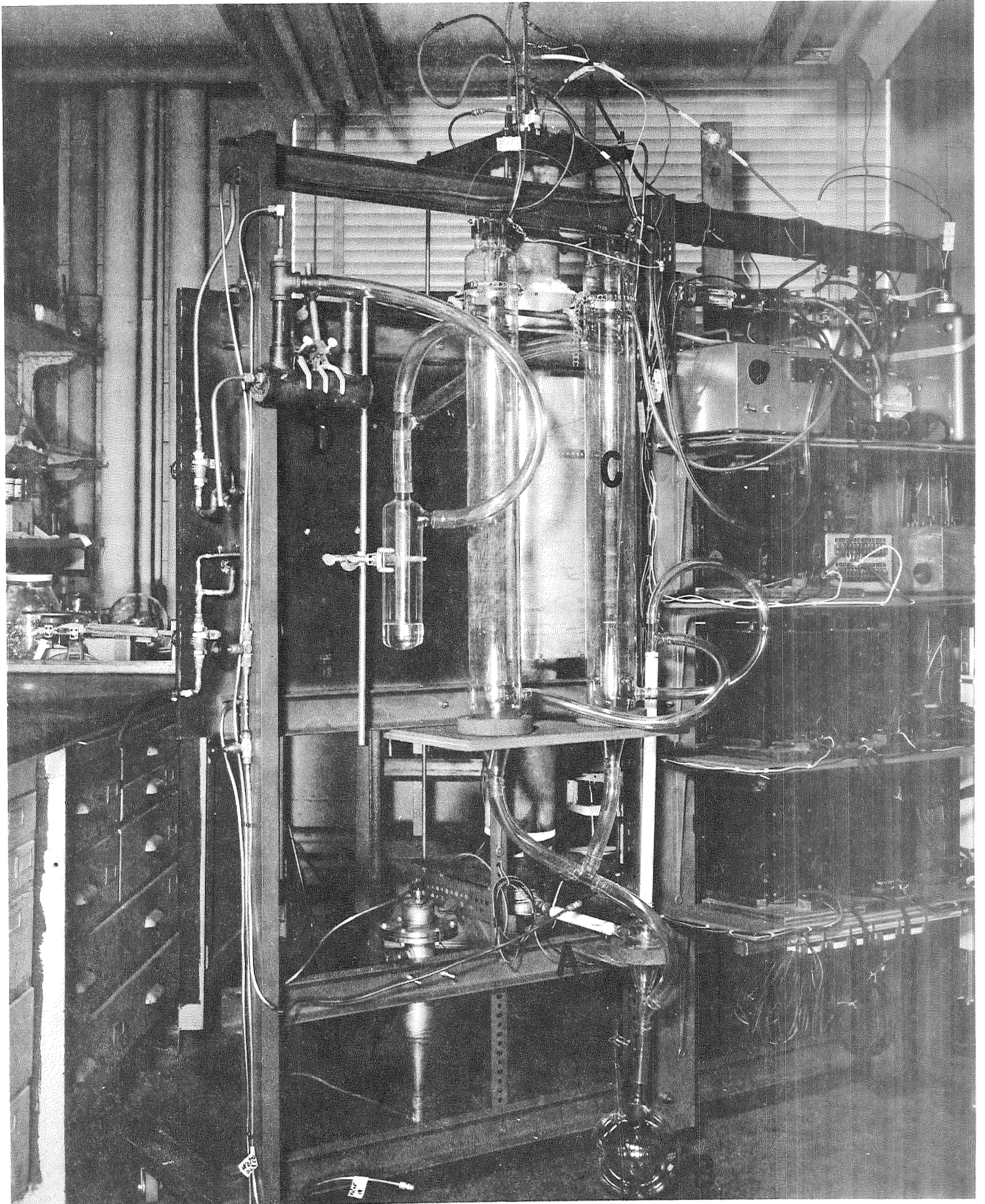


FIGURE 5. VIEW OF CHROMIUM/THORIA-POWDER-COLLECTION ASSEMBLY

The purpose of the heated CrI_2 is to react with the contaminant water normally found to be present in iodine in concentrations of 0.01 to 0.1 wt.%. The water reacts with CrI_2 to yield nonvolatile Cr_2O_3 and gaseous HI. The HI is not a contaminant, since it is one of the reduction products in the powder-preparation process. To minimize possible transport of Cr_2O_3 solid by gas entrainment, a small fritted-glass filter (labeled C in Figure 2) was placed upstream from the CrI_2 getter. However, the filter became clogged with entrained CrI_2 , and its use was discontinued early in the program.

For the continuous preparation of CrI_2 in the assembly shown in Figure 3, a predetermined mixture of helium and iodine is injected into the bed of chromium heated to 1000°C (see Figure 3 and Figure 4, Location A). The rate of iodine addition is controlled to limit the accumulation of liquid CrI_2 in the CrI_2 generator. The helium- CrI_2 mixture is injected into the hydrogen-filled chamber through a nozzle at Location B. Helium is fed through Tube C of Figure 4 to a tube concentric with the helium- CrI_2 feed tube, to prevent the contact of the CrI_2 with hydrogen and thereby prevent deposition of chromium by the hydrogen-reduction reaction. Also, a small amount of iodine is fed along with the helium-shroud gas to prevent deposition by thermal dissociation on dilution with the helium. The concentration of iodine in the helium required to prevent deposition on 50 percent dilution is calculated to be 0.25 mole percent.

Hydrogen is added through the 1/2-in. (1.27 cm) diameter stainless steel tube visible in Figures 3 and 4, Location D. The steel tube is wound with a sheathed heating element, which preheats the hydrogen before it enters a second heating chamber formed by the space between the wall of the 5-in. (12.7 cm) ID-quartz housing and the iodination chamber. The heated hydrogen passes molybdenum discs visible in Figures 3 and 4 on entering the reaction chamber.

Thoria is fed from the feeder partially visible in Figures 2 and 5 and labeled E in both figures. The feeder is constructed of stainless steel tubing,

2-1/2 in. (6.35 cm) OD x 19 in. (48.2 cm) overall height, and provided with "O"-ring seals located in the top flange, and a two-stage conical bottom. The first stage consists of a cone having a 40° included angle attached to a 3/4-in. (1.91 cm) ID x 1 in. (2.54 cm) long straight section which is welded to the second cone having a 20° included angle. Chromium granules, 60 x 120 mesh, are contained in the first stage where they are fluidized with hydrogen admitted through a small line at the bottom of the feeder. The fluidized chromium bed distributes the gas and prevents channeling of the thoria contained in the second stage. The use of chromium at this point was chosen to avoid the effects of possible attrition and entrainment of some foreign material into the system. Additional hydrogen is introduced above the fluidized bed of thoria particles to facilitate entrainment. The entrained particles are accelerated to near sonic velocity in a 47-mil (0.119 cm) ID tube, where they deagglomerate. These particles are then injected into the reaction chamber.

The chromium-thoria-powder product is carried by entrainment toward the bottom of the 5-in. (12.7 cm) ID-quartz tube where it is deflected by a 15-mil (0.038 cm) thick sheet of molybdenum cut to form an ellipse that rests at a 45° angle in the bottom closure of the quartz tube. The exhaust gas and entrained product exit through a 1/2-in. (1.27 cm) stainless steel pipe connected with Teflon to a glass cyclone separator visible in Figure 5, Location A. The cyclone was fabricated from a 500-ml Erlenmeyer flask provided with 1.9 cm tubular-glass inlet and outlet for the gases. The powder product that is disentrained in the cyclone falls into the product flask at B in Figure 5. The powder product that escapes the cyclone is collected in the Cottrell precipitators labeled C in Figure 5. In operation, the 1-in. (2.54 cm) ID plastic tubing connecting the bottoms of the cyclone and precipitators is closed with clamps so that the gas must flow through the top opening of the cyclone. The exhaust gas from the precipitators is bubbled through dibutylphthalate and then cleaned in a water-spray

scrubber located at D in Figure 5 prior to being exhausted into a vented hood. The spray scrubber is constructed of black-iron fittings with a spray nozzle housed just below the pipe "T" and is directed downward into a water reservoir provided with a drain.

The powder products from both the precipitator and the cyclone are transferred by gravity with vibration to the product flask. Since the product contains some unreacted CrI_2 , it is transferred from the flask to a 4-in. (10.2 cm) diameter x 20-in. (50.8 cm) long Vycor bulb for heat treatment in hydrogen at 700°C to reduce the CrI_2 to chromium. The heat-treated product is then transferred back into a product flask for storage until the consolidation step is undertaken. All transfers are made in a purified helium atmosphere.

Experimental Operation of the Powder-Preparation Unit

In all, 13 powder-preparation runs were made. The first eight runs did not yield significant quantities of chromium powder as a result of early termination forced by operational difficulties. Effective modifications of the coating unit were identified and used in the last five preparations for the preparation of 133 to 250 gram lots of powder products. The preparations are summarized in Table 1.

The primary operational problem involved the formation of a chromium deposit on the nozzle that injects the CrI_2 -helium mixture into the hydrogen-filled reaction zone. Initially, the chromium deposit on the nozzle deflected the CrI_2 -helium gas stream and led to an inefficient reaction as a result of inadequate mixing with hydrogen. Eventually, the chromium deposit formed a gas-tight plug. It was recognized at the outset of the program that it would be difficult to inject the thermally unstable gaseous compound, CrI_2 , at high temperature into a hydrogen-filled chamber. Dissociation of the CrI_2 can occur by

TABLE 1. SUMMARY OF DATA ON PREPARATION OF CHROMIUM POWDER (1)

Run No.	Nozzle Design (2)	Velocity of CrI ₂ -He Mixture from Nozzle, cm/sec	Re-action Temp., °C	Time in Operation, hr	Cause of Termination	Average Chromium Iodination Rate, g/hr	Chromium Powder-Preparation Rate Total Powder Formed, g/hr	Powder Collected in Product Flask, g/hr
27180-11-1	A	4,000	1,000	2	CrI ₂ -He nozzle plugged with Cr	44	Not measured, but yield was low	-
27180-17-2	A	4,000	1,000	1	"	-	"	-
27180-18-3	A	4,000	1,000	5	"	31	5 ⁽³⁾	2
27180-22-4	B	11,000	1,000	4	"	34	2 ⁽⁴⁾	-
27180-26-5	B	11,000	940	3	Collection system overloaded with CrI ₂	29	< 1	-
27180-29-6	C	600	1,000	3.5	CrI ₂ -He nozzle nearly plugged	38	10 ⁽⁵⁾	5.8
27180-33-7	C	2,000	1,000	Operating conditions not attained	CrI ₂ -He nozzle plugged with Cr	Negligible	Negligible	-
27180-35-8	E	900	1,000	1	Electrical short on I ₂ feed line heater	33	21	8.6

TABLE 1. (Continued)

Run No.	Nozzle Design (2)	Velocity of CrI ₂ -He Mixture from Nozzle, cm/sec	Reaction Temp., °C	Time in Operation, hr	Cause of Termination	Average Chromium Iodination Rate, g/hr	Chromium Powder Formed g/hr	Chromium Powder Collected in Product Flask, g/hr
27180-37-9	E	900	1,000	11.5	CrI ₂ -He nozzle nearly plugged	60	22.4	12.2
27180-41-10	F	1,000	1,000	11	Color change detected in product indicating poor reaction efficiency	63	32.8	22.7
27180-49-11	F	1,000	1,000	8	Small-bore thoria-transport tube plugged with thoria	59.4	38.5	22.1
27180-57-12	F	1,000	1,000	5.5	Plug developed in water scrubber on exhaust line as a result of corrosion	55.2	37	24.2
27180-61-13	F	1,000	1,000	9	Color change in product observed. However, no problems were detected on inspection of the dismantled unit.	60.3	42.3	25.8

TABLE 1. (Continued)

- (1) The gas composition used for all of the runs is near that used in the previous research program (NASA-10492). The composition is 23.8 to 23.9 mole % helium, 75.5-75.9 mole % hydrogen, and 0.27 to 0.66 mole % CrI_2 .
- (2) See Figures 6 and 7.
- (3) A thermocouple housed in a 7-mm-OD well was supported from the bottom of the preparation unit and positioned axially with the termination of the closed end of the well and the thermocouple bead at a point three inches (7.6 cm) within the bottom of the reaction chamber. Chromium deposited on the well at an average rate of 4.7 g/hr. In the absence of the well, a major portion of the deposited chromium could have formed powder. Therefore, the indicated rate of powder formation could be low by as much as 4.7 g/hr.
- (4) A high-velocity (4700 cm/sec) jet of hydrogen was fed from the bottom of the reaction zone counter-current to the CrI_2 -helium flow to improve the mixing of gases. However, the jet of hydrogen may have adversely affected the temperature of the reactant gases, since it was not preheated prior to injection into the reaction chamber.
- (5) Several wire probes were located in the reaction chamber to gain information on the extent of the reaction at various points. Chromium deposited on the wire probes at an average rate of 4.3 g/hr. In addition, chromium deposited across the large nozzle at an average rate of 5 g/hr. In the absence of the added surfaces, up to 9.3 g/hr of additional powder could have been formed.

dilution with an inert gas as well as by hydrogen reduction. Consequently, the general approach to the problem was to sweep the hydrogen away from the nozzle with an inert gas and thereby prevent the hydrogen reduction of CrI_2 on the nozzle. To prevent the thermal decomposition by dilution at the nozzle, iodine was fed at a predetermined concentration along with the inert sweep gas. The approach was basically sound as indicated by the successful preparation of useful quantities of powder product. However, the identification of a nozzle configuration that made effective use of the iodine-doped sweep gas involved considerable effort as indicated in the discussion that follows.

The formation of an irregular chromium deposit on the nozzle not only caused eventual termination of a preparation run due to complete blockage of the gas flow, but by altering the flow characteristics also caused unknown and uncontrolled changes in the mixing of the reactants in the reaction chamber. The changes in mixing of the reactants in turn caused wide variations in the reaction efficiency, and, as a result, a variable powder-yield rate was obtained. In addition, if the CrI_2 -helium mixture was deflected toward the wall of the reaction chamber, chromium was deposited there in massive form rather than as the desired powder. The problem was not only decreased powder-production efficiency, but the inability to predict the amount of chromium powder being prepared, which must be known to establish the rate of ThO_2 feed for a desired alloy composition.

The nozzle designs evaluated are shown in Figure 6. The initial approach was to use high velocities of the CrI_2 -helium mixture and shroud the end of the nozzle with helium containing 0.23 to 0.55 mole percent iodine. The high gas velocities effectively prevented blockage for about five hours of operation. However, as information on the yield of powder was obtained, it became apparent that the powder-preparation rate decreased with increasing gas velocities through the nozzle.

Nozzle	Outer Tube, mm ID	Inner Tube, mm ID	Z, mm
A	8	5	0
B	7	3	4
C	17	13	2

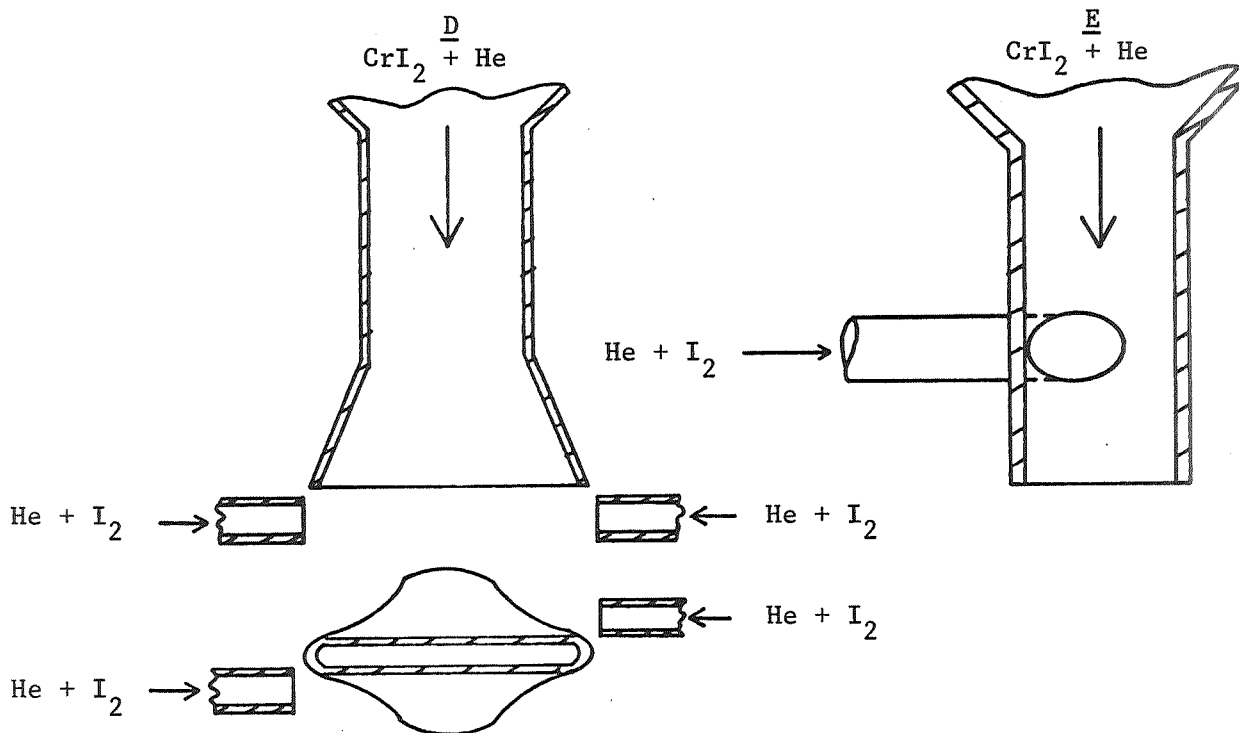
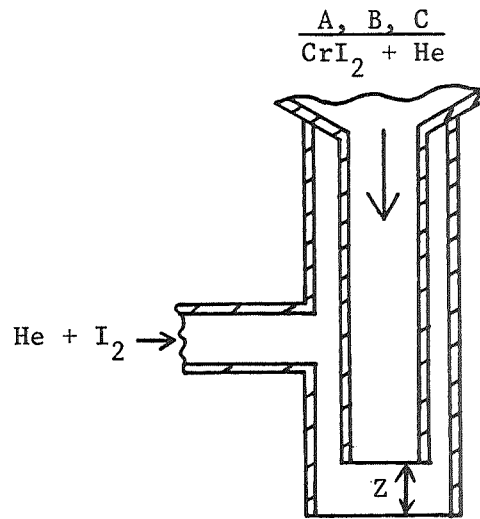


FIGURE 6. NOZZLE DESIGNS USED TO INJECT THE CrI_2 -HELIUM MIXTURE INTO THE HYDROGEN-FILLED REACTION ZONE

Nozzles A and B of Figure 6 are nozzles that operate at relatively high gas velocities, i.e., 4,000 and 11,000 cm/sec, respectively. Nozzle C of Figure 6 was operated with a gas velocity of 600 cm/sec and, as indicated by the data included in Table 1, its use resulted in the first improvement in the rate of powder formation. Nozzles D and E of Figure 6 were then designed to either spread gases injected at high velocity or effectively use a low velocity. Nozzle D was found to be ineffective. Nozzle E was designed to operate at relatively low gas velocity, 900 cm/sec, with a helium-0.5 mole percent iodine shroud gas injected tangentially to the CrI_2 -helium mixture. The design involving tangential injection showed promise and was expanded to include the tangential feed of the helium-iodine mixture to both a shroud and an inner CrI_2 -helium injection nozzle, as shown in Figure 7. With the latest nozzle design, up to about 1/2 pound (227 g) quantities of chromium or chromium/thoria powder were prepared in single preparation runs of about 10 hours duration. Preparation runs of up to 20 hours duration to yield one-pound (454 g) quantities of powder product now appear to be attainable with existing apparatus and operational experience.

Calibration of the Thoria Feeder

Control of composition with respect to thoria depends on being able to predict the rate of formation of chromium powder throughout the preparation run so that the rate of thoria feed can be adjusted accordingly. When the development of the powder preparation unit progressed to the extent that the rate of chromium powder formation was predictable, operating conditions for the thoria feeder were identified to deliver the required amount of thoria. The thoria feeder, described in detail in an earlier section of this report, consists mainly of a two-stage fluidized-bed unit provided with a small bore tube to transport entrained thoria powder to the hydrogen-filled reaction chamber of the powder-preparation unit.

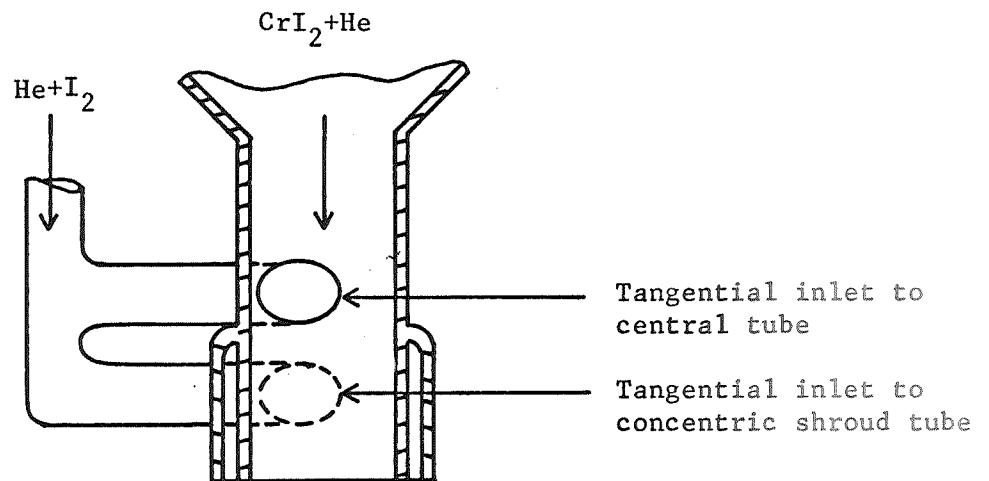


FIGURE 7. NOZZLE DESIGN USED TO INJECT THE CrI_2 -HELIUM MIXTURE INTO THE HYDROGEN-FILLED REACTION ZONE

The first stage of the fluidized bed feeder contained chromium granules to distribute the gas fed to the bed of thoria contained in the second stage.

To calibrate the feeder, 150 grams of Vitro* thoria was charged. This thoria was specified to be nominally 0.02 to 0.05 μ m in size, but actually contained some 0.1 to 1.5 μ m size particles. An electron micrograph of the starting ThO₂ powder is shown in Figure 8. It is seen that most of the particles are smaller than about 800 Å (0.08 μ m). However, large particles such as the one in Figure 8 were observed frequently. These were generally in the size range 0.1 to 1.5 μ m.

The small bore exhaust tube for the thoria feeder was connected to a weighed electrostatic precipitator. The weight of thoria collected at constant



FIGURE 8. ELECTRON MICROGRAPH OF STARTING ThO₂ POWDER, 60,000X

The particles were suspended in a solution of ethyl alcohol and sprayed onto an electron microscopy grid covered with a carbon film.

* This ThO₂ was procured from Vitro Laboratories of West Orange, New Jersey. A discussion regarding selection of this ThO₂ source is given in Appendix A.

gas flow rates in the electrostatic precipitator was determined after successive one-hour periods of operation. Based on a predetermined total chromium-feed rate of 60 grams per hour in the powder-preparation unit, thoria feed rates of 1.9 and 4.0 grams per hour were expected to be required for nominal powder compositions of 2 to 3, and 5 to 6 v/o thoria, respectively.

It was expected from previous experience that the condition of the thoria in the feeder had to be taken into account in order to obtain a desired feed rate. In an entrainment-type feeder, a high rate of feed is obtained with a fresh charge of thoria. The rate of thoria feed at constant gas flow rate decreases rapidly within several hours of operation and then becomes more constant, presumably as a result of a more steady state of agglomeration and compaction of the charge. Consequently, calibration of the feeder for each chromium/thoria run was considered to be necessary in order to compensate for changes in charge size and condition of the thoria charge.

To identify the condition required for a desired thoria feed rate of 1.9 gram per hour, 30 one-hour calibration runs were made. It was ascertained that a nearly constant thoria feed rate of 1.9 grams per hour could be obtained with (1) a conditioned charge of 110 grams of thoria, (2) a hydrogen gas flow rate of 5 liters per minute, and (3) an additional 5 liters per minute injected at the bottom of the thoria bed.

For the 1.9 gram per hour thoria feed rate, a small-bore 47-mil (0.119 cm) ID transport tube was satisfactory. However, in calibrating the feeder for a feed rate of 4 grams per hour, plugging of a 47-mil (0.119 cm) transport tube was found to be a problem. A 63-mil (0.16 cm) ID transport tube was substituted to avoid the plugging and, with the larger bore transport tube, it was established that nearly the same hydrogen gas flow rates used with the smaller bore transport were required for a 4 gram-per-hour thoria feed rate. However, at the higher feed rate, the amount of thoria fed from a preconditioned 150-gram charge

decreased gradually with use. To compensate for the decreasing delivery rate the hydrogen gas flow rate through the bed of chromium was held constant at 5 liters per minute, while the 5-liter-per-minute flow rate injected into the thoria was increased 0.2 liter per minute on an hourly basis. This procedure was defined in the calibration work.

Preparation of Powders for Consolidation and Mechanical-Property Measurement

The final modification of the CrI_2 -helium injection nozzle, shown in Figure 7, was used to prepare 250 grams of pure chromium powder, 177 grams of chromium-1.41 v/o ThO_2 , 133 grams of chromium-2.35 v/o ThO_2 , and 232 grams of chromium 2.60-v/o ThO_2 in runs numbered 27180-41-10 through 27180-61-13 (Table 1). Vacuum-fusion and spectrographic analyses were obtained for the pure chromium powder, while the chromium/ ThO_2 powders were analyzed only for thoria.

The results of the analyses of the pure chromium powder indicated that the purity was consistent with the purity of chromium powder prepared during the previous research program⁽¹⁾. Spectrographic analyses indicated the presence of only traces of iron (< 100 ppm), silicon (< 100 ppm), and copper (< 50 ppm). Other metallic contaminants were sought, but not detected. Vacuum-fusion analyses of a sample of chromium powder, contained in a helium-filled tin capsule to avoid exposure to air on loading in the vacuum-fusion apparatus, indicated oxygen and nitrogen contamination to be 830 ppm and < 40 ppm, respectively. The 830 ppm of oxygen is consistent with oxygen contamination (> 320 ppm but < 1145 ppm) obtained in pure chromium powder prepared during the previous research program. However, the oxygen content is greater than the desired target concentration of < 150 ppm.

Control of the composition with respect to thoria does not appear to be as good as was obtained in the previous program with a small powder-preparation unit. This is indicated by the analytical results in Table 2 obtained for three

TABLE 2. COMPARISON OF CHEMICAL ANALYSES
OF POWDER AND ROLLED SHEET

<u>Powder Analyses</u>						
Run No. (a)	Intended Comp., v/o ThO ₂	Wt % ThO ₂	Vol % ThO ₂	Wt % Oxygen (b)	Wt % Nitrogen (b)	Trace, Wt % (d)
10		0	0	0.083	< 0.004	< 0.01 Fe, < 0.01 Si, < 0.005 Cu
11	2 to 3	1.95	1.41	--	--	--
12	5 to 6	3.25	2.35	--	--	--
13	5 to 6	3.59	2.60	--	--	--
<u>Analyses of Rolled Sheet</u>						
Sheet No. (a)	Origin of Analysis	Wt % ThO ₂	Vol % ThO ₂	Wt % Oxygen (b)	Wt % Nitrogen (c)	
10-1a	Battelle	0	0	0.127	0.006	
11-1b	Battelle	2.72	1.96	--	0.010	
11-1b	NASA	3.55	2.57	--	--	
12-1b	Battelle	2.99	2.16	--	0.017	
12-1b	NASA	3.58	2.60	--	--	
13-1	Battelle	3.12	2.26	--	0.007	
13-1	NASA	3.68	2.66	--	--	

(a) The first number in the sheet designation (10, 11, 12, 13) corresponds to material produced from the powder run with the same number.

(b) Vacuum fusion analysis for oxygen and nitrogen.

(c) Micro-Kjeldahl analysis for nitrogen.

(d) Spectrographic analysis.

preparations of chromium/thoria powder. Here it is appropriate to compare analyses of the powder with those of the final rolled sheet, since there are some differences. Additional work would be required to identify the cause of the poor control of composition in the powder. However, the composition of the chromium/thoria powder was considered to be satisfactory for consolidation and mechanical-property measurements.

The three ThO₂-containing alloy sheets have in general ~ 3 w/o ThO₂, or ~ 2.2 v/o ThO₂. The NASA analyses on sheet were consistently higher than the Battelle analyses. However, the trend in increasing ThO₂ content from Sheets 11 to 13 is the same for both analyses. The ThO₂ contents of powders produced on Runs 12 and 13 are consistent with the respective analyses on the rolled sheet. However, the powder analysis for Run 11 (1.95 w/o) is considerably lower than the corresponding sheet analyses (2.72-3.55 w/o). The reason for this discrepancy is not known. For convenience in subsequent discussion, the following designations will be used:

Sheet 10-1a	Pure Cr
Sheet 11-1b	Cr-2.72 w/o ThO ₂
Sheet 12-1b	Cr-2.99 w/o ThO ₂
Sheet 13-1	Cr-3.12 w/o ThO ₂

All of the powder products were heated in hydrogen for 30 hours (700°C for the first 20 hours and 750°C for the remaining 10 hours) to remove (by evaporation and/or reduction) residual CrI₂ which had been collected along with the powder product. The finished powders were then transferred to helium-filled glass ampules for storage prior to the forthcoming consolidation by hot isostatic pressing.

Fewer powder compositions than were initially planned have been made in this program because problems in "scaling-up" the powder preparation unit were more extensive than anticipated.

POWDER CONSOLIDATION AND HOT ROLLINGConsolidation of Chromium and Cr-ThO₂ Powder

A rectangular die was designed and fabricated from air-hardening tool steel for the cold pressing of Cr-ThO₂ powder into billets prior to final densification by HIP. With appropriate shims and platens, the die (shown in Figure 9) can be used to fabricate several different sizes of billets dictated by the available amounts of Cr-ThO₂ powder.

In order to avoid oxygen and nitrogen contamination of the chromium and Cr-ThO₂ powders by air, all processing steps involving handling of the powders or green-pressed billets were carried out under a protective argon atmosphere. Each lot of powder was weighed before loading it into the pressing die. The die was assembled, sealed with rubber diaphragms, and removed from the dry box. Removal of the argon atmosphere from the die cavity prior to pressing was carried out by evacuation through a hypodermic needle inserted into one of the rubber diaphragms. The entire die assembly was then sealed in a rubber bladder and hydrostatically pressed to consolidate the powder fill. After clean-up and removal of the rubber bladder, the sealed die assembly was returned to the protective argon atmosphere where it was disassembled and the green-pressed billet removed and placed in a closely fitting tantalum can lined with 0.001-in. (0.00254 cm) thick tungsten foil to act as a diffusion barrier between the chromium and tantalum during HIP. A summary of the hydrostatic pressures used to green press six billets appears in Table 3, along with the powder weights and compositions. The 30,000 psi (207 MN/m²) used to compact Billet No. 10-1 proved to be inadequate in terms of the green strength achieved, because considerable cracking and delamination occurred during removal of this compact from the die. The

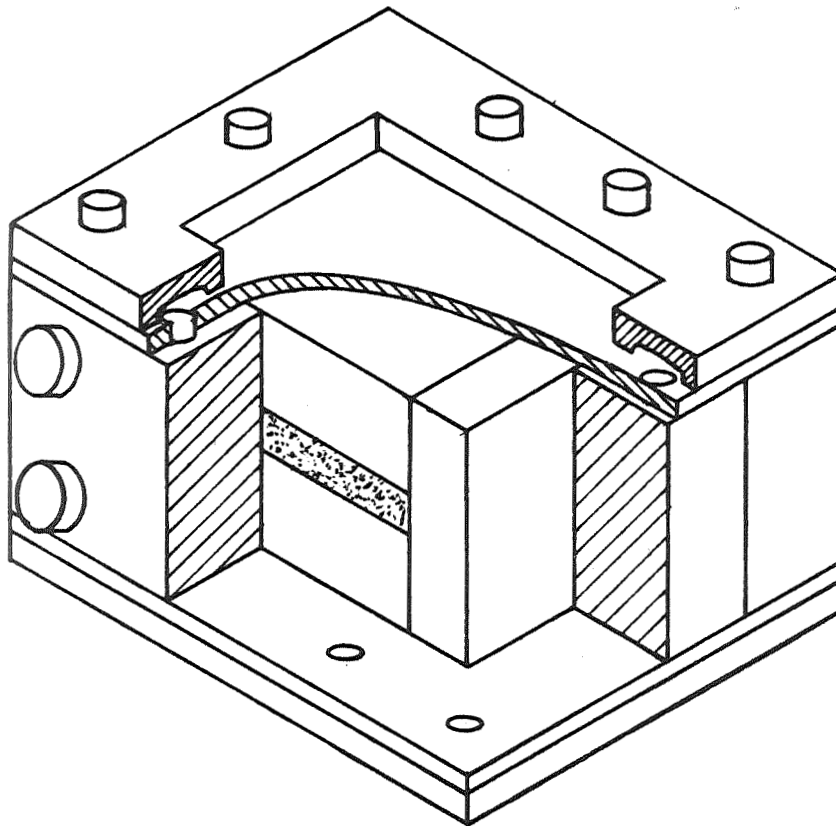


FIGURE 9. DIE FOR HYDROSTATIC PRESSING OF Cr-ThO₂ POWDER

TABLE 3. SUMMARY OF PRE-CONSOLIDATION PARAMETERS

Billet Number	Composition	Powder Weight, g	Hydrostatic Compaction Pressure	
			psi	MN/m ²
10-1	Pure Cr	129.3	30,000	207
10-2	Pure Cr	129.3	50,000	345
11-1	Cr-2.72 Wt % ThO ₂	173.3	50,000	345
12-1	Cr-2.99 Wt % ThO ₂	133.7	50,000	345
13-1	Cr-3.12 Wt % ThO ₂	116.2	50,000	345
13-2	Cr-3.12 Wt % ThO ₂	116.2	50,000	345

remainder of the specimens were compacted at 50,000 psi (345 MN/m²) and successfully extracted from the die and placed in the tantalum cans.

Each tantalum- and tungsten-clad (but not sealed) specimen was then vacuum outgassed at 816°C one hour to remove any traces of CrI₂ which might have remained from the CVD powder-preparation process. Because of the close proximity of the chromium and Cr-ThO₂ compacts to the weldment, it was found that the tantalum cladding could not be sealed by welding. The clad billets were therefore over-clad first with stainless steel and then with mild steel as added protection against leakage during HIP. Both the stainless and mild-steel-clad layers were sealed under a vacuum of approximately 10⁻⁵ torr (1.33 x 10⁻³ N/m²) by electron-beam welding. Each seal was leak checked by pressurizing the specimens to 400 psi (2.8 MN/m²) in helium. No leaks were detected either by submersion in alcohol or by "sniffing" with a helium mass spectrometer leak detector.

All six of the billets were densified at one time by HIP for two hours at 1093°C and 10,000 psi (69 MN/m²) in helium. Removal of the clad layers after HIP was begun by leaching away the mild steel in hot nitric acid. The

stainless steel, tantalum, and tungsten layers were then ground and peeled away from the billets which could now be safely exposed to the air. The surfaces were ground flat and parallel preparatory to surface replication and recladding for rolling.

All of the billets were inspected after grinding by the Zygló technique. Surface and edge cracks were revealed in all of the billets with the exception of the two small pieces cut from Billet No. 11-1. Billets Nos. 10-2 and 13-2 were particularly bad, 10-2 having a network of large cracks, possibly from the decladding operation; and 13-2 having an extensive network of small surface and edge cracks, possibly resulting from the grinding operation. Enough crack-free areas were present in the remaining billets (Nos. 10-1, 12-1, and 13-1) to permit their being sectioned into either one or two smaller specimens which could still be used for rolling experiments. The compositions and sizes of the specimens suitable for rolling are summarized in Table 4. Each of these billets was Zygló-inspected after sectioning and only minimal edge cracking was revealed. Included in Table 4 are the densities achieved after HIP. The ThO_2 -containing alloys all had densities in excess of 98%. However, the pure chromium was only about 90% dense. The reason for this lack of densification is not known.

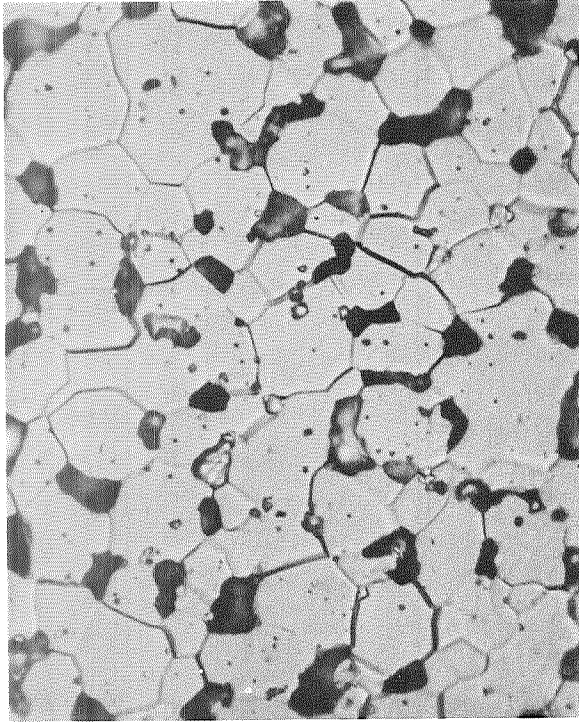
Structure of Hot Isostatically Pressed Alloys

After hot isostatic pressing, small pieces were sectioned from several billets and these were metallographically prepared and examined by optical microscopy and replica electron microscopy. Figures 10 and 11 show the microstructures as observed by optical and replica electron microscopy respectively. In the three ThO_2 -containing alloys it appears that most of the ThO_2 particles are at the grain boundaries, which correspond to the surfaces of the original

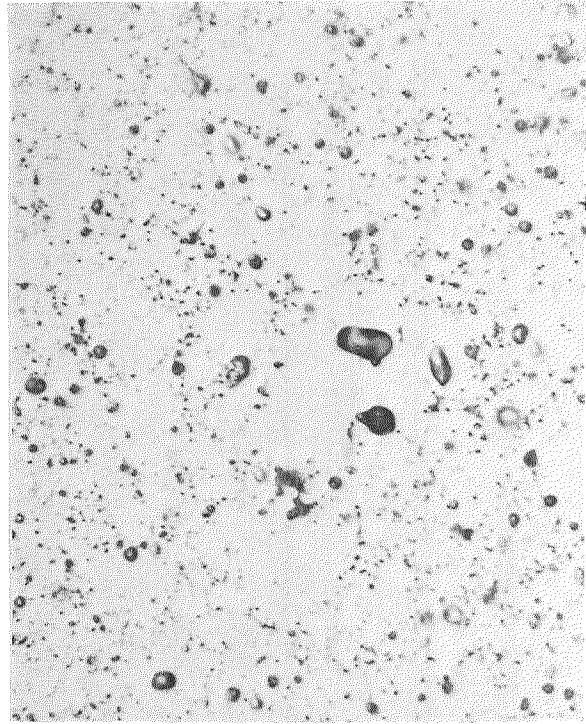
TABLE 4. STARTING DIMENSIONS OF CHROMIUM AND Cr-ThO₂ BILLETS WHICH WERE HOT ROLLED

Billet Number	Composition Wt % ThO ₂	Length,		Width,		Thickness		$\frac{\text{g/cm}^3}{\text{Density (a)}}$ % of Theoretical	
		in.	cm.	in.	cm.	in.	cm.		
10-1a	Pure Cr	1.57	4.00	1.00	2.53	0.20	0.51	6.49	90.2
10-1b	Pure Cr	1.60	4.06	1.05	2.65	0.20	0.51	6.49	90.2
11-1a	Cr-2.72 ThO ₂	1.31	3.33	0.94	2.39	0.19	0.47	7.14	98.7
11-1b	Cr-2.72 ThO ₂	1.40	3.56	1.01	2.57	0.18	0.46	7.14	98.7
12-1a	Cr-2.99 ThO ₂	1.31	3.32	1.09	2.78	0.18	0.46	7.18	98.8
12-1b	Cr-2.99 ThO ₂	1.22	3.11	1.09	2.76	0.18	0.46	7.18	98.8
13-1	Cr-3.12 ThO ₂	1.37	3.47	0.95	2.41	0.15	0.38	7.19	98.9

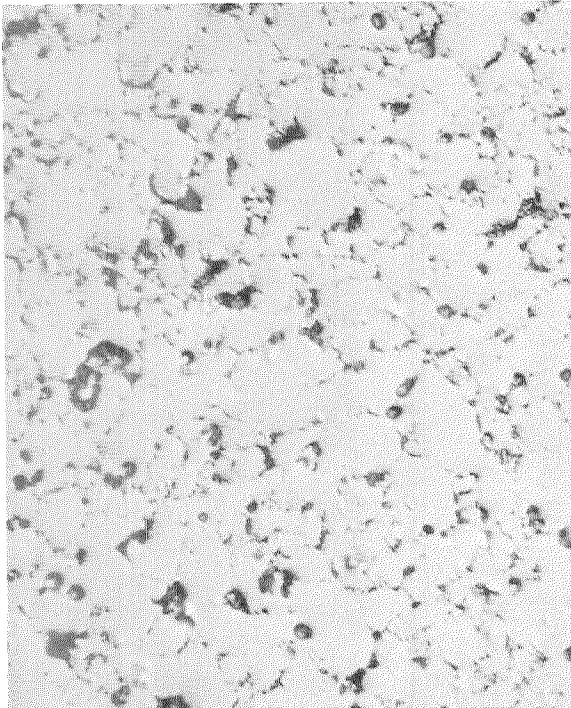
(a) Specimen volume determined by buoyancy in carbon tetrachloride.



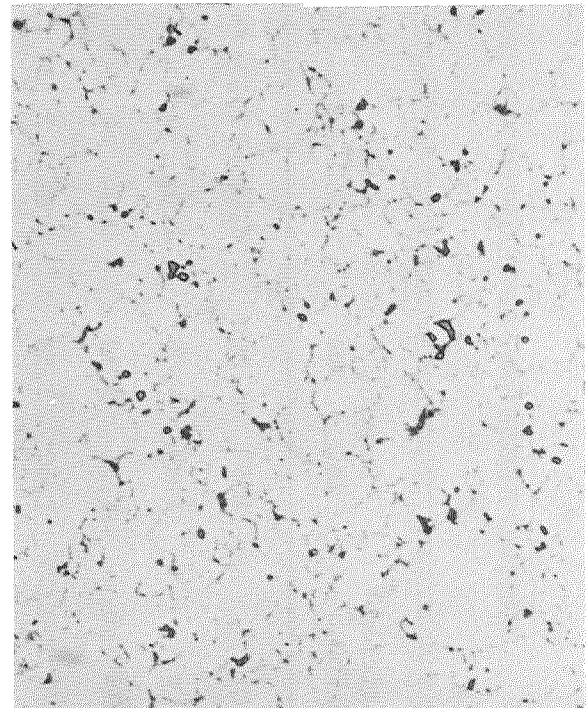
(a) Pure Cr (Billet 10-1a)



(b) Cr-2.72 w/o ThO₂ (Billet 11-1b)

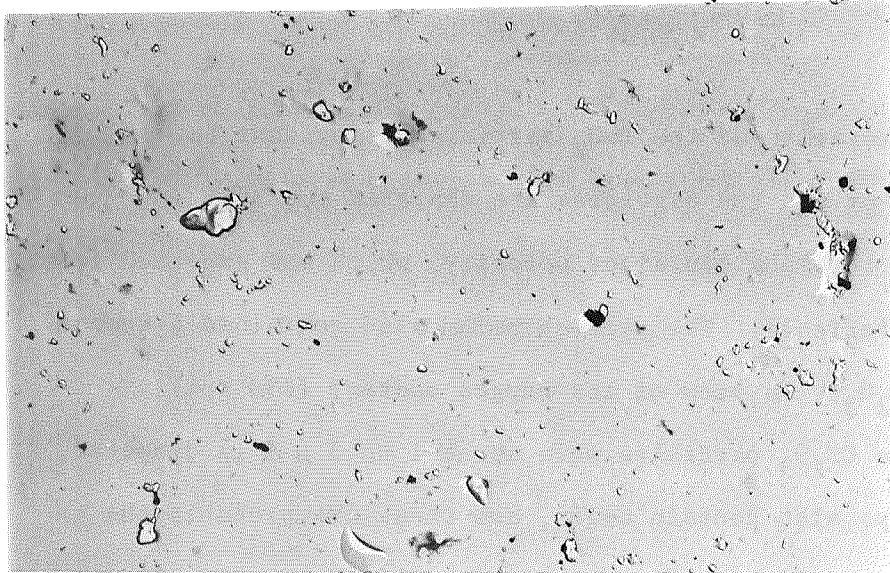


(c) Cr-2.99 w/o ThO₂ (Billet 12-1b)

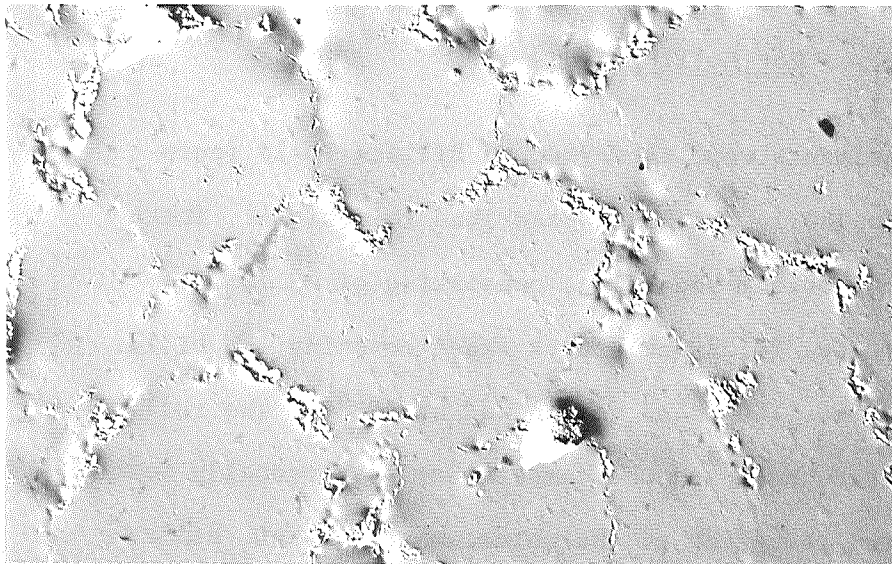


(d) Cr-3.12 w/o ThO₂ (Billet 13-1)

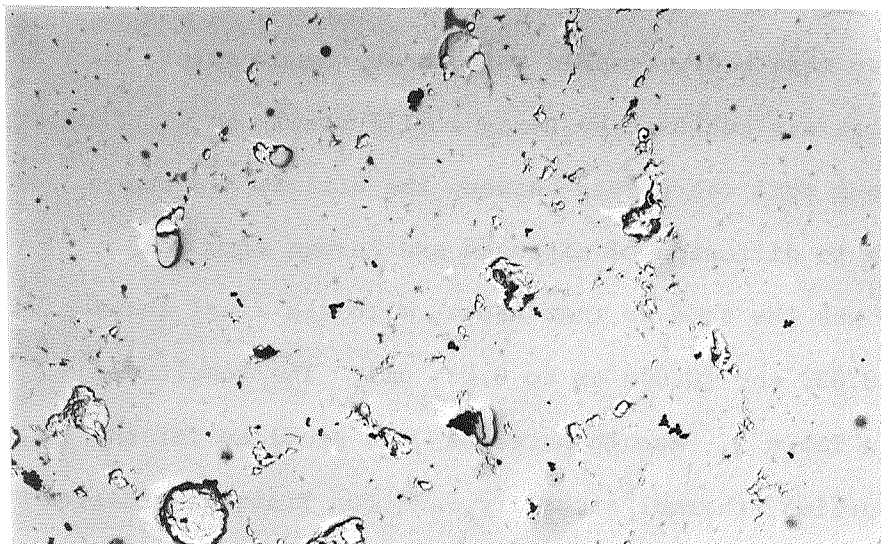
FIGURE 10. OPTICAL MICROGRAPHS OF HOT ISOSTATICALLY PRESSED Cr AND Cr-ThO₂ ALLOYS, ALL 1000 X.



(a) Cr-2.72 w/o ThO₂
(Billet 11-1b)²



(b) Cr-2.99 w/o ThO₂
(Billet 12-1b)²



(c) Cr-3.12 w/o ThO₂
(Billet 13-1)²

FIGURE 11. REPLICA ELECTRON MICROGRAPHS OF HOT ISOSTATICALLY PRESSED Cr-ThO₂ ALLOYS, ALL 4000X.

chromium crystals. Some agglomeration of the ThO_2 particles is evident but it is not possible to say whether or not the particles are sintered together. Figure 10a shows that the pure chromium contained porosity, which was expected from the low density (90.2% of theoretical). The pure chromium also contained a number of particles presumed to be Cr_2O_3 . In view of its oxygen content (830 ppm) this was to be expected. These Cr_2O_3 particles were about 1 to 3 μm in diameter. Each of the three Cr- ThO_2 alloys also contain Cr_2O_3 , and these are probably the larger particles in Figures 10 and 11.

Hot Rolling

Initial rolling experiments were performed on Billets 10-1b (pure chromium) and 11-1a (Cr-2.72 w/o ThO_2), which are described in Table 4. These billets were encapsulated in molybdenum sheathing, consisting of a 1/2 in. (1.27 cm) wide frame with 0.090 in. (0.229 cm) thick sheet covering the billet faces. Hot rolling was started at 1100°C and terminated at 700°C. The rolling reductions were 10% per pass throughout and the temperature was gradually reduced as rolling proceeded. The total reduction of the chromium and Cr- ThO_2 billets was from ~ 0.2 in. (~ 0.51 cm) to 0.055 in. (0.14 cm). When the sheets were decanned it was found that they were badly cracked throughout. Successful rolling of the remaining billets was achieved by using a mild steel can in place of the molybdenum. A molybdenum foil was placed between the billets and the mild steel to act as a barrier to diffusion of nitrogen and carbon from the steel. The rolling procedure was the same as that above, with the final sheet thickness being 0.026 in. to 0.033 in. (0.066 cm to 0.084 cm). The results of the sheet rolling are given in Table 5. Enough material was provided for the evaluation of mechanical properties, thermal stability, and for limited oxidation studies.

TABLE 5. RESULTS OF CHROMIUM AND Cr-ThO₂ SHEET ROLLING

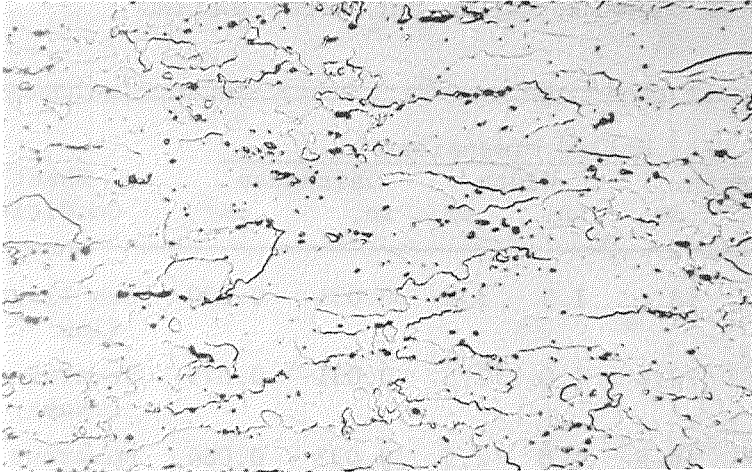
Sheet No.	Alloy	Rolled Dimensions						Sheet Condition
		Length		Width		Thickness		
		in.	cm	in.	cm	in.	cm	
10-1a	Pure Cr	7.3	18.5	1.3	3.3	0.031	0.079	One large flaw
11-1b	Cr-2.72 w/o ThO ₂	8.9	22.6	1.0	2.5	0.031	0.079	Several edge cracks
12-1a	Cr-2.99 w/o ThO ₂	7.3	18.5	1.0	2.5	0.033	0.084	Numerous edge cracks
12-1b	Cr-2.99 w/o ThO ₂	7.9	20.1	1.3	3.3	0.026	0.066	Excellent
13-1	Cr-3.12 w/o ThO ₂	7.3	18.5	1.0	2.5	0.027	0.058	Excellent

RESULTS OF EVALUATION

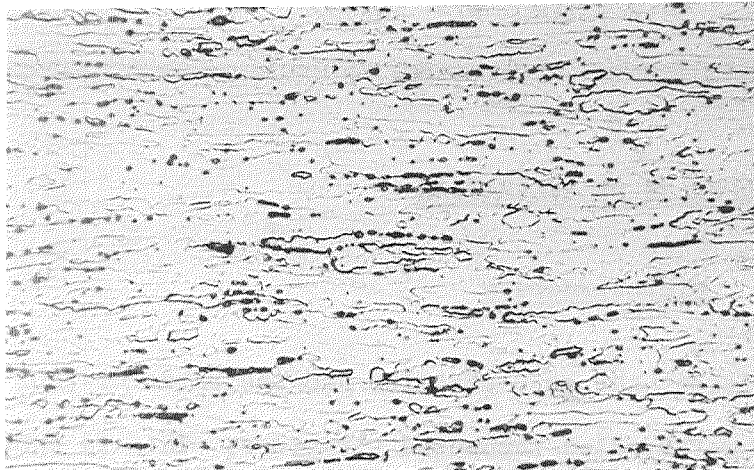
Microstructure

In the as-rolled condition, the pure chromium and the three Cr-ThO₂ alloys had essentially a cold-worked plus recovered structure. This is shown in Figures 12 and 13 (optical microstructures), 14 and 15 (replica electron micrographs), and 16 (transmission electron micrographs). All three as-rolled ThO₂-containing alloys had essentially the same microstructure. The optical micrographs in Figure 12 show the pure chromium structure on the sheet surface, on the longitudinal sheet thickness, and on the transverse sheet thickness; and Figure 13 is a similar series for the Cr-2.72 w/o ThO₂ material. In both cases the grain structure is elongated in the rolling direction, and it appears that the pure chromium grain structure is somewhat coarser than that of the Cr-ThO₂ alloys.

The Cr₂O₃ particles in the pure chromium and the ThO₂ (and Cr₂O₃) particles in the Cr-ThO₂ alloys are strung out in the rolling direction.



(a) Sheet surface, rolling direction is horizontal



(b) Longitudinal sheet thickness (parallel to rolling direction)

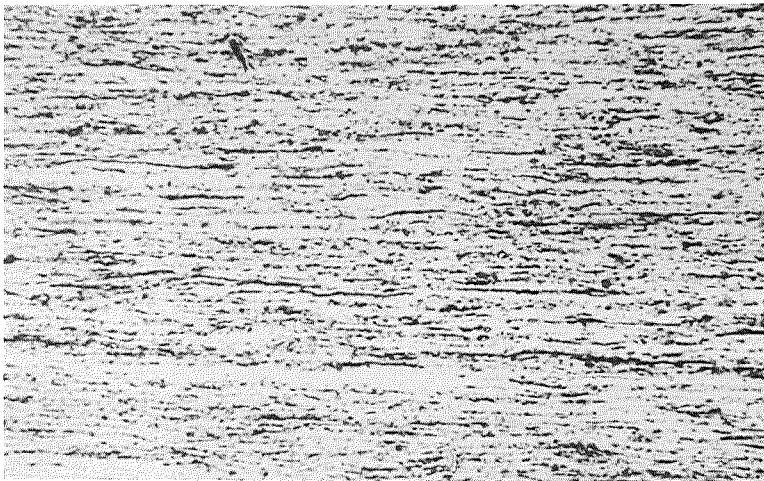


(c) Transverse sheet thickness (normal to rolling direction)

FIGURE 12. OPTICAL MICROGRAPHS OF AS-ROLLED PURE CHROMIUM (SHEET 10-1a); ALL 500 X.



(a) Sheet surface, rolling direction is horizontal



(b) Longitudinal sheet thickness (parallel to rolling direction)

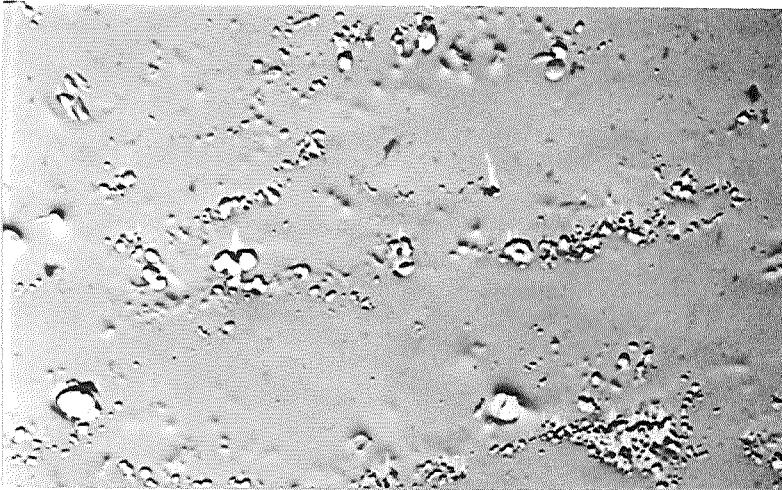


(c) Transverse sheet thickness (normal to rolling direction)

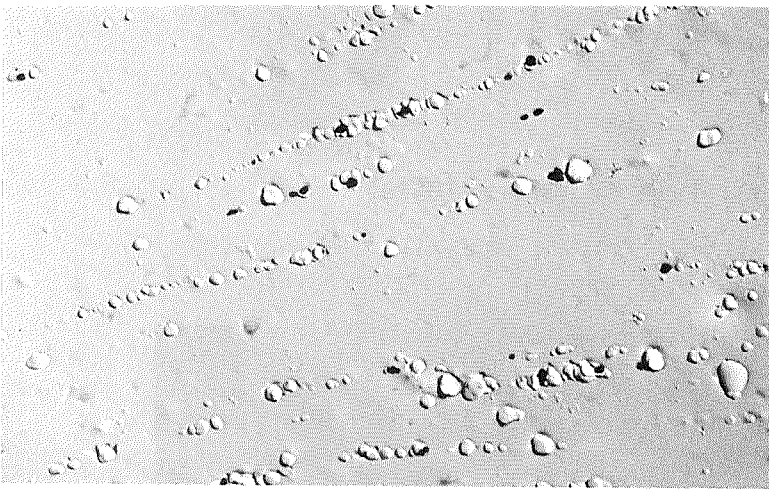
FIGURE 13. OPTICAL MICROGRAPHS OF AS-ROLLED Cr-2.72 w/o Th₂O₃ (SHEET 11-1b); ALL 500 X. THESE ARE TYPICAL OF THE OTHER TWO Cr-Th₂O₃ ALLOYS AS WELL.



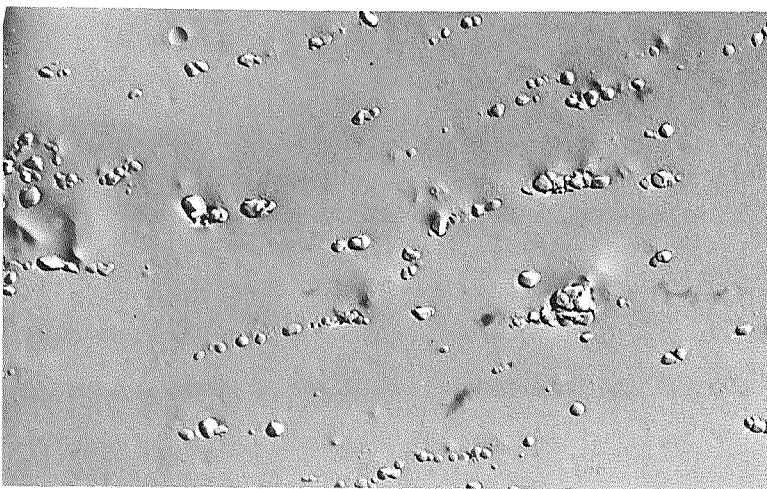
FIGURE 14. REPLICA ELECTRON MICROGRAPH OF AS-ROLLED PURE CHROMIUM (SHEET 10-1a) ON THE SHEET SURFACE, SHOWING Cr_2O_3 PARTICLES, 4000 X.



(a) Sheet surface, rolling direction is nearly horizontal

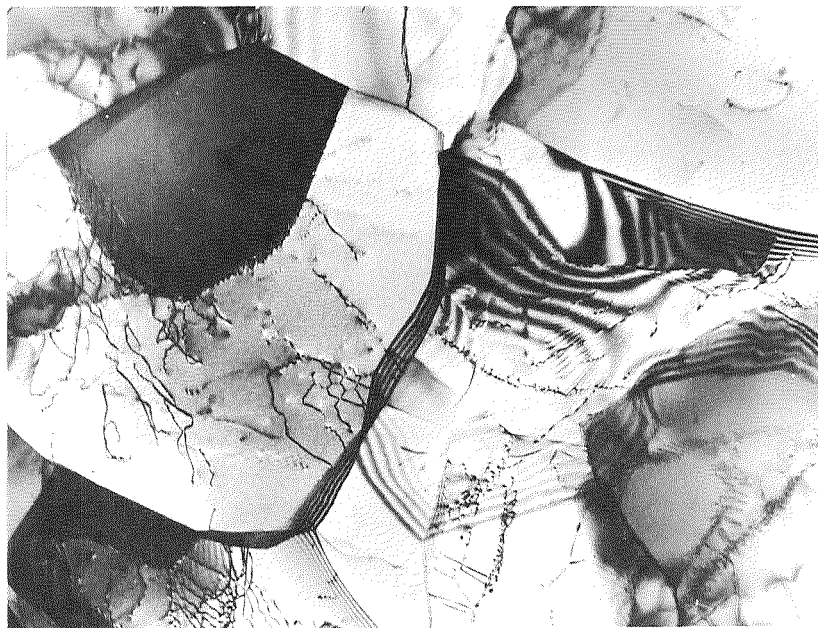


(b) Longitudinal sheet thickness (parallel to rolling direction)

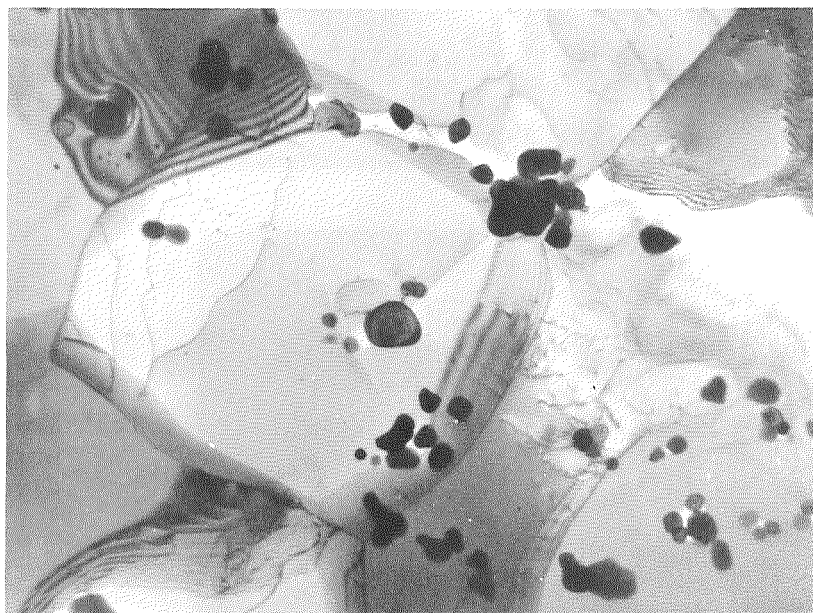


(c) Transverse sheet thickness (normal to rolling direction)

FIGURE 15. REPLICA ELECTRON MICROGRAPHS OF AS-ROLLED Cr-3.12 w/o ThO₂ (SHEET 13-1): ALL 10,000X. THESE ARE TYPICAL OF THE OTHER TWO Cr-ThO₂ ALLOYS AS WELL.

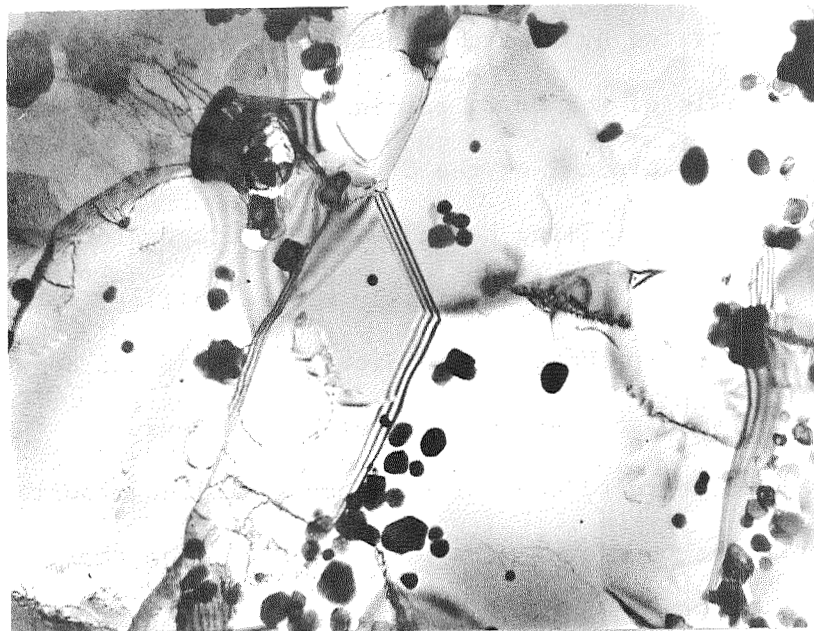


(a) Pure Cr (Sheet 10-1a)



(b) Cr-2.72 w/o ThO₂ (Sheet 11-1b)

FIGURE 16. TRANSMISSION ELECTRON MICROGRAPHS OF AS-ROLLED CHROMIUM AND Cr-ThO₂ ALLOYS, ALL 30,000X.



(c) Cr-2.99 w/o ThO₂ (Sheet 12-1b)



(d) Cr-3.12 w/o ThO₂ (Sheet 13-1)

FIGURE 16. (Continued).

Figure 13a (sheet surface) shows that the particle distribution is not uniform. This is better illustrated by replica electron micrographs in Figure 15. Figure 14 shows details of the Cr_2O_3 particles in pure chromium and Figure 15 illustrates three views typical of the Cr-Th O_2 alloys. The stringing out of particles parallel to the rolling helped make the dispersion more uniform, compared with that of the hot isostatically pressed billets (Figure 15 compared with Figure 11). However, the particle distribution is not as uniform as that in commercial dispersion-strengthened nickel-base alloys.

The substructure of each of the four as-rolled materials is seen in the transmission electron micrographs of Figure 16. The thoriated alloys often had particles at the subgrain boundaries. An interesting feature of Figure 16 is that the subgrain size of the pure chromium is essentially the same as that of the thoriated alloys ($\sim 1.2 \mu\text{m}$). This is somewhat surprising since the optical micrographs in Figures 12 and 13 indicate that the pure chromium is more recovered than the thoriated alloys. Table 6 lists the average subgrain size for each of the four alloys in the as-rolled condition. Also listed here are the subgrain or grain sizes of each alloy after a high temperature anneal (1200°C , 1 hour); these results are discussed later.

Recrystallization and Thermal Stability

It is well known that chromium and chromium alloys generally have a lower DBTT in the as-worked condition than after a high temperature exposure which causes recrystallization. For example, heavily drawn pure chromium wire exhibited some ductility (1-2% elongation) at temperatures as low as -150°C ⁽⁴⁾. However, after complete recrystallization at 950°C , such wire had no measurable ductility at room temperature.

TABLE 6. AVERAGE SUBGRAIN OR GRAIN SIZE OF CHROMIUM AND Cr-ThO₂ ALLOYS^(a)

Alloy	Condition	Subgrain Size, μ m
Pure Cr (Sheet 10-1a)	As-rolled	1.1
Cr-2.72 w/o ThO ₂ (Sheet 11-1b)	"	1.2
Cr-2.99 w/o ThO ₂ (Sheet 12-1b)	"	1.2
Cr-3.12 w/o ThO ₂ (Sheet 13-1)	"	1.2
Pure Cr (Sheet 10-1a)	Annealed 1 hr, 1200°C	33.0 ^(b)
Cr-2.72 w/o ThO ₂ (Sheet 11-1b)	"	2.4
Cr-2.99 w/o ThO ₂ (Sheet 12-1b)	"	2.4
Cr-3.12 w/o ThO ₂ (Sheet 13-1)	"	2.1

(a) In each case the subgrain size is the average of about 50 measurements from transmission electron micrographs.

(b) This is grain size as measured from optical micrographs. No subgrains were evidenced by transmission electron microscopy.

In the present work, the recrystallization behavior of the pure chromium and Cr-ThO₂ alloys was studied. In addition, the stability of ThO₂ particles after prolonged high temperature annealing (100 hours at 1316 and 1427°C) was investigated. The hardness change of as-rolled chromium and Cr-ThO₂ alloys as a function of annealing is given in Table 7, and these results are plotted in Figure 17. The as-rolled hardness of pure chromium was 135 VHN and that of the three Cr-ThO₂ alloys was 156-167 VHN. The higher hardness of the thoriated alloys must be associated with dispersion strengthening, since the substructure size is the same in all four alloys (see Figure 16 and Table 6). One hour anneals at 800-1200°C in purified argon decreased the hardness of pure chromium to 99-90 VHN.

TABLE 7. EFFECT OF ANNEALING ON VICKERS MICROHARDNESS
OF CHROMIUM AND Cr-ThO₂ ALLOYS (a)

Alloy	As- Rolled (b)	1 Hour (c)					100 Hours (c)	
		800°C	900°C	1000°C	1100°C	1200°C	1316°C	1427°C
Pure Cr (Sheet 10-1a)	135	99	94	99	96	90	64	59
Cr-2.72 ThO ₂ (Sheet 11-1b)	157	160	138	124	125	109	101	102
Cr-2.99 ThO ₂ (Sheet 12-1b)	167	149	146	124	115	115	107	100
Cr-3.12 ThO ₂ (Sheet 13-1)	156	136	120	122	124	114	102	98

(a) Annealing was done in purified argon. Hardness was measured on metallographically polished sheet surfaces, 50 g load.

(b) Average of 21 hardness readings.

(c) Average of 3 hardness readings.

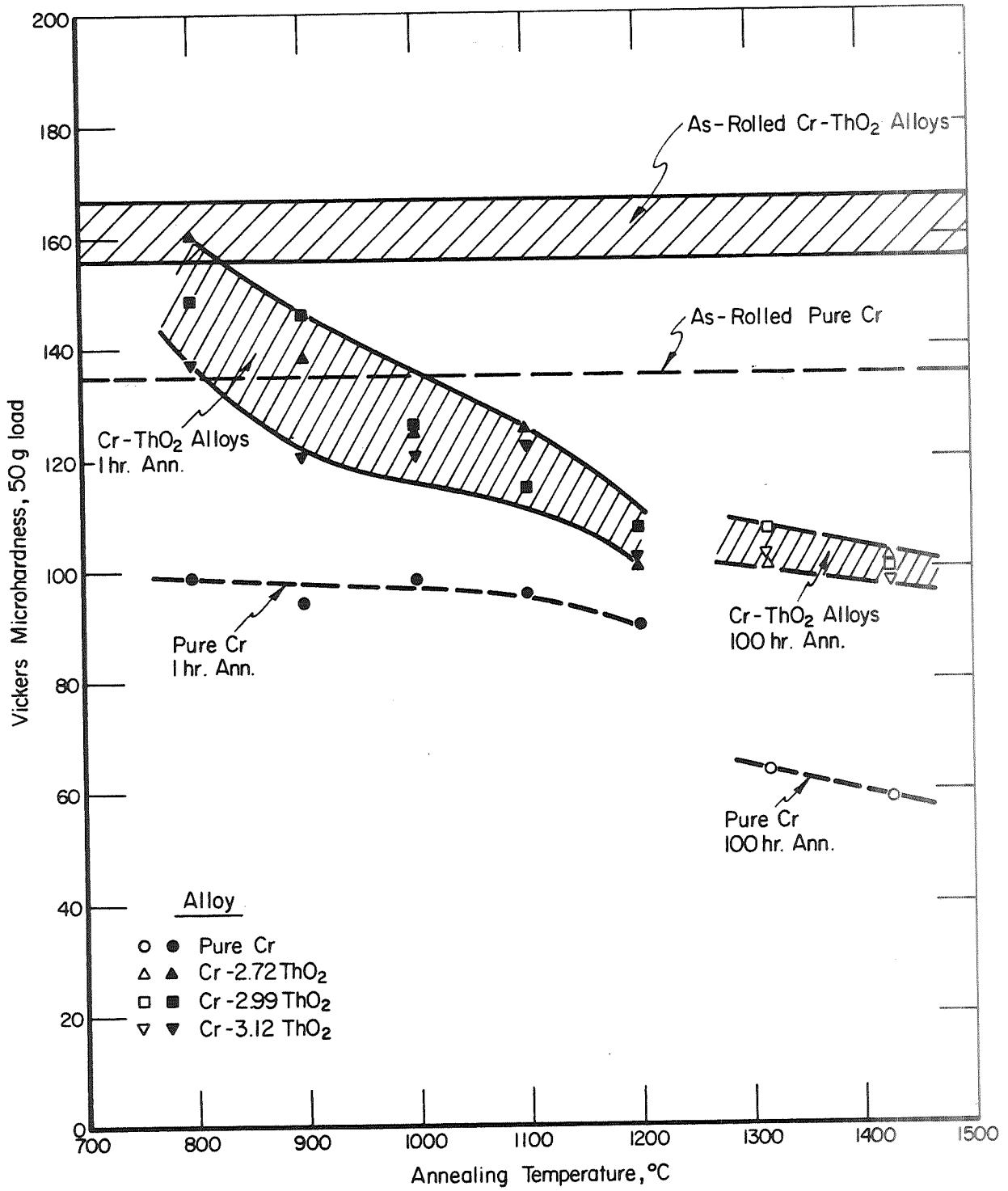


FIGURE 17. EFFECT OF ANNEALING ON ROOM TEMPERATURE HARDNESS OF CHROMIUM AND Cr-ThO₂ ALLOYS

Optical microscopy showed that these annealing treatments were sufficient to completely recrystallize the pure chromium. However, the slightly decreased hardness of the Cr-ThO₂ alloys after one hour at 800°C indicates that in this case recovery was only beginning. After one hour at 1200°C the hardness of the Cr-ThO₂ alloys decreased to 109-115 VHN. Prolonged exposure for 100 hours at 1316°C and 1427°C further decreased the hardness of the chromium too (to 59-64 VHN), but caused only a slight additional decrease in hardness of the thoriated alloys.

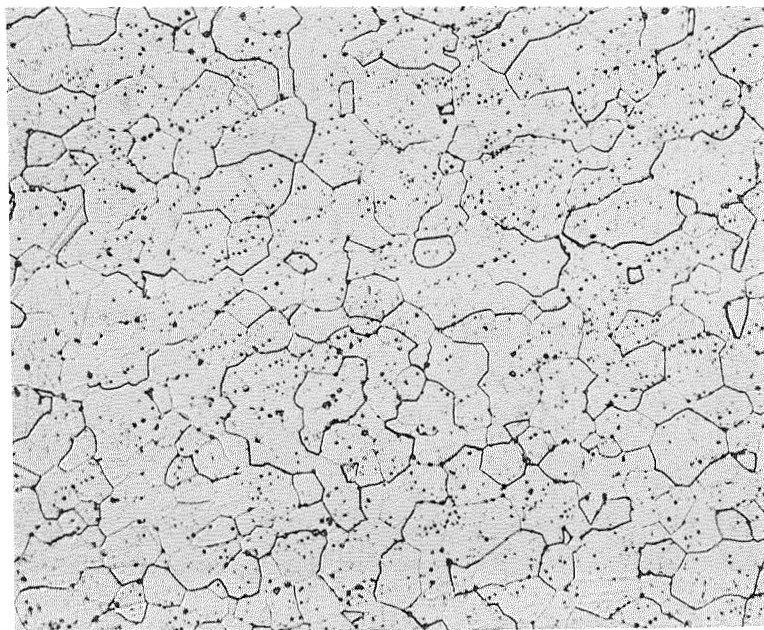
It was decided that a standard anneal of one hour at 1200°C in purified argon would be given specimens from each material for subsequent mechanical property determinations. The microstructures resulting from this treatment are shown in Figures 18-20:

Figure 18, Optical micrographs of pure chromium

Figure 19, Optical micrographs of Cr-2.99 w/o ThO₂

Figure 20, Transmission electron micrographs of all four materials.

The optical micrographs of pure chromium in Figure 18 reveal that complete recrystallization occurred, with a resulting equiaxed grain size of 33 μm (Table 6). Very little dislocation substructure was present as shown in the transmission electron micrograph in Figure 20a. However, the thoriated alloys did not recrystallize after the one hour anneal at 1200°C, as seen in Figure 19. The structure coarsened somewhat compared with the as-rolled microstructure (compare Figures 13 and 19). The transmission electron micrographs in Figure 20b, c, and d indicate that the annealing caused additional recovery of the thoriated alloys (compare with Figure 16), and the subgrain size increased to 2.1 to 2.4 μm. Figures 20c and d show several examples where boundaries are being held up by ThO₂ particles. A comparison of Figures 20 and 16 indicates that the one hour anneal at 1200°C did not measurably coarsen the ThO₂ particles. The three annealed thoriated alloys generally had very few dislocations within the



(a) Sheet surface, rolling direction is horizontal

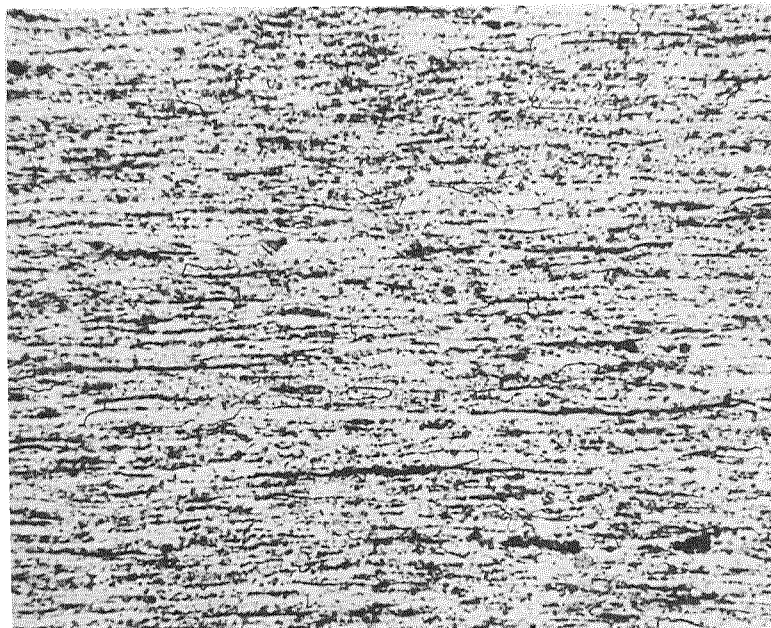


(b) Longitudinal sheet thickness, rolling direction is horizontal

FIGURE 18. OPTICAL MICROGRAPHS OF PURE CHROMIUM (SHEET 10-1a) AFTER ANNEALING FOR ONE HOUR AT 1200°C, 200 X.



(a) Sheet surface, rolling direction is horizontal

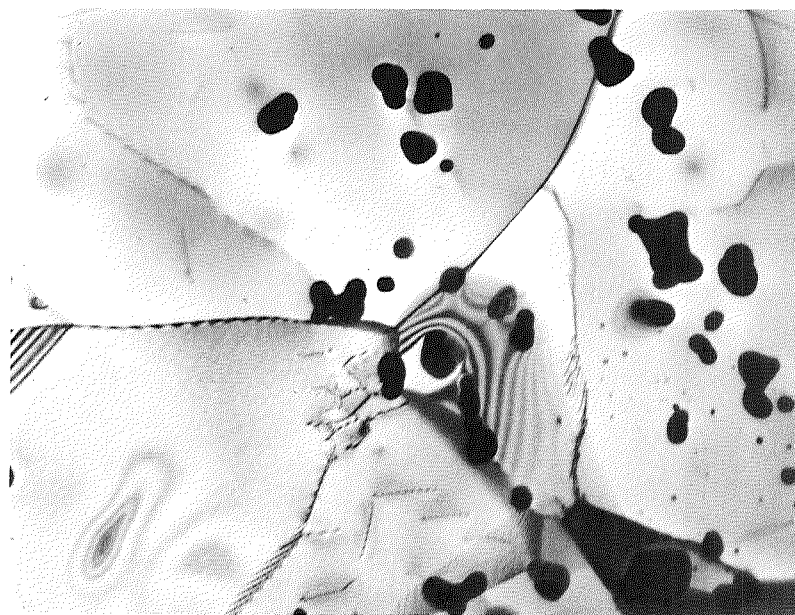


(b) Longitudinal sheet thickness, rolling direction is horizontal

FIGURE 19. OPTICAL MICROGRAPHS OF Cr-2.99 w/o ThO₂ (SHEET 12-1b) AFTER ANNEALING FOR ONE HOUR AT 1200°C, 500X. THE OTHER TWO THORIATED ALLOYS HAD SIMILAR STRUCTURES.

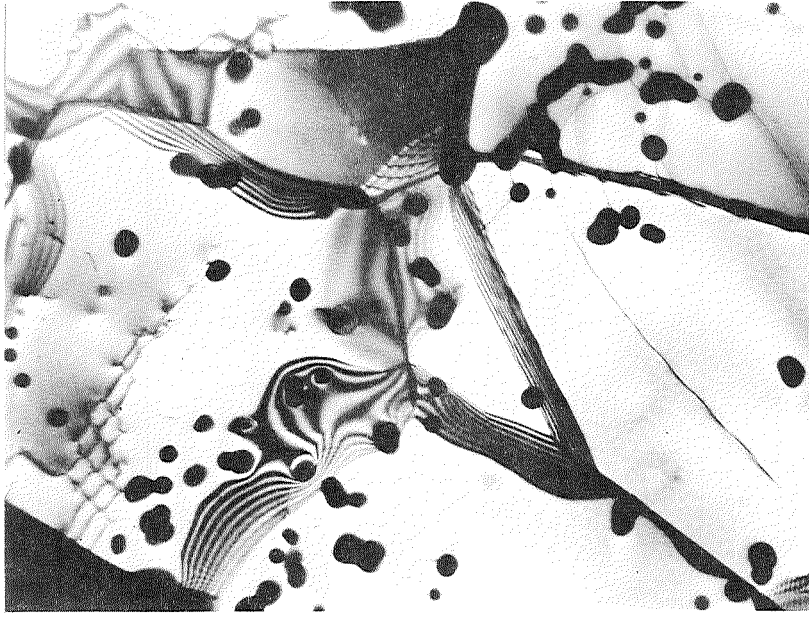


(a) Pure Chromium (Sheet 10-1a)

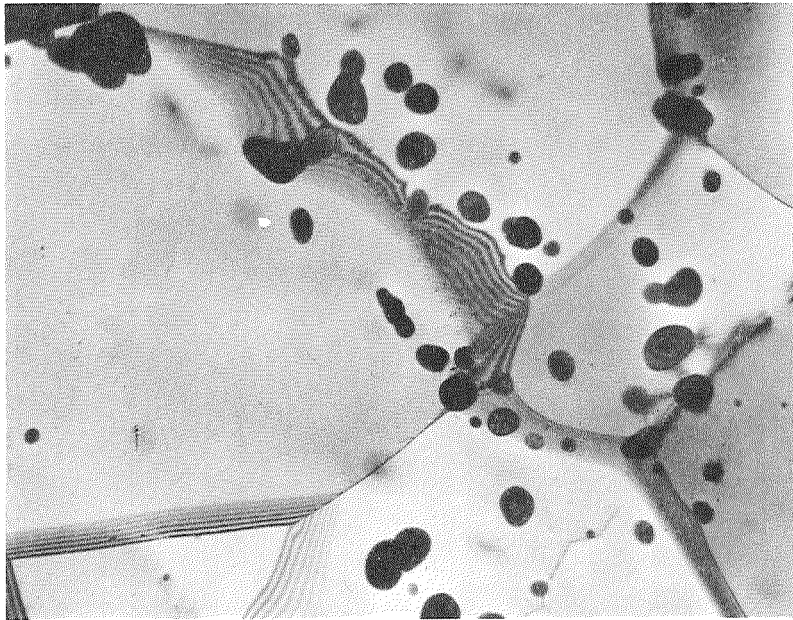


(b) Cr-2.72 w/o ThO₂ (Sheet 11-1b)

FIGURE 20. TRANSMISSION ELECTRON MICROGRAPHS OF CHROMIUM AND Cr-ThO₂ ALLOYS AFTER ANNEALING ONE HOUR AT 1200°C, ALL 30,000 X.



(c) Cr-2.99 w/o ThO_2 (Sheet 12-1b)



(d) Cr-3.12 w/o ThO_2 (Sheet 13-1)

FIGURE 20. Continued.

subboundaries. Figure 21 shows one example where individual dislocations were observed in a region away from boundaries. Here it is evident that the ThO_2 particles have strongly pinned the dislocations.

Prolonged annealing for 100 hours at 1316°C and 1427°C coarsened the equiaxed grain size of the pure chromium to $\sim 90 \mu\text{m}$ for both temperatures. However, the same treatments did not produce an equiaxed recrystallized grain structure in the three thoriated alloys. Instead, an elongated grain structure resulted, which is reminiscent of recrystallized doped tungsten and recrystallized TD Nickel and TD Nickel-Chromium. This is illustrated in Figure 22, for the Cr-2.72 w/o ThO_2 (Sheet 11-1b) alloy annealed for 100 hours at 1427°C . The replica electron micrograph in Figure 23a shows ThO_2 particles of the Cr-3.12 w/o ThO_2 alloy (Sheet 13-1) after the specimen had been annealed for 100 hours at 1427°C . Comparison of this micrograph with the same material in the as-rolled condition (Figure 23b) indicates that the long-time high-temperature anneal did

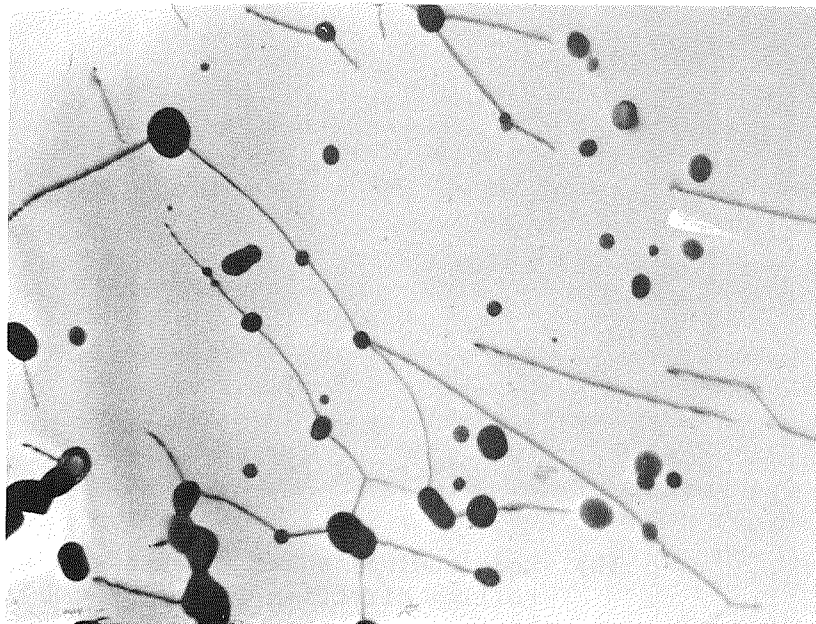


FIGURE 21. Cr-3.12 w/o ThO_2 ANNEALED ONE HOUR AT 1200°C , SHOWING DISLOCATIONS PINNED BY ThO_2 PARTICLES, 30,000X.

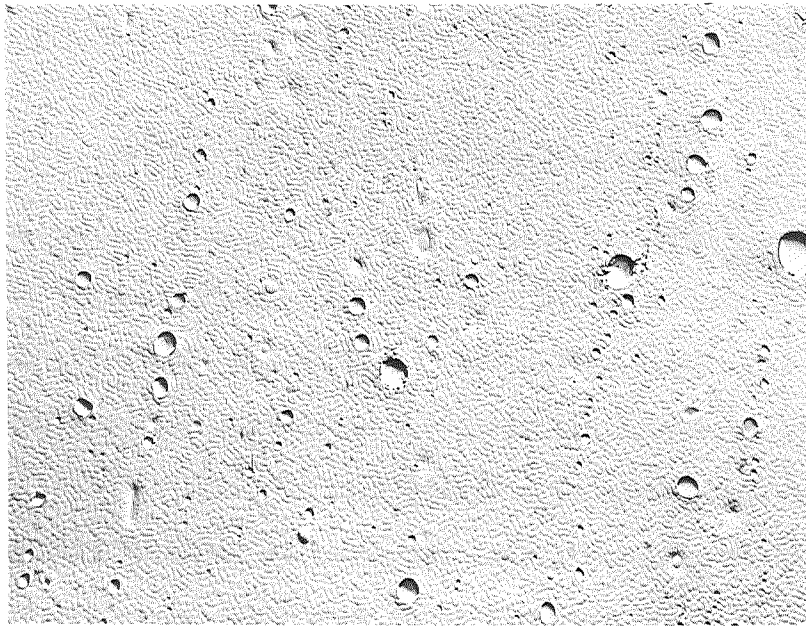


(a) Sheet surface, rolling direction is horizontal

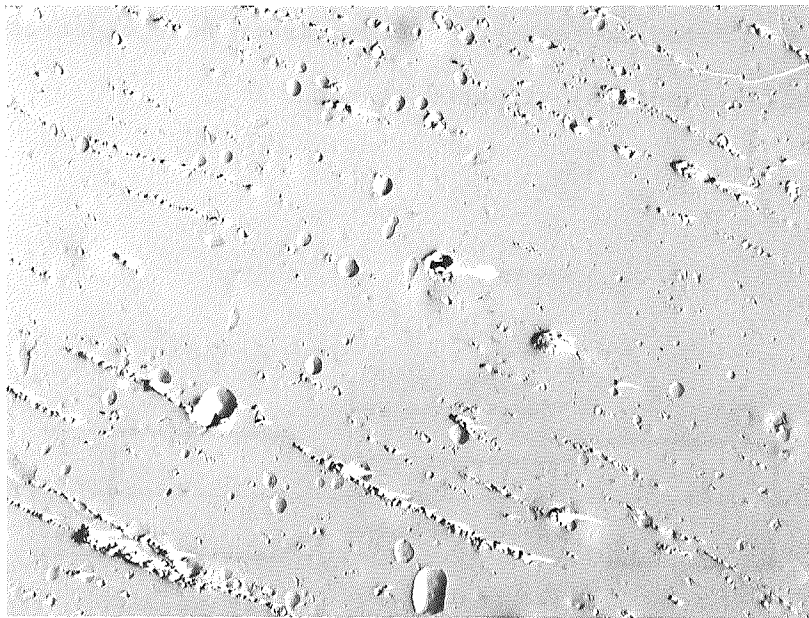


(b) Longitudinal sheet thickness, rolling direction is horizontal

FIGURE 22. OPTICAL MICROGRAPHS Cr-2.72 w/o ThO₂ (SHEET 11-1b) AFTER ANNEALING 100 HOURS AT 1427°C, 200X.



(a) Annealed 100 hours, 1427°C



(b) As-rolled

FIGURE 23. REPLICA ELECTRON MICROGRAPHS OF Cr-3.12 w/o ThO₂ (SHEET 13-1) TAKEN ON THE LONGITUDINAL SHEET THICKNESS SURFACE, 4000X.

not significantly coarsen the particles. It is probable that the larger particles in both micrographs are Cr_2O_3 .

Ductile-to-Brittle Transition (DBTT)

The tensile DBTT was determined for the pure chromium and the three thoriated alloys in the as-rolled condition and after annealing for one hour at 1200°C . Tensile specimens, having the dimensions in Figure 24, were cut from the various sheets by electrical discharge machining. All specimens were tested in an Instron Testing Machine at a strain rate of $1.7 \times 10^{-4} \text{ sec}^{-1}$. The specimens were clamped in split serrated grips. In order to minimize stress concentrations in the shoulders due to the serrated edges, thin foils of copper were cemented with Sauereisen to the specimen shoulders. This allowed tight clamping of the specimens without damage to the shoulders, and in subsequent testing all specimens failed in the gage length. Prior to testing, all specimens were electropolished in 90% glacial acetic acid--10% perchloric acid at about 0°C .

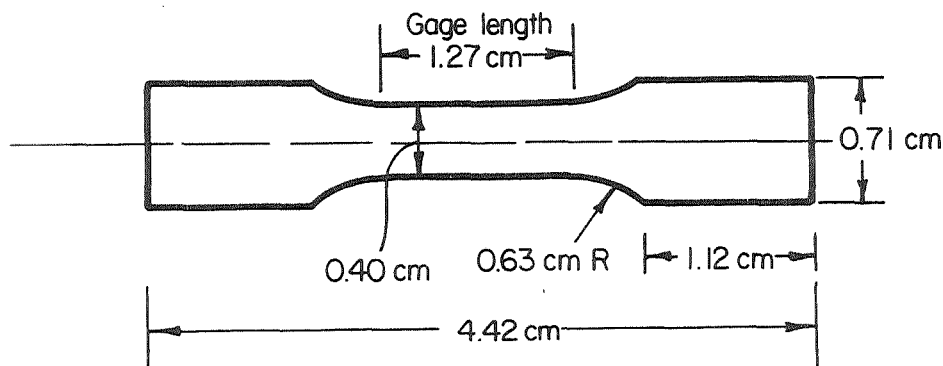


FIGURE 24. DESIGN OF CHROMIUM AND Cr-ThO_2 TENSILE SPECIMENS.

The mechanical property results for the four materials in the as-rolled condition are listed in Table 8. Plots of pertinent ductility and strength values as a function of test temperature are shown in Figures 25-27. Similarly, Table 9 presents results for the alloys tested after annealing one hour at 1200°C, and Figures 28-30 illustrate corresponding plots of ductility and strength versus test temperature.

The ductility versus test temperature plots in Figure 25 show that in the as-rolled condition the Cr-ThO₂ alloys are considerably more ductile than pure chromium. The DBTT values from both elongation and reduction in area results are 15°C for the Cr-ThO₂ alloys and 140°C for pure chromium. These values represent the temperature corresponding to the point where the plots were extrapolated to 0% ductility. The temperatures corresponding to a ductility of 5% elongation are 20°C and 175°C for Cr-ThO₂ alloys and pure chromium, respectively. At temperatures above the DBTT, the total elongations ranged from 6.9 to 10.8% for the Cr-ThO₂ alloys and 7.4 to 7.9% for the pure chromium. However, corresponding reduction-in-area values were much higher, ranging from 14.6 to 26.9% for the Cr-ThO₂ materials and 21.6 to 22.8% for pure chromium.

The true fracture stress, σ_f (load at fracture divided by cross-sectional area at fracture), is plotted in Figure 26a as a function of test temperature. As is typical with many BCC metals, the true fracture stress at the DBTT is high when the materials are ductile and lower when brittle. However, there is a strong temperature dependence of both the ductile and brittle fracture stress, σ_f decreasing with increasing temperature in both cases. The brittle fracture stress plot for the Cr-ThO₂ alloys merges with the plot for pure chromium. Similarly, when extrapolated to higher temperatures, the ductile fracture stress of the Cr-ThO₂ alloys would merge with that of pure Cr. Thus at a given temperature, there appears to be very little difference between σ_f (brittle or ductile) for Cr-ThO₂ and pure chromium. Yet the tensile DBTT values differ by 125°C.

TABLE 8. MECHANICAL PROPERTIES OF AS-ROLLED CHROMIUM AND Cr-ThO₂ ALLOYS

Alloy	Test T, °C	Prop. Lim.		0.2% Y.S.		UTS		True Fracture Stress		Unif. Elong. %	Total Elong. %	Red. in Area %
		10 ³ psi	MN/m ²	10 ³ psi	MN/m ²	10 ³ psi	MN/m ²	10 ³ psi	MN/m ²			
Pure Cr	25	68.3	472	81.5	562	86.0	593	86.0	593	0.5	0.5	~ 0.2
"	75	--	--	--	--	78.9	544	78.9	544	0	0	0
"	146	68.3 (a)	472 (a)	77.4 (b)	533 (b)	78.1	538	79.5	548	1.0	1.0	1.8
"	195	76.5 (a)	527 (a)	75.3 (b)	520 (b)	78.5	541	87.0	600	4.6	7.4	22.8
"	242	75.7 (a)	523 (a)	73.7 (b)	507 (b)	76.5	527	85.5	588	4.5	7.9	21.6
Cr-2.72 w/o ThO ₂	- 26	101.5	700	111.0	765	113.0	779	113.0	779	0.9	0.9	~ 0.2
"	25	77.0	531	86.2	595	101.0	696	123.0	849	5.5	9.2	24.0
"	98	75.0	517	83.5	576	91.7	633	103.5	714	5.3	7.7	16.8
"	142	77.0	531	87.0	600	88.4	609	98.9	682	5.0	7.5	18.4
"	194	75.5	521	84.3	581	85.5	588	98.5	679	4.0	8.3	20.4
Cr-2.99 w/o ThO ₂	- 75	--	--	--	--	94.8	654	94.8	655	0	0	0
"	3	--	--	--	--	89.0	613	89.0	613	0	0	0
"	25	76.5	527	87.0	600	104.0	717	114.0	787	7.4	10.8	17.0
"	105	75.7	523	86.8	599	95.9	661	113.5	783	6.5	10.5	23.5
Cr-3.12 w/o ThO ₂	- 57	--	--	--	--	130.0	896	130.0	896	0	0	0
"	25	72.5	500	87.7	605	106.0	732	135.5	934	6.9	6.9	15.9
"	62	72.2	497	81.6	563	94.9	654	111.0	765	7.3	7.3	14.6
"	82	75.5	521	87.7	605	99.1	683	118.0	813	5.8	9.4	26.9

(a) Upper yield point.

(b) Lower yield point.

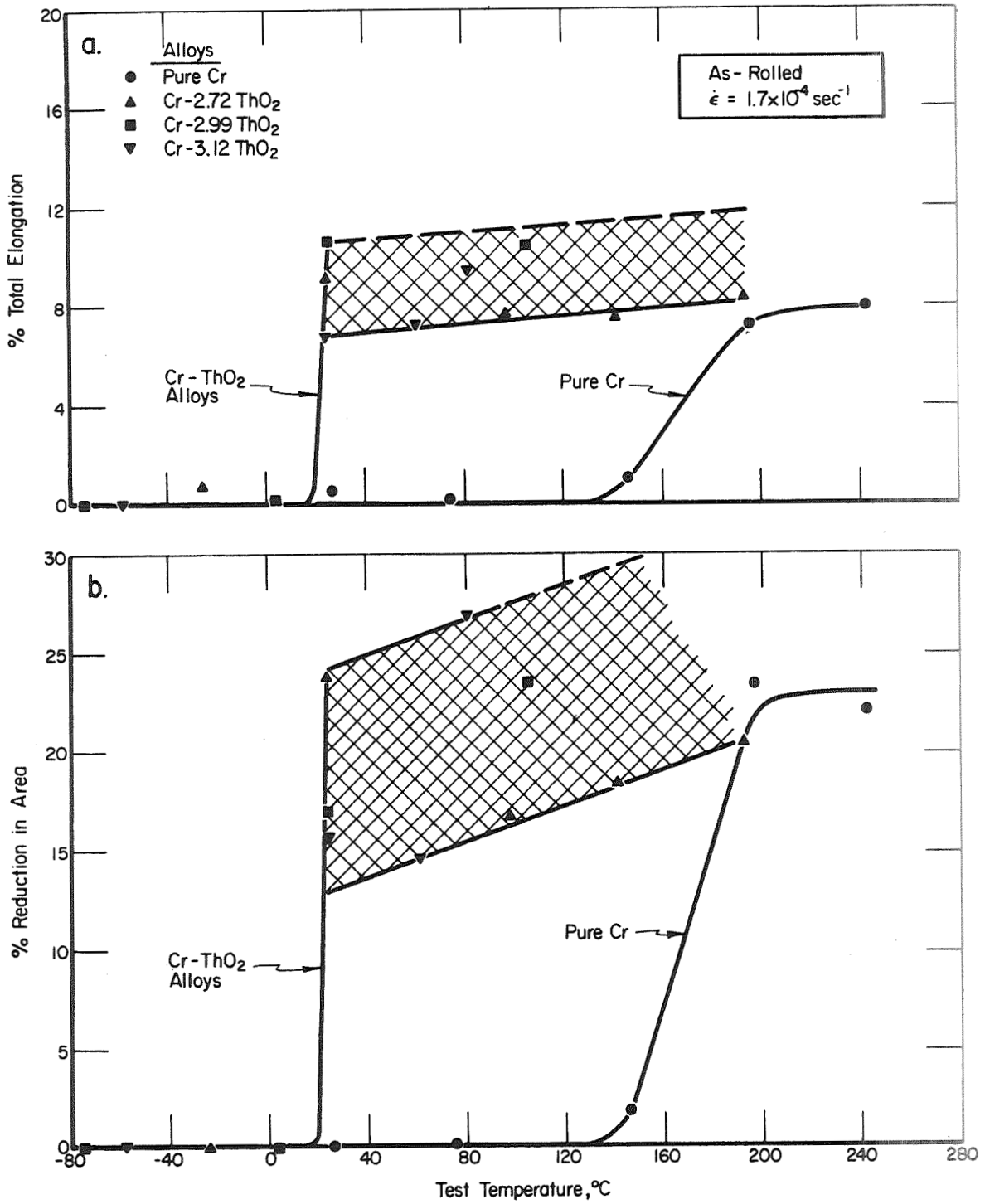


FIGURE 25. TENSILE DUCTILE-TO-BRITTLE TRANSITION OF AS-ROLLED CHROMIUM AND Cr-ThO₂ ALLOYS

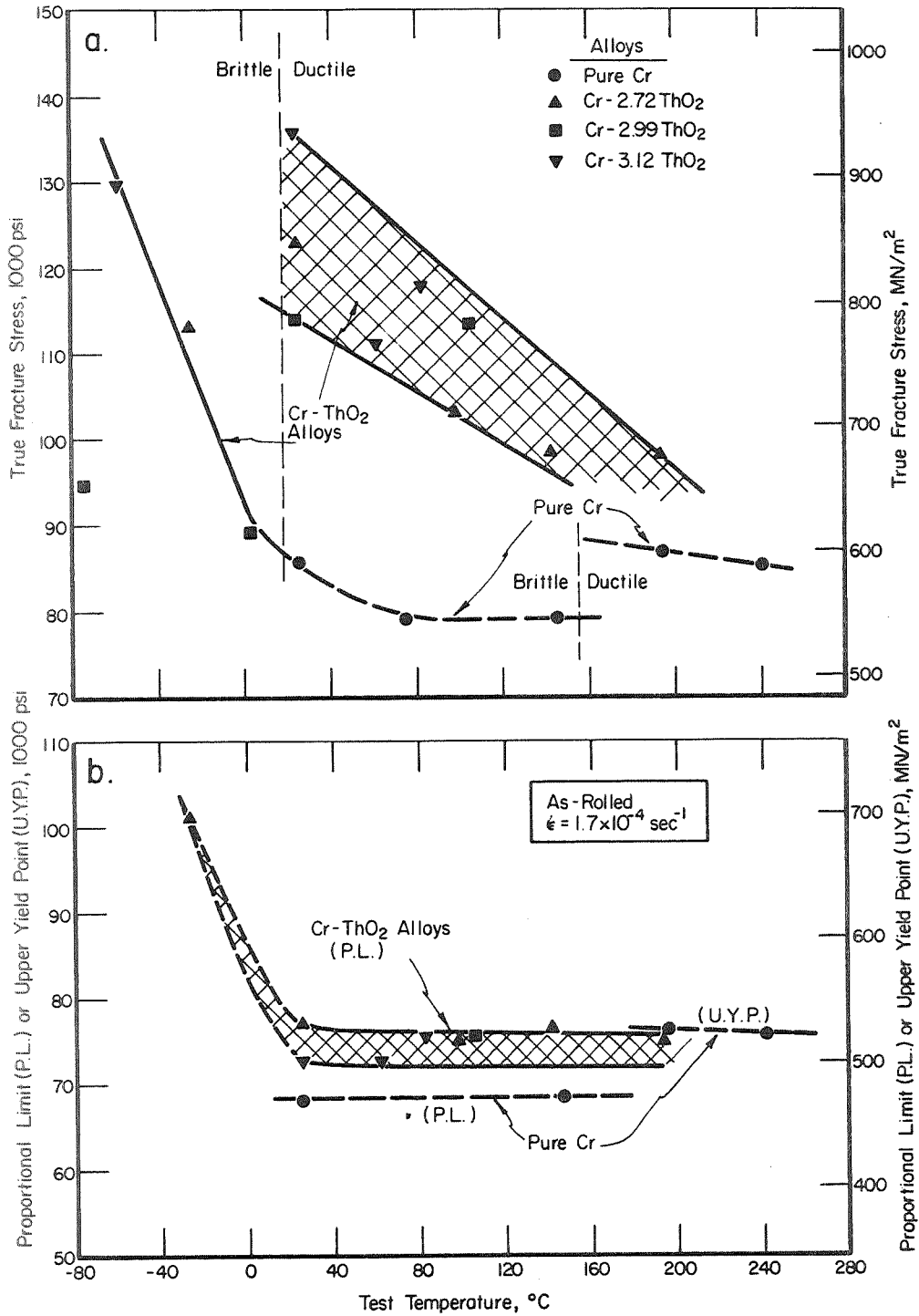


FIGURE 26. TENSILE PROPORTIONAL LIMIT, UPPER YIELD STRENGTH AND TRUE FRACTURE STRESS OF AS-ROLLED CHROMIUM AND Cr-ThO₂ ALLOYS AS A FUNCTION OF TEST TEMPERATURE.

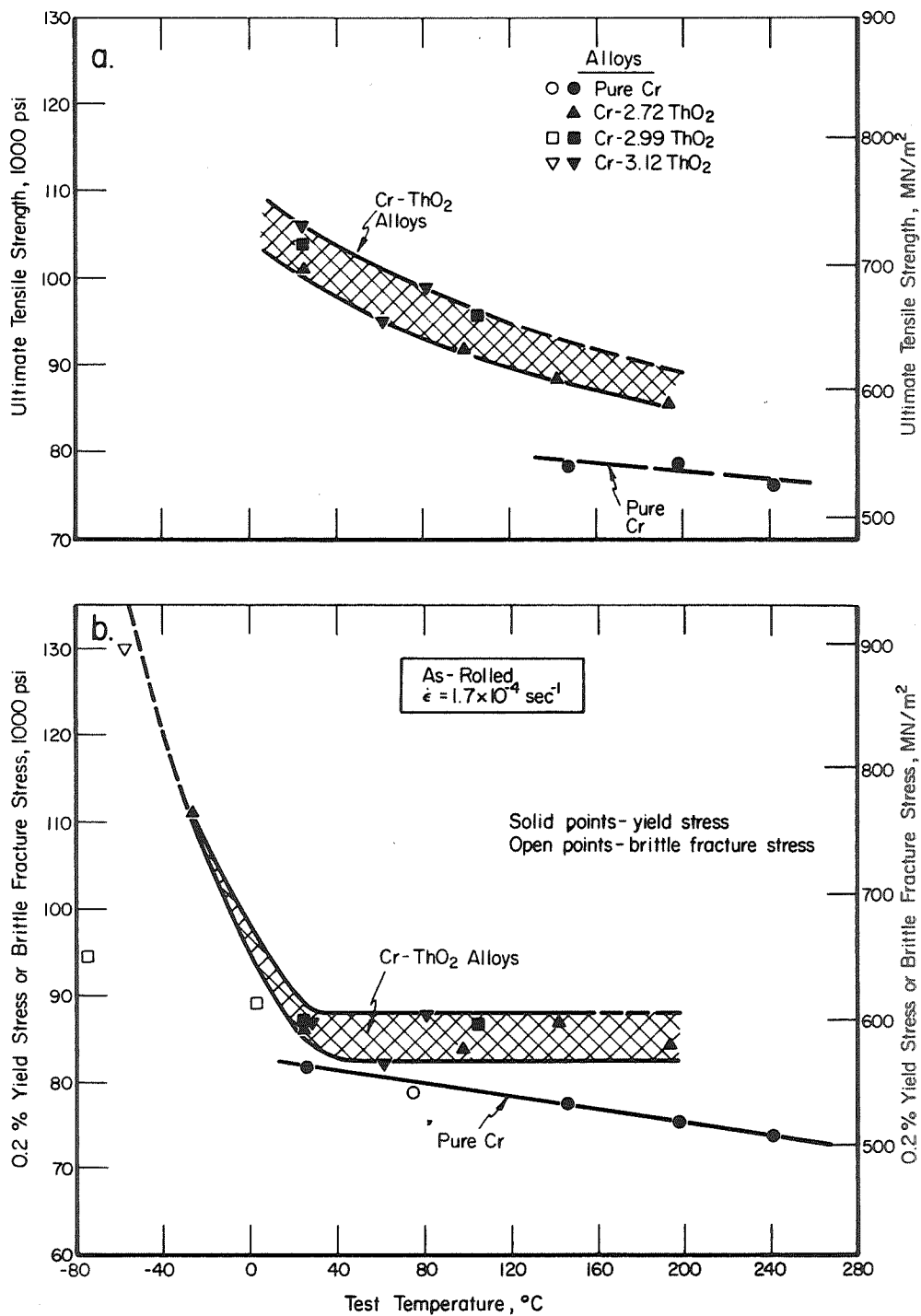


FIGURE 27. TENSILE YIELD STRESS, BRITTLE FRACTURE STRESS AND ULTIMATE TENSILE STRENGTH OF AS-ROLLED CHROMIUM AND Cr-ThO₂ ALLOYS AS A FUNCTION OF TEST TEMPERATURE

TABLE 9. MECHANICAL PROPERTIES OF CHROMIUM AND Cr-ThO₂ ALLOYS AFTER ANNEALING
1 HOUR AT 1200°C

Alloy	Test T, °C	Prop. Lim.		0.2% Y.S.		UTS		True Fracture Stress		Unif. Elong. %	Total Elong. %	Red. in Area %
		10 ³ psi	MN/m ²	10 ³ psi	MN/m ²	10 ³ psi	MN/m ²	10 ³ psi	MN/m ²			
Pure Cr	58	--	--	--	--	38.5	265	38.5	265	0	0	0
"	80	--	--	--	--	37.0	255	37.0	255	0	0	0
"	135	26.4	182	28.7	198	36.4	251	36.4	251	0.6	0.6	~0.2
"	152	24.4 (a)	167 (a)	24.4 (b)	169 (b)	42.3	292	47.3	326	19.7	20.3	17.2
"	200	16.1 (a)	111 (a)	15.2 (b)	105 (b)	39.1	269	63.3	437	38.2	43.0	48.9
Cr-2.72 w/o ThO ₂	35	--	--	--	--	51.2	352	51.2	352	0	0	0
"	45	--	--	--	--	42.0	289	42.0	289	0	0	0
"	161	36.0	249	39.6	273	54.5	375	74.3	513	24.5	30.4	35.1
"	197	28.0	193	39.8	275	51.0	351	76.0	524	25.1	30.1	42.4
Cr-2.99 w/o ThO ₂	- 10	61.5	425	--	--	65.3	451	65.3	451	0.1	0.1	~0
"	55	44.5	307	47.3	327	59.4	408	60.8	420	6.0	6.0	2.3
"	75	44.0	304	44.0	304	63.2	435	82.3	567	16.0	19.6	27.2
"	100	47.8	331	47.8	331	62.7	433	78.0	538	21.0	25.9	29.3
Cr-3.12 w/o ThO ₂	25	--	--	--	--	48.5	334	48.5	334	0	0	0
"	145	29.5	204	34.2	236	53.5	369	74.7	515	26.3	31.5	35.1

(a) Upper yield point.

(b) Lower yield point.

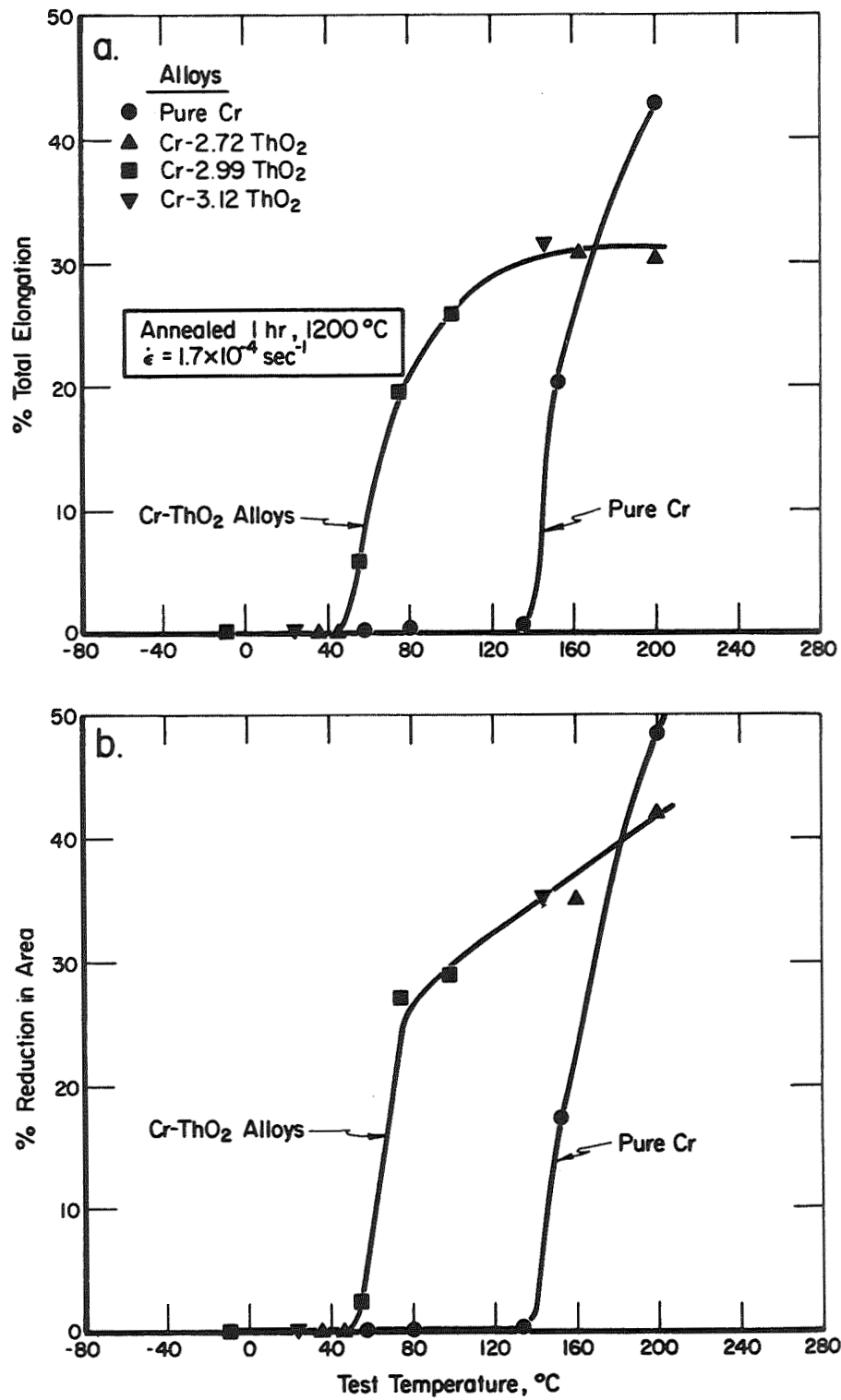


FIGURE 28. TENSILE DUCTILE-TO-BRITTLE TRANSITION OF ANNEALED (1 HR, 1200°C) CHROMIUM AND Cr-ThO₂ ALLOYS

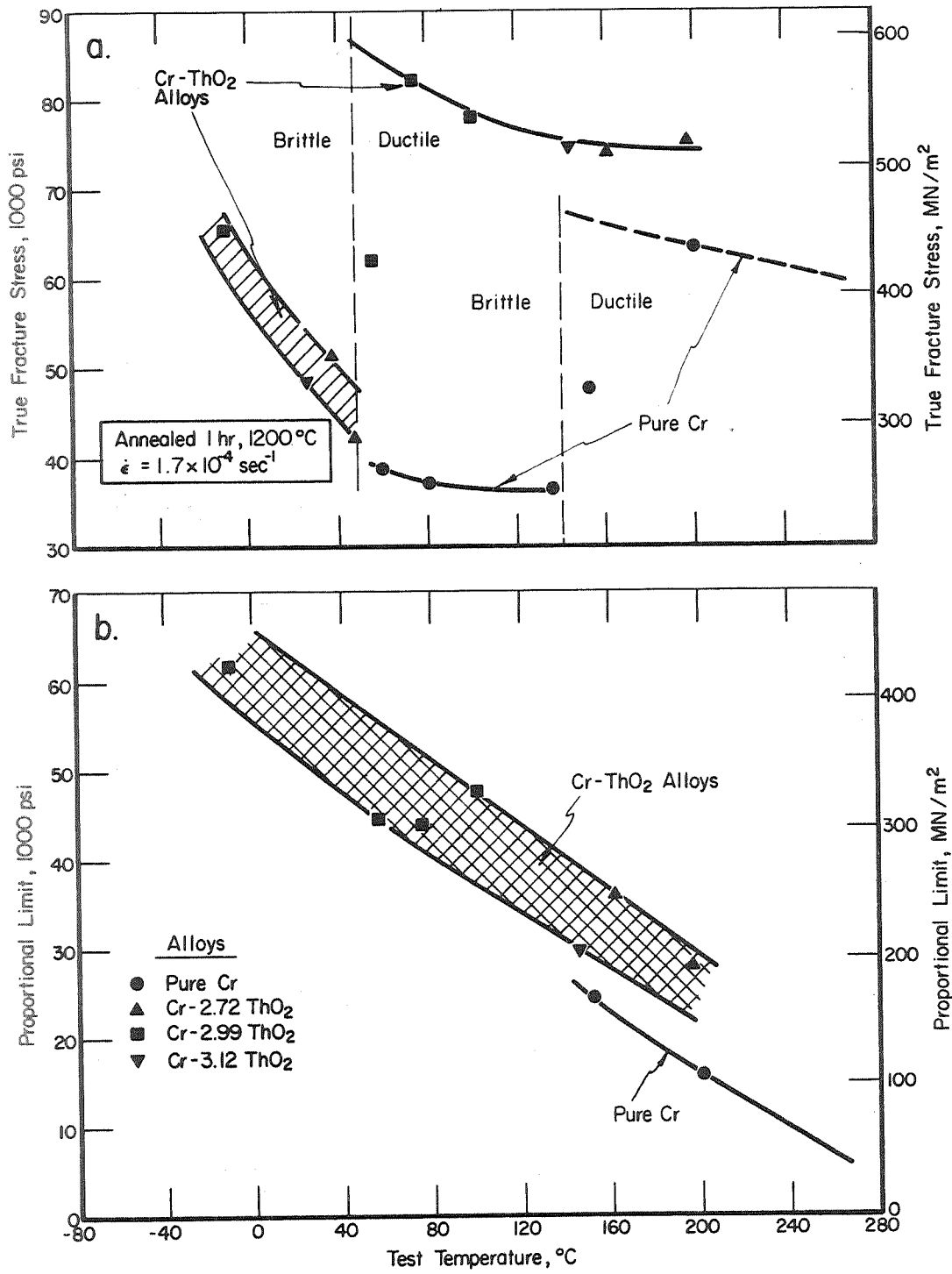


FIGURE 29. TENSILE PROPORTIONAL LIMIT AND TRUE FRACTURE STRESS OF ANNEALED (1 HR, 1200°C) CHROMIUM AND Cr-ThO₂ ALLOYS AS A FUNCTION OF TEST TEMPERATURE

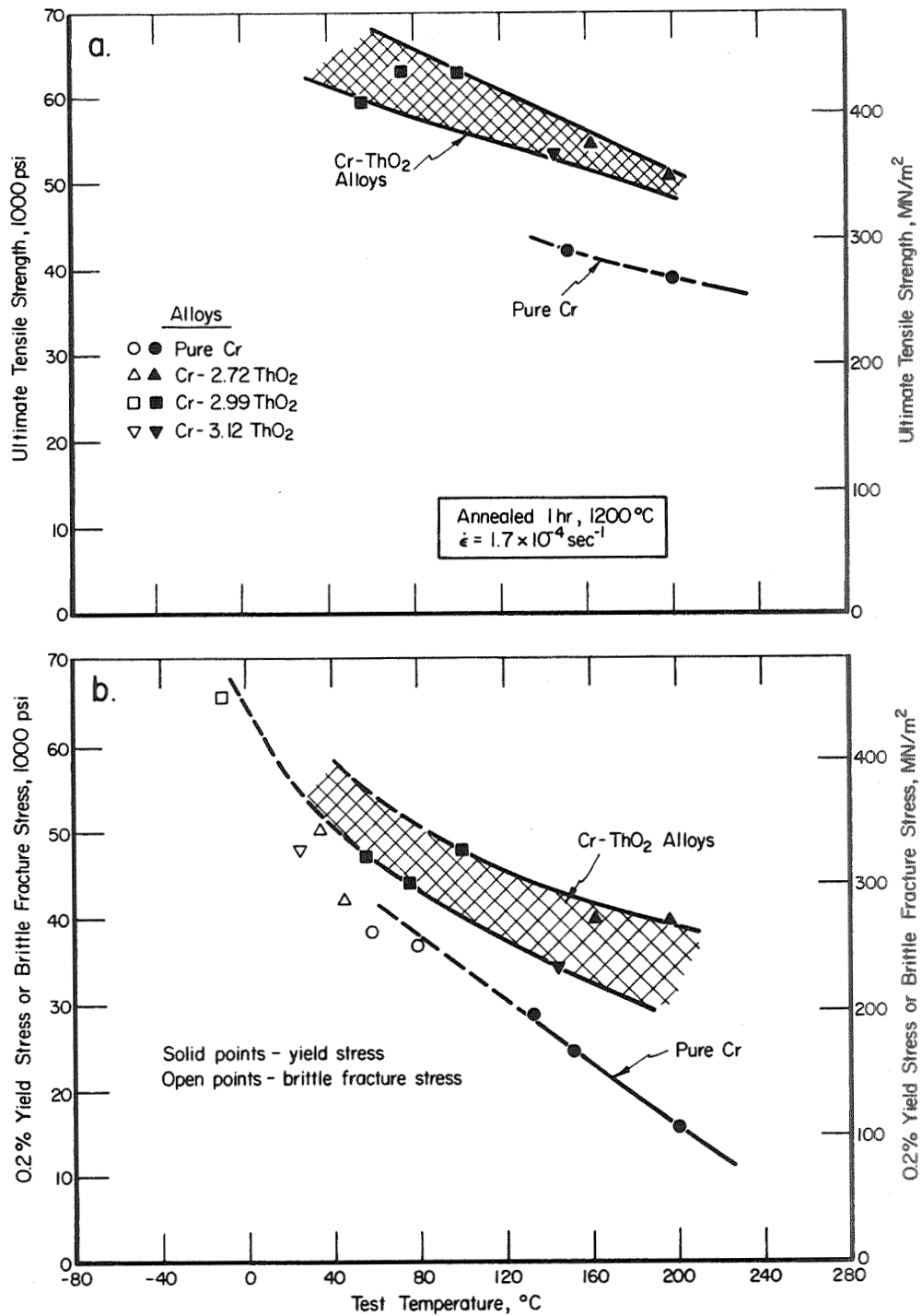


FIGURE 30. TENSILE YIELD STRESS, BRITTLE FRACTURE STRESS, AND ULTIMATE STRENGTH OF ANNEALED (1 HR, 1200°C) CHROMIUM AND Cr-ThO₂ ALLOYS AS A FUNCTION OF TEST TEMPERATURE

The as-rolled Cr-ThO₂ alloys showed no yield point, and pure chromium exhibited a yield drop only at $T \gtrsim 195^{\circ}\text{C}$. The upper yield stress of pure chromium is approximately the same as the proportional limit of the Cr-ThO₂ alloys, as seen in Figure 26b. Over the temperature range 25 to 195°C the proportional limit of the Cr-ThO₂ alloy is independent of temperature, and the stress levels are somewhat higher than the proportional limit of pure chromium, indicating some dispersion strengthening by the ThO₂ particles.

Figures 27a and b illustrate how the ultimate strength and yield strength, respectively, of the materials vary with test temperature. Both yield and ultimate strengths of the thoriated chromium are somewhat higher than corresponding values for pure chromium. Also plotted in Figure 27b are values of the brittle fracture stress (open points). These values lie slightly below the yield strength at any temperature, but have essentially the same temperature dependence as the yield strength. This is evidence for the occurrence of slip-induced brittle cleavage, which is often observed in other BCC metals below the DBTT.

The deformation and fracture behavior of pure chromium and the Cr-ThO₂ alloys after annealing for one hour at 1200°C had the same general characteristics as in the as-rolled condition. The DBTT (Figure 28) of the Cr-ThO₂ alloys was 50°C and the pure chromium had a DBTT of 140°C , determined by extrapolation to 0% elongation and reduction in area. The temperatures corresponding to 5% elongation were 55°C and 145°C for the Cr-ThO₂ alloys and the pure chromium, respectively. Compared with the as-rolled results, annealing for one hour at 1200°C increased the DBTT of the Cr-ThO₂ alloys by 35°C , but caused no change in the DBTT of pure chromium. The latter is surprising, since normally BCC metals have a lower DBTT in the worked condition than after recrystallization. At temperatures above the DBTT the elongation and reduction in area values were much greater after annealing than in the as-rolled condition

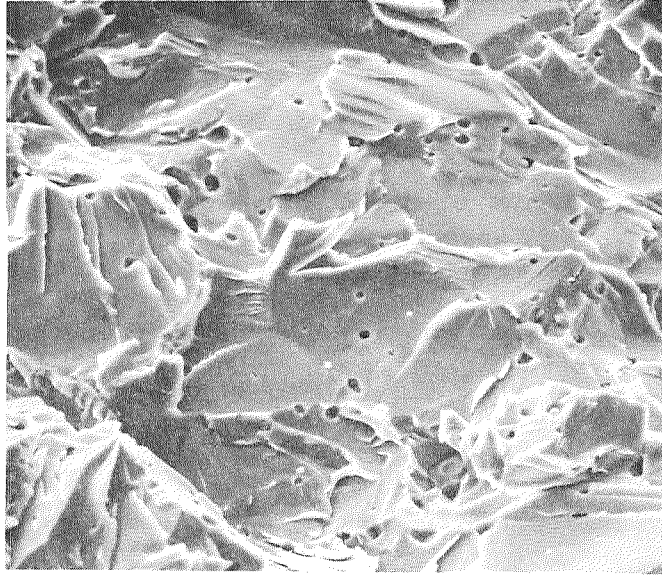
(compare Figures 25 and 28). Total elongations as high as 43% for pure chromium and 30% for Cr-ThO₂ specimens were obtained, compared with the relatively low values of ~ 7 to 11% for as-rolled specimens.

Graphs of true fracture stress and proportional limit (Figure 29) and ultimate and yield strength (Figure 30) for annealed materials show the same general features as noted earlier for the alloys tested in the as-rolled condition (see Figures 26 and 27). There is some dispersion strengthening in the thoriated alloys, but not as much as would be expected if the ThO₂ dispersion had been more uniform. This relative lack of dispersion strengthening is discussed later. Comparison of Figures 26 and 27 (as-rolled) with Figures 29 and 30 (annealed) shows that the one hour, 1200°C anneal lowered the strength of both the pure chromium and the Cr-ThO₂ alloys. For example, the 0.2% yield strengths were decreased by annealing, as shown below:

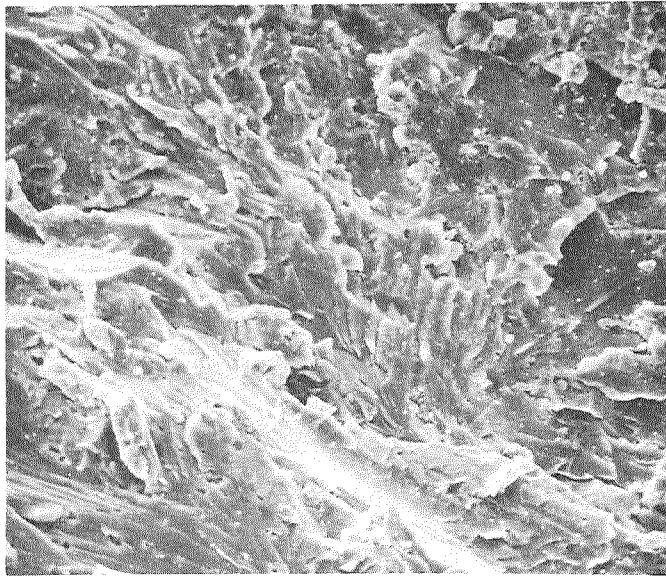
<u>Condition</u>	<u>Pure Cr, 150°C</u>	<u>Cr-ThO₂ Alloys, 60°C</u>
As-rolled	77 ksi (530 MN/m ²)	82-88 ksi (566-607 MN/m ²)
Annealed	24 ksi (166 MN/m ²)	46-53 ksi (317-365 MN/m ²)

These temperatures were selected for comparison, since they are just above the highest DBTT for the pure chromium and the thoriated materials.

The fracture characteristics of the as-rolled pure chromium and Cr-ThO₂ alloys were similar. Below the DBTT, fracture was almost entirely by cleavage, while above the DBTT, mixed cleavage and ductile tearing was observed. The one hour anneal at 1200°C caused the pure chromium to recrystallize, but the Cr-ThO₂ alloys still had a worked (plus recovered) structure. Below the DBTT the annealed pure chromium failed by mixed cleavage and grain boundary fracture and the thoriated alloys almost entirely by cleavage. Above the DBTT the annealed pure chromium and the thoriated alloys failed by ductile tearing, with some grain boundary fracture in the pure chromium. Figure 31a shows the mixed transgranular



(a) Pure chromium, tested at 135°C (0.6% El., 0.2% RA).



(b) Cr-2.99 w/o ThO₂, tested at 55°C (6.0% El., 2.3% RA).

FIGURE 31. SCANNING ELECTRON FRACTOGRAPHS OF ANNEALED CHROMIUM AND Cr-ThO₂ SPECIMENS, 1000X.

cleavage and grain boundary fracture of an annealed pure chromium specimen tested at 135°C (0.6% El., 0.2% RA). The craters apparent on the fracture surface correspond to Cr₂O₃ particles (or their holes). The mixed ductile-tear/cleavage fracture of an annealed Cr-2.99 w/o ThO₂ specimen tested at 55°C is shown in Figure 31b. This specimen had 6% elongation and 2.3% reduction in area.

High Temperature Deformation

Due to the limited amount of material available, only a few preliminary tensile tests were made on the Cr-ThO₂ alloys at elevated temperatures (1093°C). The specimen configuration was the same as that used for the DBTT determinations (Figure 24), and specimens were clamped in split serrated grips made from Mo-TZM. Tests were performed at a strain rate of $1.7 \times 10^{-4} \text{ sec}^{-1}$ in an Instron with a Brew vacuum furnace attached. During testing the vacuum was 10^{-5} torr ($1.33 \times 10^{-3} \text{ N/m}^2$).

The results are listed in Table 10. At 1093°C there is little difference in strength between the as-rolled and annealed conditions, although the total elongation of the as-rolled specimens is about twice that of annealed specimens. The yield and ultimate strength values of both the Cr-2.99 w/o ThO₂ and Cr-3.12 w/o ThO₂ alloys are essentially the same as values for pure chromium at 1093°C reported in the literature.^(5,6) The reasons for lack of high temperature dispersion strengthening are discussed later.

Preliminary Oxidation Studies

Several selected oxidation tests were made on the pure chromium and one Cr-ThO₂ alloy (Cr-3.12 w/o ThO₂). Thermogravimetric measurements of weight gain versus time were made at 900 and 1100°C in 100 torr ($1.33 \times 10^4 \text{ N/m}^2$) of

TABLE 10. MECHANICAL PROPERTIES OF Cr-ThO₂ ALLOYS AT 1093°C

Alloy	Condition	Prop. Lim.		0.2% Y.S.		UTS		Unif. Elong. %	Total Elong. %	Red. in Area %
		10 ³ psi	MN/m ²	10 ³ psi	MN/m ²	10 ³ psi	MN/m ²			
Cr-2.99 w/o ThO ₂	As-rolled	8.1	55.8	9.7	66.8	11.0	75.9	4.5	13.2	8.1
Cr-2.99 w/o ThO ₂	Annealed (a)	7.9	54.5	9.6	66.2	10.1	69.7	1.8	7.6	6.0
Cr-3.12 w/o ThO ₂	As-rolled	5.3	36.5	7.7	53.2	9.2	63.4	4.0	11.7	10.4
Cr-3.12 w/o ThO ₂	Annealed (a)	5.6	38.6	7.2	49.7	7.7	53.1	1.5	6.0	3.6

(a) Annealed at 1200°C, 1 hour in argon.

static oxygen, with the results shown in Figure 32. The specimens were from the shoulders of broken tensile specimens, which had been tested in the annealed condition. Prior to oxidation, the specimens were re-electropolished. Details of the oxidation procedures have been described elsewhere.⁽⁷⁾

Oxidation, as measured by weight gain, appears to be more rapid for the pure chromium than for the Cr-ThO₂ alloy at both 900 and 1100°C. This is similar to previous work on TD Ni-Cr (Ni-20Cr-2ThO₂) and its ThO₂-free counterpart^(8,9). In TD Ni-Cr oxidation at $T \lesssim 1000^\circ\text{C}$ appears to be a balance between weight gain by scale (Cr₂O₃) formation and weight loss by evaporation of external CrO₃. Under some conditions this can result in a total weight loss in TD Ni-Cr oxidized for long periods of time. This behavior, however, does not appear to happen in Ni-20Cr, or even in Ni-30Cr where Cr₂O₃ scales form during oxidation. The differences between the pure chromium and Cr-ThO₂ results in Figure 32 may be the result of a similar situation, although the mechanism of the ThO₂ effect is not apparent.

Scanning electron micrographs of sectioned pure chromium and Cr-3.12 w/o ThO₂ specimens oxidized for 24 hours at 1100°C are shown in Figure 33. The average Cr₂O₃ scale thicknesses are $\sim 15 \mu\text{m}$ for the pure chromium and $\sim 5 \mu\text{m}$ for the Cr-ThO₂ alloy. The scale on the pure chromium is buckled (Figure 33a) and spalled on cooling from the oxidation temperature. The Cr₂O₃ scale on the Cr-3.12 w/o ThO₂ alloy is adherent in places, and appears to be severely fragmented (Figure 33b). This could have occurred during cooling. An interesting feature in Figure 33b is the appearance of ThO₂ particles (white) in the scale. This identification was possible by using the back-scattered mode in the scanning electron microscope. The presence of ThO₂ in the Cr₂O₃ scale has also been observed in oxidized TD Ni-Cr⁽⁹⁾, and is possible evidence that oxidation proceeds by inward oxygen diffusion in thoriated alloys.

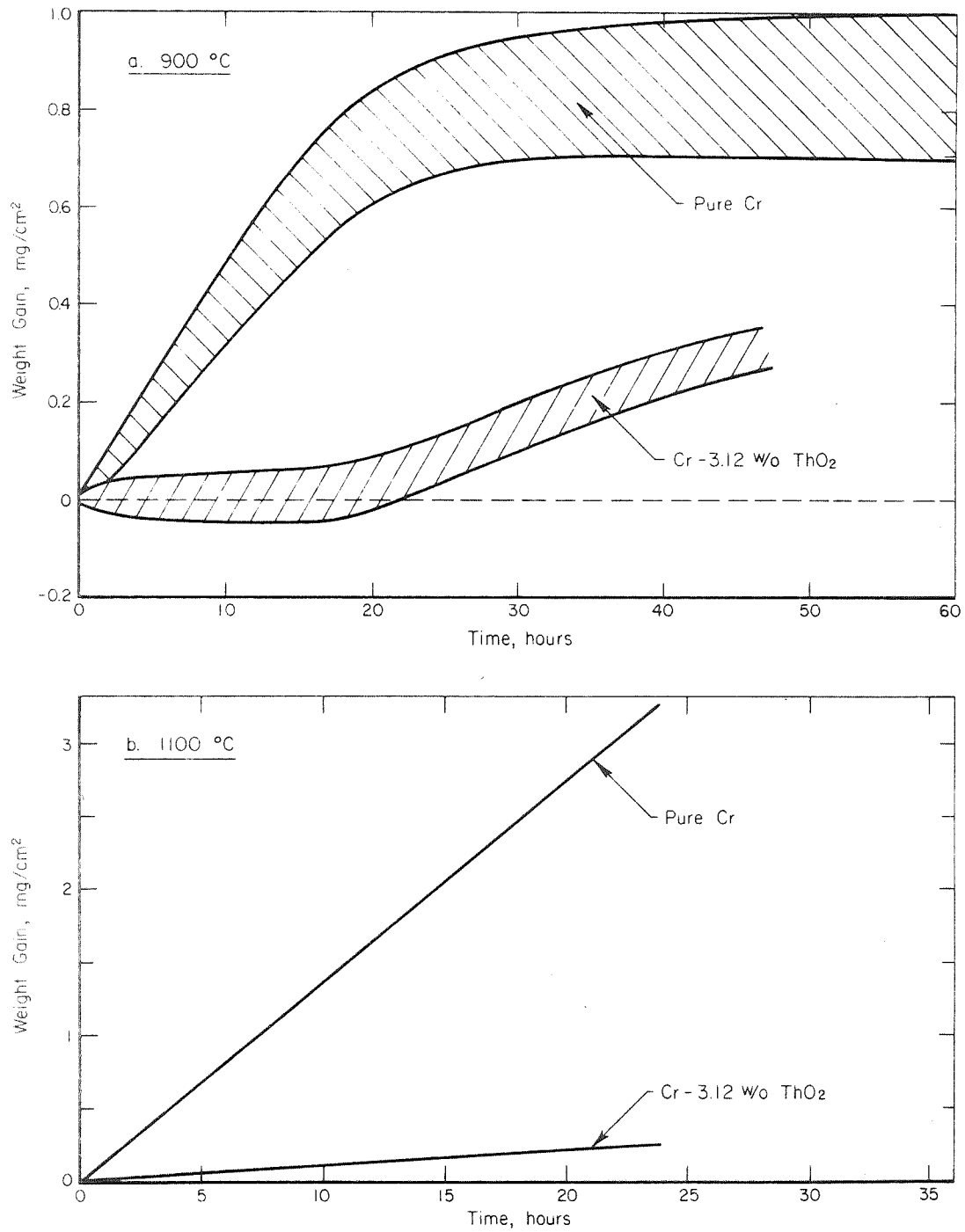
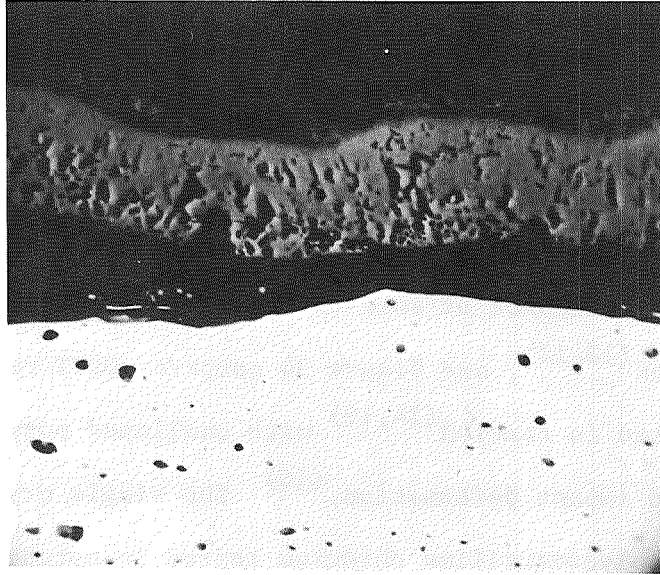
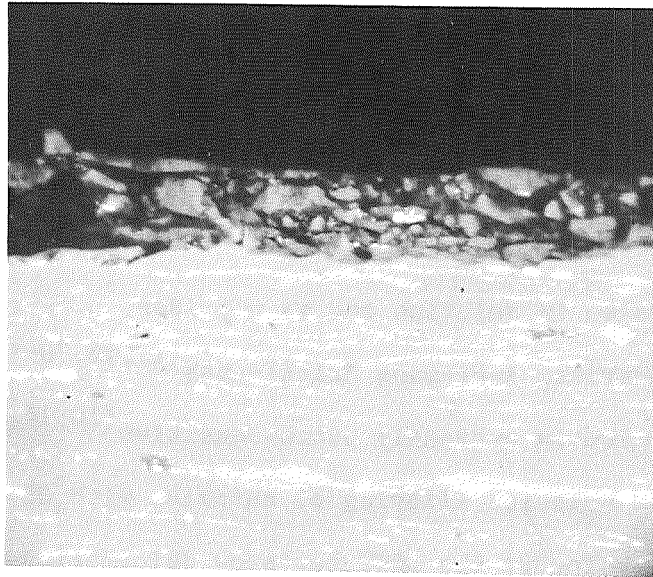


FIGURE 32. STATIC ISOTHERMAL OXIDATION OF PRE-ANNEALED PURE CHROMIUM AND Cr-3.12 w/o ThO₂ AT 900 AND 1100°C IN 100 TORR (1.33×10^4 N/m²) OF OXYGEN. NOTE DIFFERENT WEIGHT GAIN AND TIME SCALES IN (a) AND (b).



(a) Pure Cr, 1000X



(b) Cr-3.12 w/o ThO₂, 2000X

FIGURE 33. SCANNING ELECTRON MICROGRAPHS OF SECTIONED SPECIMENS WHICH HAVE BEEN OXIDIZED FOR 24 HRS AT 1100°C IN 100 TORR (1.33×10^4 N/m²) OXYGEN

Discussion

The ductile-to-brittle transition temperature of unalloyed chromium has been shown to be a function of material parameters such as grain size, density of mobile dislocations, impurities (e.g., nitrogen and grain boundary nitrides) as well as rate of deformation and type of testing (e.g., notched impact, slow tension, etc.). The influence of some of these factors has been reviewed in recent communications⁽¹⁰⁻¹³⁾, and Figure 34 compares DBTT results for chromium single crystals tested in tension^(14,15) with unalloyed polycrystalline chromium subjected to notched impact deformation.⁽¹⁶⁾ The single crystals had a DBTT of -80°C , whereas the polycrystalline chromium tested in notched impact had a DBTT of 370°C .

Although some factors regarding the DBTT of chromium are not completely clear, several generally accepted conclusions have been reached:

- (a) The DBTT of wrought chromium is lower than that of recrystallized material^(16,17,19,22,25,34).
- (b) Brittle fracture is slip-induced and the critical stage of fracture is crack initiation^(10,15,30).
- (c) Nitrogen in solution and as nitrides, especially at grain boundaries, increases brittleness^(17,18,20-23,34-36).
- (d) Chromium is extremely notch-sensitive^(10,14,21).
- (e) Solid solution alloying of chromium with 35 at/o rhenium substantially lowers the DBTT for slow deformation rates^(10,12,39).
- (f) Prestraining to produce mobile dislocations increases the subsequent ductility of chromium^(24,31-33,37).
- (g) Increasing the deformation rate increases the DBTT of chromium^(10,26-29).

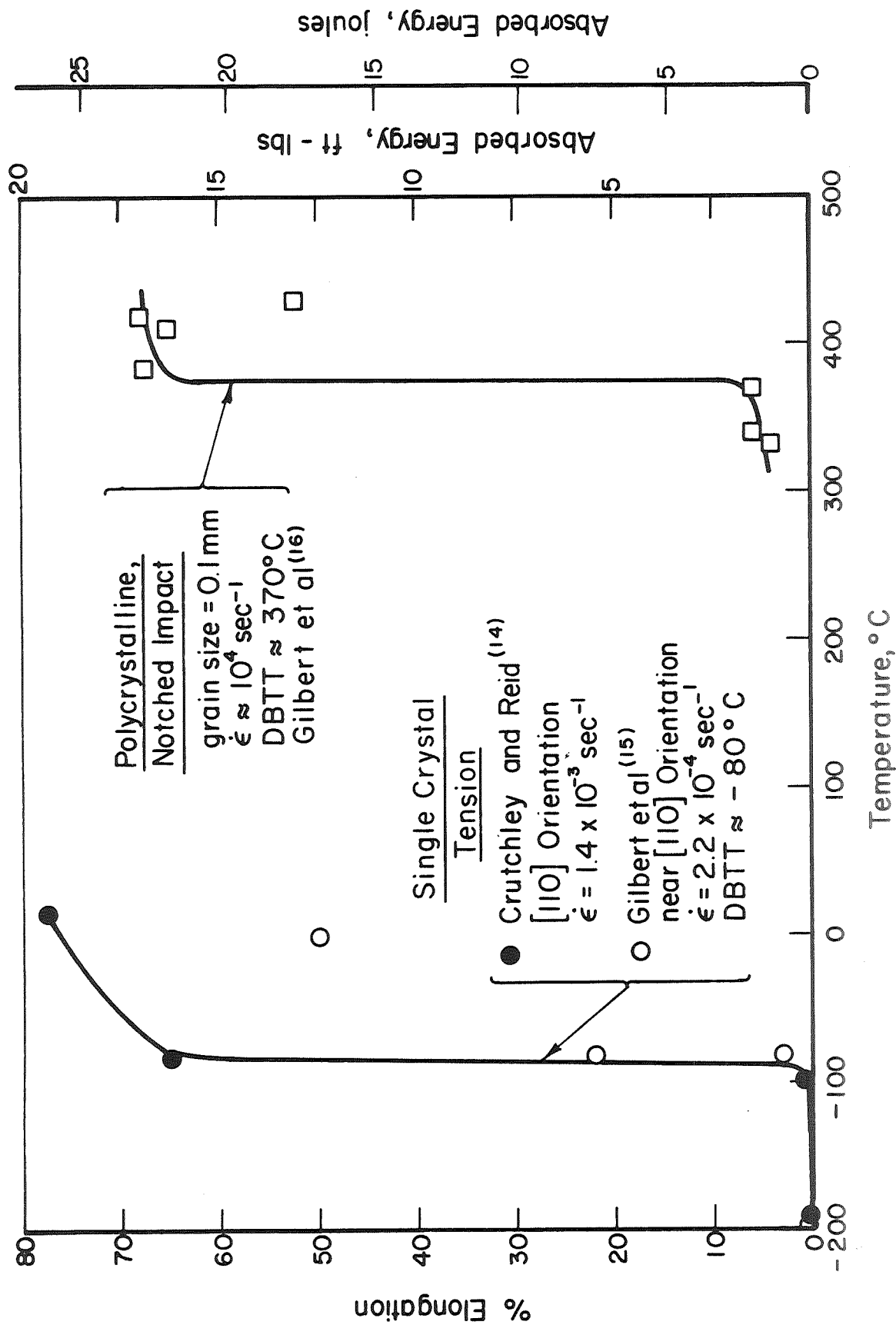


FIGURE 34. VARIATIONS IN DBTT BEHAVIOR OF UNALLOYED CHROMIUM.

The present investigation has shown that ThO_2 particles in chromium lower the DBTT by 125°C in the as-rolled condition and by 90°C for material that has been annealed for one hour at 1200°C . This enhanced ductility could not be due to a difference in substructure, since as shown in Table 6, both the pure chromium and Cr- ThO_2 alloys had $\sim 1 \mu\text{m}$ diameter subgrains in the as-rolled condition. Neither could the apparent ThO_2 -induced ductilizing be due to a difference in nitrogen content. As seen in Table 2 the nitrogen analysis for pure chromium was 60 ppm compared with 70-170 ppm for the thoriated material. If nitrogen embrittlement were apparent, the thoriated alloys should have been more embrittled. Grain size effects probably did not affect the DBTT values. For example, the as-rolled pure chromium with a fine elongated (somewhat recovered) grain structure had the same DBTT, 140°C , as did material after annealing for one hour at 1200°C , where the structure was completely recrystallized with a grain size of $33 \mu\text{m}$.

As noted in Conclusion (b) above, there is general agreement that brittle fracture in chromium is slip-induced. Further, in polycrystalline chromium tested in tension, evidence points to the fact that the initial crack formed is a result of slip-induced grain boundary parting⁽¹⁰⁾, which initiates cleavage and final fracture. Maykuth and Gilbert⁽¹⁰⁾ have presented strong evidence for slip-induced fracture by comparing the temperature dependence of the tensile brittle fracture stress, from Weaver⁽³⁶⁾, with the temperature dependence of the compressive yield stress, from Marcinkowski and Lipsitt⁽³⁸⁾. The two stress versus temperature plots were parallel over the temperature range -100 to $+100^\circ\text{C}$, which suggests that some yielding on a fine scale must occur before brittle fracture is initiated. The results of the present work confirm this conclusion. Figures 27b and 30b show that the brittle fracture stress has the same temperature dependence as the 0.2% yield strength, with the values of brittle fracture stress lying slightly below the yield-strength-versus-temperature plots.

The brittle-versus-ductile fracture of chromium, then, is a competition between slip-induced crack initiation and macroscopic flow. If the stress required to produce macro-yielding is higher than the brittle fracture stress, the material will be brittle. Conversely, if flow can take place at stresses substantially below the brittle fracture stress, the material will be ductile.

Several mechanisms may be operative, although it is not possible to pinpoint with certainty which is most important: (1) ThO_2 particles may disperse slip, making it more difficult to achieve slip induced grain boundary crack nucleation either due to the attainment of a critical stress or critical strain condition; (2) second phase particles may act as dislocation sources, and thus provide mobile dislocations in this normally source-poor-material; and (3) particles in grain boundaries may serve to help transmit slip across boundaries by injecting mobile glide dislocations into an adjacent grain and thereby inhibit grain boundary cracking.

The first mechanism is considered with the help of the schematic illustration in Figure 35, which essentially reflects the model of Hahn and Rosenfield⁽²⁾. A similar concept has been employed by Hodgson and Tetelman⁽⁴²⁾ to steel containing spheroidized carbides, for their case where particles were not cracked by slip bands. The numerous well known theories of brittle fracture, e.g., Griffith, Cottrell, Stroh, Petch, all predict that the cleavage strength, σ_c , varies as $(1/L)^{1/2}$, where L is the length of a slip band, or dislocation pileup, and this often may be the grain diameter. All other things being equal, a higher value of L will lower σ_c . It is possible that the role of the ThO_2 particles is to disperse slip, as shown in Figure 35, such that lower effective values of L are achieved. If this is accomplished, less severe stress concentrations are produced at grain boundaries or other potential sites for crack nucleation, and the cleavage strength is raised. However, particles cannot only raise the cleavage strength, but can also

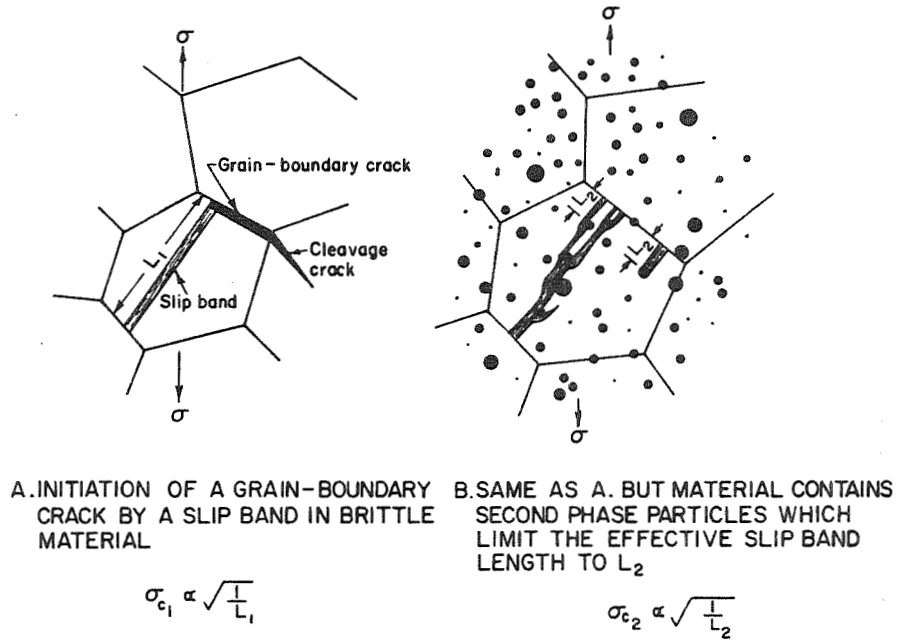
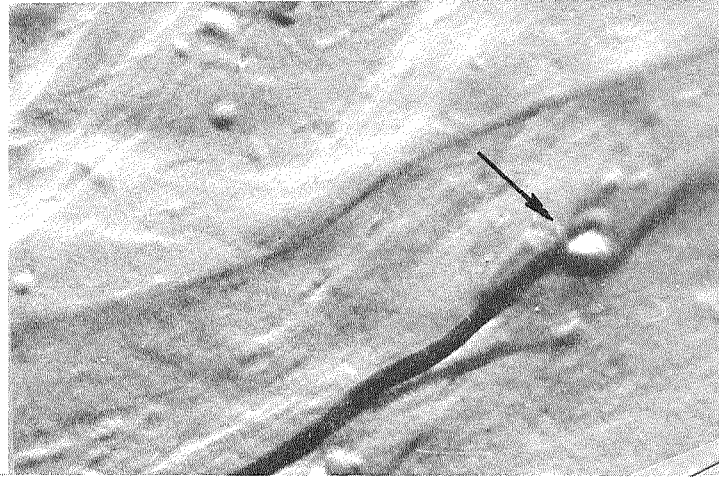


FIGURE 35. SCHEMATIC DIAGRAMS ILLUSTRATING EFFECT OF SECOND-PHASE PARTICLES ON SLIP BAND LENGTH, L , AND CLEAVAGE STRENGTH, σ_c . $L_1 > L_2$, so $\sigma_{c_1} < \sigma_{c_2}$.

increase the yield strength. The stress concentrations exerted on a potential site for crack nucleation by localized slip can be relieved by more extensive general slip in the same region, thus avoiding brittle fracture. The onset of more extensive slip would coincide with the general yielding of the specimen. For the DBTT to be lowered by particles, the cleavage strength must be increased more than the yield strength. This apparently is the case for the Cr-ThO₂ alloys. Thus the relatively small amount of dispersion strengthening by ThO₂ in chromium is useful in helping to promote a lower DBTT.

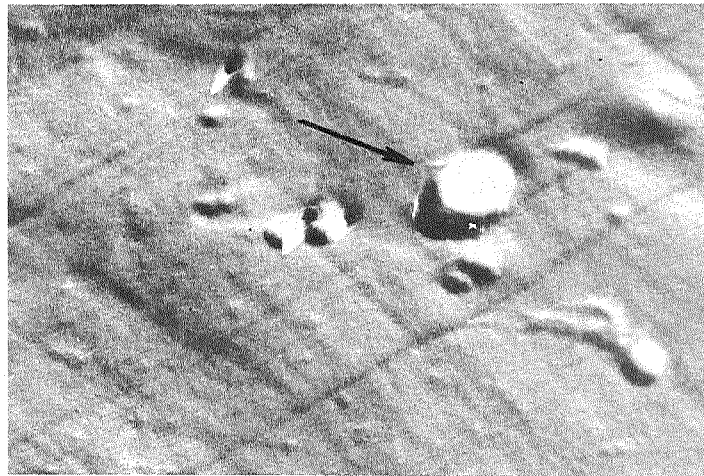
Some evidence in support of this model is shown by the replica electron micrographs in Figure 36. These were taken on an annealed Cr-3.12 w/o ThO₂ specimen deformed to fracture above the DBTT (T = 145°C, 31.5% total elongation and 35.1% reduction in area). The purpose of the experiment was to determine whether or not slip bands on the surface had interacted with ThO₂ particles. A similar experiment was performed on a Cr-ThO₂ specimen fractured below the DBTT. However, this was unsuccessful because no surface slip offsets were visible in the areas examined. The arrows on the micrographs in Figure 36 point to particles where the slip character is different on opposite sides of the particle. However, this evidence cannot be considered conclusive proof that the model is correct, since sometimes particles were intersected by slip bands with no apparent change in slip character, and the two-dimensional surface examination may not adequately represent the three-dimensional flow process.

One way to assess the influence of slip dispersion by particles on crack nucleation is to consider the question of wavy slip versus planar slip, and the relation of slip character to crack nucleation⁽⁴⁶⁾. In general, as the test temperature is raised, cross-slip increases and deformation of BCC metals changes from planar slip to slip with increasing waviness. Yet the grain size dependence of the fracture stress in BCC metals⁽⁴⁷⁾, i.e., slope of Petch plots, remains the



(a)

36,000X



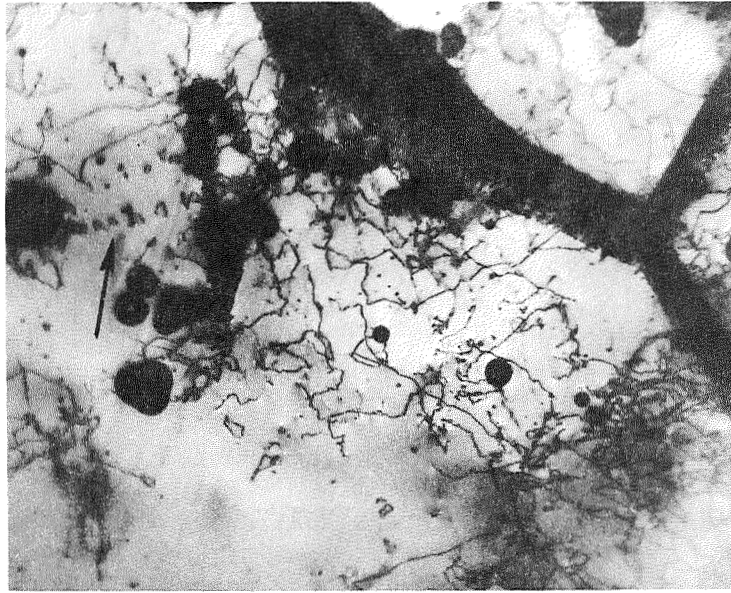
(b)

48,000X

FIGURE 36. REPLICA ELECTRON MICROGRAPHS TAKEN ON THE SURFACE OF AN ANNEALED Cr-3.12 W/O ThO₂ SPECIMEN DEFORMED TO FRACTURE ABOVE THE DBTT ($T = 145^{\circ}\text{C}$, 31.5% EL., 35.5% RA). ARROWS INDICATE PARTICLES WHICH APPEAR TO HAVE INFLUENCED THE CHARACTER OF SLIP.

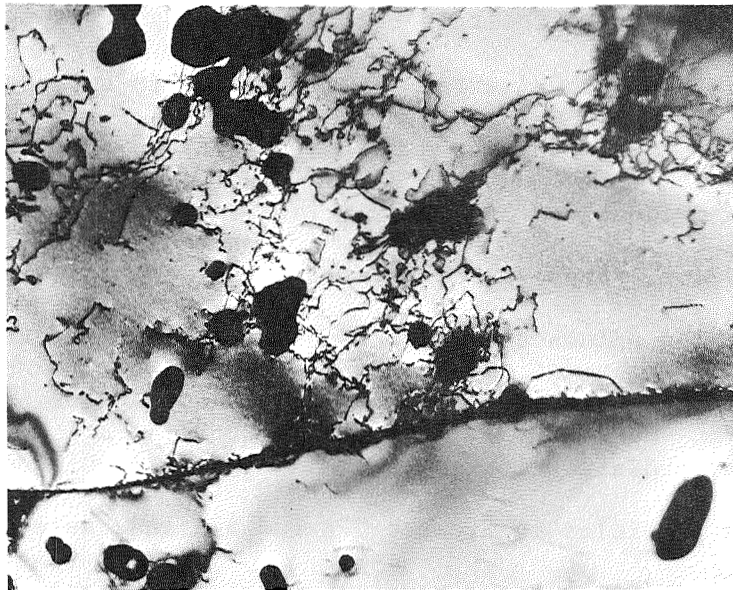
same with increasing temperature, which suggests that the character of slip in pure BCC metals may not be important in the fracture initiation process. In fact, some wavy slip lines in iron⁽⁴⁸⁾ have deviations in direction equivalent to that induced by the ThO₂ particle in Figure 36a. If this is true in chromium as well, then the dispersion of slip by particles may not lower the DBTT.

As noted previously, it is possible to lower the DBTT of chromium by first prestraining above the DBTT to produce mobile dislocations in this normally source-poor material. The prestraining can be done conventionally^(24,37) or by hydrostatic pressurization⁽³¹⁻³³⁾, and has the general effect of removing the yield point. Once mobile dislocations are available, then multiplication can occur and macroscopic flow will proceed until the material is sufficiently work-hardened that the ductile cleavage fracture stress is reached. If the second mechanism were operative, such that the ThO₂ particles acted as dislocation sources by punching out loops at stresses below the upper yield stress (and brittle fracture stress), e.g., in the microstrain region, this might act in a fashion equivalent to the prestraining experiments. Some evidence in support of this was obtained by transmission electron microscopy of a deformed specimen of Cr-2.99 w/o ThO₂ which had been preannealed at 1200°C. This specimen was fractured at 55°C and had 6% total elongation. Representative micrographs are illustrated in Figure 37. The arrow in Figure 37a points to dislocation loops which appear to have been punched from a small particle. Previous workers also have observed that particles in chromium can act as dislocation sources.^(31,49) Woolly dislocation tangles appear around other particles in Figures 37a and 37b and these may have been formed in part by source activation at the particle matrix interface. Thus ThO₂ particles acting as dislocation sources may contribute to the enhanced ductility of Cr-ThO₂ alloys. This is born out indirectly by the complete absence of yield drops in the thoriated materials and the appearance of yield drops above the DBTT in the as-rolled pure chromium and yield plateaus in the annealed pure chromium.



(a)

30,000X



(b)

30,000X

FIGURE 37. TRANSMISSION ELECTRON MICROGRAPHS OF A Cr-2.99 W/O ThO₂ SPECIMEN DEFORMED AT 55°C TO 6% TOTAL ELONGATION. THE SPECIMEN HAD BEEN ANNEALED AT 1200°C PRIOR TO TESTING.

The third possible mechanism, suggested by Embury⁽⁴⁶⁾, is an extension of the second mechanism and relies upon a slip band in one grain intersecting a boundary containing particles. These stressed particles may then inject dislocations into the adjacent grain, provided neither the particles nor the particle-matrix interface fractures. In this manner slip may be transmitted across grain boundaries, thus relieving the stress concentration at the boundary and preventing crack nucleation. Such a situation may be possible in the present case, since many ThO₂ particles were located in the elongated grain boundaries (see Figure 15b). The schematic illustration in Figure 38 represents this process, and some possible evidence in support of it is shown in Figure 39. The surface replica in Figure 39 shows slip bands intersecting a boundary containing particles, and the slip appears to be transferred across the boundary from grain A to grain B.

Although the lack of dispersion strengthening at low temperatures may have helped lower the DBTT, the absence at high temperatures is detrimental if chromium were used in high temperature structural applications. However, one useful function of ThO₂ with regard to high temperature strength was to promote the elongated grain structure during high temperature annealing. From previous work on dispersion strengthened nickel alloys⁽⁴⁰⁾ it is known that the elongated grain structure enhances the high temperature tensile and creep strength by making grain boundary sliding more difficult. It was shown that the 0.2% yield strength and creep strength all increased linearly with increasing grain aspect ratio, i.e., grain length divided by grain width.⁽⁴⁰⁾ The fact that the elongated grain structure was produced in Cr-ThO₂ alloys suggests that these materials have good potential for high temperature strength. If the dispersion cannot be made more uniform, then matrix strengthening by solid solution additions would be a logical way to proceed. Dilute additions of tantalum and niobium (≈ 1 at. %) have been shown to triple the strength of chromium over the temperature range 1000-1300°C⁽⁴¹⁾. It is possible to alloy with both tantalum and niobium in the present CVD powder production unit.

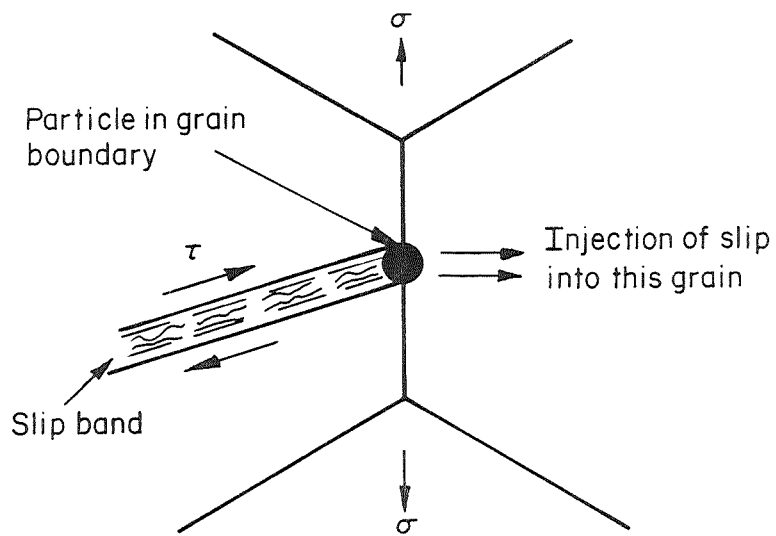


FIGURE 38. SCHEMATIC ILLUSTRATION OF A SLIP BAND INTERSECTING A PARTICLE IN A GRAIN BOUNDARY, AND THE PARTICLE INJECTING SLIP INTO AN ADJACENT BOUNDARY. ⁽⁴⁶⁾

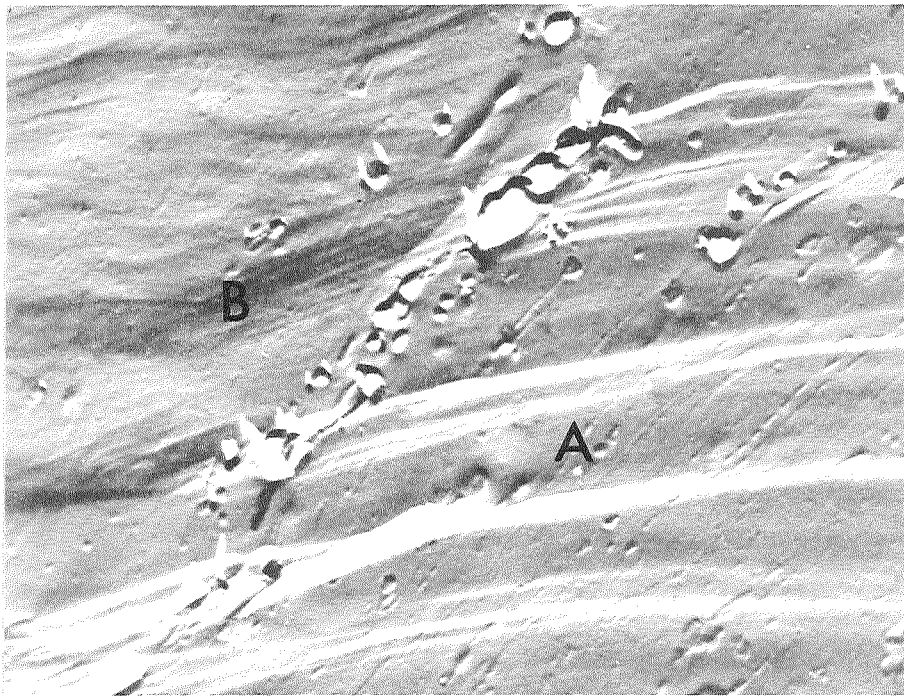


FIGURE 39. SOME POSSIBLE EVIDENCE FOR THE MECHANISM IN FIGURE 38. SPECIMEN WAS ANNEALED Cr-3.12 W/O ThO₂, DEFORMED TO FRACTURE AT 145°C (31.5% EL., 35.5% RA), 12,000X.

SUMMARY OF RESULTS AND
CONCLUSIONS

(1) A vapor-deposition apparatus has been designed, constructed, and operated for the production of chromium and Cr-ThO₂ powders in 1/4 to 1/2 pound (114-227 g) lots.

(2) One lot of pure chromium and three lots of Cr-ThO₂ containing about 3 w/o ThO₂ (2.2 v/o) were prepared, consolidated by hot isostatic pressing, and successfully rolled to sheet of 0.026 to 0.033 inch (0.066 to 0.084 cm) thickness.

(3) The ThO₂ particle distribution was more uniform in rolled sheet than in hot isostatically pressed billets. However, the dispersion was not as uniform as in commercial dispersion-strengthened nickel alloys.

(4) The tensile ductile-to-brittle-transition temperature (DBTT) at a strain rate of $1.7 \times 10^{-4} \text{ sec}^{-1}$ was lower for the three thoriated materials than for pure chromium. This ThO₂-induced ductilizing was evident for material tested in the as-rolled condition as well as for material which had been annealed for one hour at 1200°C. The DBTT values were:

<u>Material</u>	<u>As-rolled</u>	<u>Annealed</u>
Pure Chromium	140°C	140°C
Cr-ThO ₂ alloys	15°C	50°C.

(5) The improved ductility in thoriated chromium may be associated with several possible mechanisms: (1) particles may disperse slip, such that critical stress or strain concentrations for crack nucleation are more difficult to achieve, (2) particles may act as dislocation sources, thus providing mobile dislocations in this normally source-poor material, in a manner similar to prestraining, and (3) particles in grain boundaries may help to transmit slip across the boundaries, thus relieving stress concentrations and inhibiting crack nucleation.

(6) Some dispersion strengthening at lower temperatures was achieved by ThO₂ additions. The yield and ultimate strengths of the thoriated alloys were

about 10,000 psi (69 MN/m^2) higher than corresponding values for pure chromium over the temperature range 150-200°C. At 1093°C, however, the strength of thoriated materials was essentially the same as that for pure chromium.

(7) When the Cr-ThO₂ alloys were annealed at 1316 and 1427°C for 100 hours, an elongated grain structure was produced. From other work, it is known that such a structure minimizes grain boundary sliding. The elongated grains in Cr-ThO₂ alloys thus have potential for improved high temperature strength. However, matrix strengthening by solid solution alloying or a more uniform dispersion is believed to be necessary.

ACKNOWLEDGEMENTS

The authors are grateful to J. R. Stephens of NASA-Lewis Research Center for helpful discussions regarding fabrication, and to G. T. Hahn and A. R. Rosenfield for their advice concerning particle ductilizing. The scanning electron microscopy was performed by C. Price, and A. Z. Hed, and G. R. Wallwork performed the oxidation studies. The skillful technical assistance of M. R. Cantin, C. R. Barnes, R. O. Dodds, and W. Hern is gratefully acknowledged.

REFERENCES

- (1) N. D. Veigel, J. L. McCall, K. E. Meiners, and J. M. Blocher, Jr., "Chemical Vapor Deposition of Chromium on ThO_2 ", NASA CR-72404, June 30, 1968.
- (2) G. T. Hahn and A. R. Rosenfield, "A Modified Double-Pileup Treatment of the Influence of Grain Size and Dispersed Particles on Brittle Fracture", *Acta Met.*, 14, 1815 (1966).
- (3) G. T. Hahn and A. R. Rosenfield, "The Influence of a Fine Dispersion on the Cleavage Strength of Iron", *Trans. AIME*, 239, 668 (1967).
- (4) F. Henderson, F. P. Bullen, and H. L. Wain, "The Preparation and Tensile Properties of Chromium Wire", *J. Inst. Met.*, 98, 65 (1970).
- (5) J. W. Pugh, "The Tensile and Stress Rupture Properties of Chromium", *Trans. ASM*, 50, 1072 (1958).
- (6) J. W. Clark, "Development of High-Temperature Chromium Alloys", NASA CR-72731, November, 1970.
- (7) P. K. Kofstad and A. Z. Hed, "Oxidation of Co-25 w/o Cr at High Temperatures", *J. Electrochem. Soc.*, 116, 1542 (1969).
- (8) C. S. Giggins and F. S. Pettit, "The Oxidation of TD-Ni Cr Between 900 and 1200°C", to be published in *Met. Trans.*
- (9) G. R. Wallwork and A. Z. Hed, "The Oxidation of Ni-20Cr-2 ThO_2 ", to be published in *J. Oxidation of Metals*.
- (10) D. J. Maykuth and A. Gilbert, *Chromium and Chromium Alloys*, DMIC Rept. No. 234, October, 1, 1966.
- (11) J. A. Rogers and A.R.G. Brown, "The Development of Chromium-Base Alloys for Use at High Temperatures", *Metals and Materials*, 1, 246 (1967).
- (12) W. D. Klopp, "Review of Ductilizing of Group VIA Elements by Rhenium and Other Solutes", NASA TN D-4955, December, 1968.
- (13) G. T. Hahn, A. Gilbert, and R. I. Jaffee, "The Effects of Solutes on the Ductile-to-Brittle Transition in Refractory Metals", Refractory Metals and Alloys II, M. Semchyshen and I. Perlmutter, Eds., Interscience Pub., New York, p 23 (1963).
- (14) D. E. Crutchley and C. N. Reid, "Mechanical Properties of Chromium Single Crystals", 6th Plansee Seminar on High Temperature Materials, F. Benesovsky, Ed., Springer-Verlag, New York, p 57 (1969).
- (15) A. Gilbert, C. N. Reid, and G. T. Hahn, "Observations on the Fracture of Chromium", *J. Inst. Met.*, 92, 351 (1963-64).

- (16) A. Gilbert and B. C. Allen, "The Notch-Impact Behavior of Chromium and a Chromium-35 at.% Rhenium Alloy", *J. Inst. Met.*, 93, 529 (1964-65).
- (17) B. C. Allen, D. J. Maykuth, and R. I. Jaffee, "The Effect of Impurities and Structure on the Tensile Transition Temperature of Chromium", *Trans. AIME*, 227, 724 (1963).
- (18) A. Gilbert and M. J. Klein, "The Effect of Cooling Rate on the Ductile-Brittle Bend Transition Temperature of Chromium Wire", *Acta Met.*, 14, 541 (1966).
- (19) S.T.M. Johnstone, F. Henderson, and H. L. Wain, "Recrystallization and the Ductility of Chromium", *Nature*, 180, 806 (1957).
- (20) C. W. Weaver, "Strain Age Hardening and Brittleness in Chromium", *Nature*, 180, 806 (1957).
- (21) H. L. Wain, F. Henderson, and S.T.M. Johnstone, "A Study of the Room Temperature Ductility of Chromium", *J. Inst. Met.*, 83, 133 (1954-55).
- (22) H. L. Wain, F. Henderson, S.T.M. Johnstone and N. Louat, "Further Observations on the Ductility of Chromium", *J. Inst. Met.*, 86, 281 (1957-58).
- (23) K. E. Solie and O. N. Carlson, "The Effect of Nitrogen on the Brittle-Ductile Transition of Chromium", *Trans. AIME*, 230, 480 (1964).
- (24) S. Yoshida, Y. Ohba, and N. Nagata, "The Effect of Prestraining on the Ductility of Pure Chromium", *J. Japan Inst. Met.*, 1, 49 (1960).
- (25) D. J. Maykuth and R. I. Jaffee, "The Mechanical Properties of Swaged Iodide-Base Chromium and Chromium Alloys", *Trans. ASM*, 49, 948 (1957).
- (26) H. A. Johnson and G. Asai, "Room Temperature Ductile Chromium", *J. Electrochem. Soc.*, 101, 604 (1954).
- (27) A. H. Sully, E. A. Brandes, and K. W. Mitchell, "The Effect of Temperature and Purity on the Ductility and Other Properties of Chromium", *J. Inst. Met.*, 81, 585 (1952-53).
- (28) H. L. Wain, S.T.M. Johnstone, and F. Henderson, "The Effect of Rolling Temperature, Prestrain, and Strain Rate on the Ductility of Chromium", *J. Inst. Met.*, 91, 41 (1962).
- (29) R. E. Cairns and N. J. Grant, "Effects of Carbon, Nitrogen, Oxygen and Sulfur on the Ductile-Brittle Fracture Temperature of Chromium", *Trans. AIME*, 230, 1150 (1964).
- (30) A. Ball, F. P. Bullen, F. Henderson, and H. L. Wain, "Tensile Fracture Characteristics of Heavily Drawn Chromium", *Phil. Mag.*, 21, 701 (1970).
- (31) A. Ball and F. P. Bullen, "Pressurization Effects in Chromium", *Phil. Mag.*, 21, 201 (1970).

- (32) F. P. Bullen and H. L. Wain,, "The Effect of Free Dislocations on Yielding and Fracture in Body-Centered Cubic Metals", Physical Basis of Yield and Fracture, Inst. of Phys. and Phys. Soc., London, p 60 (1966).
- (33) F. P. Bullen, F. Henderson, H. L. Wain, and M. S. Patterson, "The Effect of Hydrostatic Pressure on Brittleness in Chromium", Phil. Mag., 9, 803 (1964).
- (34) R. I. Garrod and H. L. Wain, "Dislocation Arrangements and Brittleness in Chromium", J. Less-Common Met., 9, 81 (1965).
- (35) N. E. Ryan, "An Appraisal of Possible Scavenger Elements for Chromium and Chromium Alloys", J. Less-Common Met., 6, 21 (1964).
- (36) C. W. Weaver, "Tensile Properties of Annealed Chromium Between -196 and +900°C", J. Inst. Met., 89, 385 (1960-61).
- (37) R. E. Hook and A. M. Adair, "On the Recrystallization Embrittlement of Chromium", Trans. Met. Soc. AIME, 227, 151 (1963).
- (38) M. J. Marcinkoski and H. A. Lipsitt, "The Plastic Deformation of Chromium at Low Temperatures", Acta Met., 10, 95 (1962).
- (39) J. G. Booth, R. I. Jaffee, and E. I. Salkovitz, "The Mechanisms of the Rhenium-Alloying-Effect in Group VI-A Metals", 5th Plansee Seminar on Metals for the Space Age, F. Benesovsky, Ed., Springer-Verlag, New York, p 547 (1965).
- (40) B. A. Wilcox, A. H. Clauer, and W. B. Hutchinson, "Structural Stability and Mechanical Behavior of Thermomechanically Processed Dispersion Strengthened Nickel Alloys", NASA CR- , November 25, 1970.
- (41) W. D. Klopp, "Recent Developments in Chromium and Chromium Alloys", NASA TM X-1867, September, 1969.
- (42) D. E. Hodgson and A. S. Tetelman, "The Effect of Microstructure on the Cleavage Strength of Quenched and Tempered Steels", Proceedings of the Second International Conference on Fracture, P. L. Pratt, et al., Eds., Chapman and Hall, Ltd., London, p 266 (1969).
- (43) C. N. Davis (Ed.), Aerosol Science, Academic Press, London and New York, p 273 (1966).
- (44) K. R. Spurney, et al., "Aerosol Filtration by Means of Nuclepore Filters, Structural and Filtration Properties", Environmental Science and Technology, 3, 453 (1969).
- (45) C. E. Lapple, "Characteristics of Particles and Particle Dispersoids", Stanford Research Institute Journal, Third Quarter, 1961.
- (46) J. D. Embury, MacMaster University, Hamilton, Ontario, private communication.

- (47) N. J. Petch, "The Ductile Fracture of Polycrystalline α -Iron", *Phil. Mag.*, 1, 186 (1956).
- (48) J. D. Boyd, G. T. Hahn, A. R. Rosenfield, and E. Votava, "Character of Slip Bands in Iron and a Mild Steel with Manganese", *Trans. ASM*, 62, 206 (1969).
- (49) N. E. Ryan, "The Influence of a Carbide Dispersion on the Recrystallization Behavior of Chromium", Rept. ARL/Met. 64, Aeronautical Research Laboratories, Melbourne, March, 1967.

APPENDIX A

PROCUREMENT AND EVALUATION OF THORIA POWDER

APPENDIX A

PROCUREMENT AND EVALUATION OF THORIA POWDER

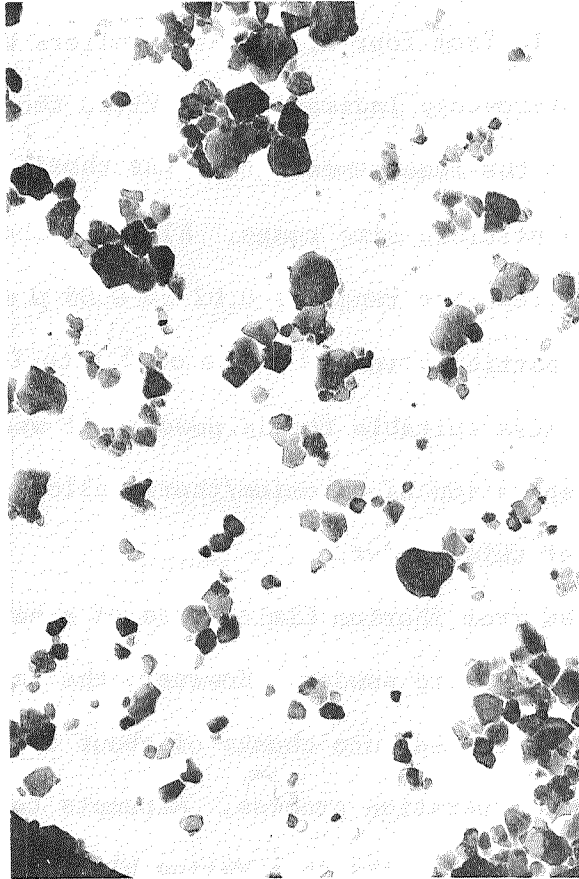
Samples of thoria from four different suppliers were evaluated. The evaluation by electron microscopy indicated that Vitro thoria was the best available with respect to the requirements that the thoria must be a free-flowing powder and have a narrow particle size range. Although the Vitro thoria is predominantly in the desired size range of 0.02 to 0.05 μ m, it contains a significant fraction of particles in the range of 0.1 to 1.5 μ m. Due to the unavailability of a more suitable thoria powder, it was decided to use the Vitro thoria for the preparation of chromium/thoria alloys. Figure 8 shows an electron micrograph of this powder.

Thoria obtained from Thorium Limited was of a narrower size range (0.04 to 0.08 μ m) than the Vitro powder. However, the fact that the Thorium Limited material was agglomerated into chunks of about 1/8-in. (0.32 cm) size ruled out its use in the preparation process. Attempts to de-agglomerate an alcohol slurry of these thoria chunks in a Waring blender showed some promise, but on removal of the alcohol, the thoria re-agglomerated. An electron micrograph of the Thorium Limited ThO₂ is shown in Figure A-1.

Samples of thoria from seven lots obtained from a third supplier and a single sample from a fourth supplier were evaluated and judged to be unsuitable because of the wide range of particle sizes observed.

Upgrading Thoria Powder by Filtration

The possibility that oversized thoria particles in the Vitro ThO₂ could be trapped by filtration of particles entrained in hydrogen was considered. The approach appeared to have some potential, since filters are now



60,000X

FIGURE A-1. ThO₂ PARTICLES OBTAINED FROM THORIUM LIMITED, LONDON, ENGLAND. THE STARTING CHUNKS OF ThO₂ (~ 0.3 cm DIA.) WERE SUSPENDED IN A SOLUTION OF ETHYL ALCOHOL AND SPRAYED ONTO AN ELECTRON MICROSCOPE GRID COVERED WITH A CARBON FILM.

available with known pore sizes in the range of interest. For example, filters with pore sizes of 0.01, 0.05, 0.1, 0.22, 0.3, 0.45, 0.65, 0.80, 1.2, 3.0, 5.0, and 8.0 μ m are commercially available. In addition, the geometry of the pores of available filters approximates a close-packed array of capillary tubes. In discussions at Battelle's Columbus Laboratories with personnel knowledgeable in the field of aerosols, it was learned that the fundamentals for filtration of airborne particles are not sufficiently developed to predict the suitability of the approach. This conclusion is in agreement with a statement of Davis⁽⁴³⁾ that "in spite of the fact that membrane filters (MF) are widely used and manufactured, the filtration process itself is not understood. In comparison with fibrous filters, MF filtration has been studied very little experimentally and theory is entirely lacking. A somewhat naive argument is often found, stating that the high efficiency of MF's is due to strong electric charge, but any data, even of a qualitative character, are lacking".

However, recent pertinent information by Spurney⁽⁴⁴⁾ and a limited amount of experimental work indicated that the powder-preparation process requirements did not match the performance of available filters. The mismatch is associated with the size of particles retained by the filters and the concentration of the aerosol which determine the useful time before clogging occurs. In Spurney's published experimental work, the collection efficiencies are given for a range of particle sizes and filter pore sizes. Some of the published data are listed below to illustrate the finding that both the small and large particles are retained by the filter and only a fraction of the particles of intermediate size pass through the filter. Clogging was not a problem in the work of Spurney after several hours of use. However, the data indicate that clogging would be a problem for filtering ThO_2 , since the concentration of particles required in the entraining gas, i.e., 1.5×10^{10} thoria particles (0.05μ m in diameter)/ cm^3 of entraining

Aerosol Particle Diameter, μ m	Collection Efficiencies, %		
	Filter 1 pore Diameter = 0.5μ m	Filter 2 pore Diameter = 0.8μ m	Filter 3 pore Diameter = 1.0μ m
0.012	100	100	96
0.023	100	90	67
0.042	99	60	42
0.080	80	46	33
0.15	80	50	38
0.27	96	69	57
0.50	100	94	85
0.68	100	100	96

gas, is many orders of magnitude greater than those investigated in the study on filtration [1×10^5 platinum-oxide particles ($0.02\text{-}\mu$ m diameter)/ cm^3].

Use of filters in the thoria feeder was explored briefly using Linde B alumina and filters having pore sizes of 0.1, 0.45, 1.2, and 5μ m. All filters trapped the entrained Linde B, having a reported size of 0.03μ m, to the extent that no smoke was visible in the exhaust gas. The results can be explained partially by the published data and partially by the results of an electromicroscopic examination of the Linde B. The examination of the alumina feed indicated that it consisted of 0.05 to 0.1μ m-size particles fused at points of contact to form agglomerates of about one micron in size. The results of the examination explains the absence of feed through all but the 5μ m filter and could be a contributing factor for low feed rates through the larger pore size.

In the light of the presently available information, it was decided to terminate development of the upgrading of thoria by filtration. It should be noted that classification of submicron-size particles by conventional methods is not feasible. Separation of settling in various gas and liquid media has been considered. However, the problem can be properly visualized by simply observing

the smoke from a cigarette. Tobacco smoke has a particle size of 0.01 to 1.0 μ m. Obviously, the 0.01 to 0.1 μ m-size particles of interest do not readily separate in air. The reported⁽⁴⁵⁾ settling rates in air and in a normal gravitational field are 5×10^{-3} and 1×10^{-5} cm/sec for the 1.0- and 0.01 μ m-size-particles, respectively. In water, the settling velocities for 1 μ m-size particles are 5×10^{-5} cm/sec, as compared to 5×10^{-9} cm/sec for 0.01 μ m-size particles. The slow settling rates allow ample time for the formation of agglomerates of mixed particle size which then settle more rapidly than individual particles. Consequently, little or no separation is achieved on settling in either air or water.

APPENDIX B

NEW TECHNOLOGY

APPENDIX B

NEW TECHNOLOGY

The research in this report has provided New Technology, which is briefly described below, including pertinent pages in the report describing the New Technology.

A. Scale-up of Powder Production

The chemical vapor deposition unit has been scaled up to provide production of chromium and Cr-ThO₂ powders in 1/4 to 1/2 pound (114-227 g) lots in a one-day process run. (Discussion is on pp 4-22).

B. Dispersion Ductilizing of Cr by ThO₂ Particles

Addition of about 3 w/o ThO₂ (2.2 v/o) to chromium lowers the tensile ductile-to-brittle transition temperature. (Discussion is on pp 52-65, 73-80).

APPENDIX C
DISTRIBUTION LIST

DISTRIBUTION LIST FOR FINAL REPORT CONTRACT NAS3-12435

<u>ADDRESSEE</u>	<u>NUMBER OF COPIES</u>	<u>ADDRESSEE</u>	<u>NUMBER OF COPIES</u>
NASA Headquarters		NASA Marshall Space	
Washington, D. C. 20546		Flight Center	
Attention: N. F. Rekos (RAP)	1	Huntsville, Alabama 35812	
R. H. Raring (RRM)	1	Attention: Library	1
G. Deutsch (RRM)	1		
M. Comberiate (RAP)	1	NASA Manned Spacecraft Center	
J. Gangler (RRM)	1	Structures & Mechanics Div.	
		Houston, Texas 77058	
NASA Lewis Research Center		2101 Webster-Seabrook Road	
21000 Brookpark Road		Attention: Library	1
Cleveland, Ohio 44135		N. Chaffee E.B. 4	1
Attention:			
G. M. Ault MS 3-13	1	NASA Ames Research Center	
Tech, Utilization Off 3-19	1	Moffett Field, California 94035	
Library, MS 60-3	2	Attention: Library	1
Aero. Proc. Section			
L. W. Schopen MS 77-3	1	NASA Goddard Space Flight Center	
Patent Council MS 501-3	1	Greenbelt, Maryland 20771	
Report Controls Off MS 5-5	1	Attention: Library	1
Materials & Structures Div.			
R. W. Hall MS 105-1	1	NASA Flight Research Center	
J. W. Weeton MS 49-1	1	P. O. Box 273	
J. Freche MS 49-1	1	Edwards, California 93523	
M. Quatinetz MS 49-1	1	Attention: Library	1
T. K. Glasgow MS 49-1	1	D. F. Hasson	
Dr. T. Herbell MS 49-1	10	Code 714	1
S. Grisaffe MS 49-1	1		
W. D. Klopp MS 105-1	1	Air Force Materials Laboratory	
J. P. Merutka MS 49-1	1	Wright Patterson AFB, Ohio 45433	
		Attention: Dr. A. M. Lovelace	
NASA Scientific and Technical		Director (CC)	1
Information Facility		C. Lombard (LLA)	1
P. O. Box 33		Dr. H. M. Burte (LL)	1
College Park, Maryland 20740		T. D. Cooper (LLN)	1
Attention: NASA Representative		I. Perlmutter (LLP)	1
RQT-2448	2	Dr. H. Geigel (LLS)	1
		C. L. Ramsey (FBS)	1
National Technical Information		LAM Technical Library	1
Service			
Springfield, Virginia 22151	10		
NASA Langley Research Center			
Langley Station			
Hampton, Virginia 23365			
Attention: Technical Library	1		
R. Pride	1		

<u>ADDRESSEE</u>	<u>NUMBER OF COPIES</u>	<u>ADDRESSEE</u>	<u>NUMBER OF COPIES</u>
Aerospace Research Lab. Wright Patterson AFB, Ohio 45433 Attention: Dr. H. Lipsitt (ARZ)	1	Department of the Navy U.S. Navy Marine Engineering Lab. Annapolis, Maryland 21402 Attention: Dr. Klaus M. Zwilsky	1
FAA Headquarters Washington, D. C. 20553 Attention: A. K. Forney	1	Naval Air Systems Command Navy Department Attention: Mr. Philip Goodwin AIR-5203, Room 2W98 Washington, D. C. 20360	1
U.S. Atomic Energy Commission Washington, D. C. 20545 Attention: Tech. Rpt. Library	1	Aerospace Corporation P. O. Box 95085 Los Angeles, California 90245 Attention: Dr. K. Kamber	1
Air Force Office of Scientific Research 1400 Wilson Blvd. Arlington, Virginia 22209 Attention: Maj. R. Austin Dr. M. Slawsky	1 1	American Society for Metals Metals Park Novelty, Ohio 44073 Attention: Dr. Taylor Lyman	1
U.S. Army Materials and Mechanics Research Center Watertown, Massachusetts 02172 Attention: S. V. Arnold	1	Boeing Company Commercial Airplane Division Materials Research Unit P. O. Box 707 Renton, Washington 98055 Attention: Dr. D. Webster	1
U.S. Army Aviation Materials Lab. Fort Eustis, Virginia 91103 Attention: Library	1	Boeing Company P. O. Box 733 Renton, Washington 98055 Attention: W. E. Binz, Jr.	1
U.S. Army Research Office- Durham Box CM-Duke Station Durham, North Carolina 27706 Attention: Dr. H. M. Davis	1	Atomic Energy Commission Research Establishment RISO DK-4000 Roskilde Denmark Attention: Dr. N. Hansen	1
Department of the Navy Office of Naval Research Code 429 Washington, D. C. 20350 Attention: Dr. R. Roberts	1	Avco Space Systems Division Lowell Industrial Park Lowell, Massachusetts 01851 Attention: Dr. A. S. Bufferd	1
Department of the Navy Chief, Bureau of Naval Weapons Washington, D. C. 20350 Attention: RRMA-2/T. F. Kearns	1		

<u>ADDRESSEE</u>	<u>NUMBER OF COPIES</u>	<u>ADDRESSEE</u>	<u>NUMBER OF COPIES</u>
Aerojet-General Corp. Attention: Mr. Ira Petker Technical Specialist Composite Structures Dept. Azusa, California 91702	1	Central Electricity Research Lab. Attention: Dr. I. Palmer Materials Division Kingston Road Leatherhead, Surrey England	1
Battelle-Institut e.V. Wiesbadenstrasse, Postfact 1337 Frankfurt/Main, W. 13 Germany Attention: Dr. R. Scharwaechter	1	Chromalloy Corporation Attention: M. Epner Sintercast Division 169 Western Highway West Nyack, New York 10994	1
The Bendix Corporation Research Laboratories Division Southfield, Michigan 48075 Attention: E. C. Johnson	1	Defense Documentation Center (DDC) Cameron Station 5010 Duke Street Alexandria, Virginia 22314	1
Atomic Energy of Canada, Ltd. CRNL Applied Materials Research Branch Chalk River, Ontario, Canada Attention: Dr. C. D. Williams	1	Defense Metals Information Center (DMIC) Battelle Memorial Institute 505 King Avenue Columbus, Ohio 43201	1
Battelle Memorial Institute Attention: Dr. Robert I. Jaffee 505 King Avenue Columbus, Ohio 43201	1	Denver Research Institute University Park Denver, Colorado 80210 Attention: Library	1
Cambridge University Department of Metallurgy Attention: G. C. Smith Pembroke Street Cambridge, England	1	Fansteel Metallurgical Corp. 5101 Tantalum Place Baltimore, Maryland 21226 Attention: Dr. L. Klinger	1
Case-Western Reserve Univ. Dept. of Metallurgy & Materials Science University Circle Cleveland, Ohio 44106 Attention: Prof. L. Ebert Prof. L. Leonard	1 1	Frankford Arsenal Mr. Hyman Rosenthal Research Advisor Metallurgy Research Lab. Philadelphia, Pennsylvania 19137	1
		Firth Sterling, Inc. Powder Metals Research P. O. Box 71 Pittsburgh, Pennsylvania 15230	1

<u>ADDRESSEE</u>	<u>NUMBER OF COPIES</u>	<u>ADDRESSEE</u>	<u>NUMBER OF COPIES</u>
The Franklin Institute Attention: Dr. R. Jones Solid State Sciences Div. Philadelphia, Pa. 19103	1	International Nickel Company Attention: Dr. J. S. Benjamin Paul D. Merica Research Lab. Sterling Forest Suffern, New York 10901	1
General Electric Research & Development Lab. Attention: Dr. E. W. Hart Schenectady, New York	1	International Nickel Company Attention: R. R. Dewitt 67 Wall Street New York, New York 1005	1
General Electric Company Attention: C. T. Sims Bldg. 55 Materials & Process Labs. Schenectady, New York 12301	1	International Nickel Company Attention: Library Hunting, West Virginia 25701	1
General Electric Company Advanced Technology Lab. Attention: Library Schenectady, New York 12305	1	ITT Research Institute Attention: S. L. Blum Technology Center Chicago, Illinois 60616	1
General Electric Company Materials Dev. Lab. Oper. Advanced Engine & Technology Department Attention: Dr. R. E. Allen Mr. L. P. Jahnke	1 1	Jet Propulsion Laboratory Attention: Library 4800 Oak Grove Dr. Pasadena, California 91102	1
General Motors Corporation Allison Division Attention: D. K. Hanink Materials Lab. Indianapolis, Indiana 46206	1	Arthur D. Little, Inc. Attention: Dr. B. Bovarnick 20 Acorn Park Cambridge, Massachusetts 02140	1
Gordon McKay Laboratory Attention: Prof. M. F. Ashby Harvard University Cambridge, Mass. 02138	1	Lockheed Missile and Space Co. 3251 Hanover Street Palo Alto, California 94304 Attention: Dr. E. C. Burke Matls. Science Lab. Dr. T. E. Tietz Matls. Science Lab. Tech. Information Center	1 1 1 1
Illikon Corporation Attention: Dr. L. J. Bonis Natick Industrial Center Natick, Massachusetts 01762	1	Lockheed-Georgia Company Attention: Dr. W. S. Cremens Research Laboratory Marietta, Georgia 30060	1
Institute de Recherches de la Siderurgie Francaise (IRSID) Attention: Dr. L. Roesch 185, Rue President-Roosevelt St. Germain-en-Laye (S & O) France	1	Lycoming Division AVCO Attention: Mr. W. Freeman 505 S. Main Street Stratford, Conn. 06497	1

<u>ADDRESSEE</u>	<u>NUMBER OF COPIES</u>	<u>ADDRESSEE</u>	<u>NUMBER OF COPIES</u>
Massachusetts Institute of Technology Department of Metallurgy Room 8-305 77 Massachusetts Avenue Cambridge, Massachusetts 02138 Attention: Prof. N. J. Grant	1	The Ohio State University 116 West 19th Avenue Columbus, Ohio 43210 Department of Metallurgy Attention: Prof. M. G. Fontana, Chrm. Prof. R. A. Rapp	1 1
McDonnell Douglas Corporation Materials Research Division Attention: Dr. D. Killpatrick 3000 Ocean Park Blvd. Santa Monica, California 90406	1	Oxford University Attention: Dr. F. J. Humphreys Dept. of Metallurgy Oxford, England	1
McMaster University Attention: Prof. J. D. Embary Dept. of Metallurgy and Materials Science Hamilton, Ontario, Canada	1	Pennsylvania State University Attention: Prof. M. C. Inman Department of Materials Science University Park, Pennsylvania 16802	1
Michigan Technical University Attention: Prof. R. W. Guard Head, Dept. of Metll. Engrg. Houghton, Michigan 49931	1	Pratt & Whitney Aircraft Attention: Dr. D. H. Boone Advanced Materials Res. & Development Lab. Middletown, Conn. 06473	1
Narmco Res. & Dev. Division Whittaker Corporation Attention: Dr. F. J. Riel Tech. Director 3540 Aero Court San Diego, California 92123	1	P. R. Mallory and Co., Inc. Attention: Technical Library 3029 E. Washington Street Indianapolis, Indiana 46206	1
N.R.A., Inc. Attention: Dr. S. Grand 35-01 Queens Blvd. Long Island City, New York 11101	1	Pratt & Whitney Aircraft Div. United Aircraft Corporation Attention: E. F. Bradley 400 Main Street East Hartford, Connecticut 06108	1
National Research Corp. Attention: Tech. Info. Ctr. 70 Memorial Drive Cambridge, Mass. 02142	1	Pratt & Whitney Aircraft Div. United Aircraft Corporation Attention: J. Moore West Palm Beach, Florida 33402	1

<u>ADDRESSEE</u>	<u>NUMBER OF COPIES</u>	<u>ADDRESSEE</u>	<u>NUMBER OF COPIES</u>
Rensselaer Polytechnic Institute Attention: Prof. F. V. Lenel Department of Materials Science Troy, New York 12180	1	Cabot Corporation Stellite Division Attention: Technical Library Technology Department Kokomo, Indiana 46901	1
Sherritt Gordon Mines, Ltd. Attention: Dr. D. J. I. Evans Research and Development Div. Fort Saskatchewan Alberta, Canada	1	University of Birmingham Attention: Prof. R. E. Smallman Dept. of Physical Metallurgy Edgebaston Birmingham, England	1
Solar Division International Harvester Attention: J. V. Long 2200 Pacific Highway San Diego, California 92112	1	University of California at Los Angeles Attention: Dr. G. Hoffman Los Angeles, California 90024	1
Stanford Research Institute Attention: F. A. Halden Menlo Park, California 94025	1	University of California Attention: Prof. J. E. Dorn Hearst Mining Bldg. - Room 268 Berkeley, California 94720	1
Stanford University Attention: Prof. Oleg Sherby Department of Materials Science Palo Alto, California 94305	1	Universal-Cyclops Steel Corporation Attention: L. W. Lherbier Bridgeville, Pennsylvania 15017	1
Sylvania Electric Products, Inc. Attention: Dr. J. S. Smith Chemical & Metallurgical Div. Towanda, Pennsylvania 18848	1	University of Kentucky Attention: Prof. Hans Conrad Dept. of Metallurgy Lexington, Kentucky 40506	1
TRW, Inc. Attention: Dr. E. Steigerwald TRW Electromechanical Div. 235555 Euclid Avenue Cleveland, Ohio 44117	1	Wah Chang Corporation Attention: S. Worster Albany, Oregon 97321	1
		Westinghouse Research Lab. Attention: R. T. Begley Metallurgy Department Pittsburgh, Pennsylvania	1